

POLITECNICO DI TORINO

Master's Degree in Nanotechnologies for ICTs



Master's Degree Thesis

Characterization of ion exchange membranes for energy harvesting and storage devices

Supervisors

Dr. Mara SERRAPEDE

Prof. Andrea LAMBERTI

Candidate

Claudio BAUDINO

December 2020

Table of Contents

1	Introduction	5
2	Energetic situation	7
2.1	Energy demand	7
2.2	Renewable energy sources	9
2.2.1	DSSC	12
2.3	Storage devices requirements	15
2.3.1	Supercapacitors	16
2.4	Integrated HS devices	18
2.4.1	Configurations	19
2.4.2	Parameters to evaluate	23
2.4.3	Reviews	24
3	Microelectrodes	27
3.1	Differences with respect to macroelectrodes	28
3.2	Polishing procedures	31
4	Redox mediators	37
4.1	Diffusion coefficient of $K_3Fe(CN)_6$	37
4.1.1	Setup	39
4.1.2	Cyclic voltammetry	41
4.1.3	CV results	43
4.1.4	Chronoamperometry	55
4.1.5	CA results	57
4.1.6	Impedance spectroscopy	63
4.1.7	FRA results	65
4.2	Calibration with different concentration	69
4.2.1	CV results	70
4.2.2	CA results	71
4.2.3	FRA results	74
4.3	Comparison between the three techniques	75

5	Ion exchange membranes	78
5.1	Theory	78
5.2	Activation	81
5.3	H cell	81
5.4	Reference electrode	83
5.5	Permselectivity	85
	5.5.1 Results	89
5.6	Determination of redox mediator concentration variations	91
	5.6.1 Results	92
6	Carbon electrodes for supercapacitor	96
6.1	Realization of electrodes	96
6.2	Results for Glassy Carbon	101
6.3	Results for activated carbon electrodes	103
	6.3.1 Comments on the different configurations	104
	6.3.2 Deposition on Glassy Carbon	106
	6.3.3 Deposition on Titanium foil	108
6.4	Results for active carbon disc electrodes	114
7	Conclusions	120
	Bibliography	123

Chapter 1

Introduction

This thesis work was finalized to the characterization of an ion exchange membrane. This has been done by considering, as ultimate scope, inserting the studied membrane in an integrated Harvest and Storage device.

HS devices consist in a new family of tools which integrate in the same block both the operations of production and stock of energy. They will be presented and treated in chapter 2. In particular, an important look will be given to the most used components (Dye-Sensitized Solar Cell and supercapacitor), their working principles and a review of projects of HS devices up to now.

The need for HS devices starts from the increasing energy demand in the world. A short overview of the variation of energy request will also be presented in chapter 2, with data until 2018.

In order to build in future an integrated HS device, made up of a DSSC and a supercapacitor, a fundamental step is to characterize the ion exchange membrane. This, in turn, requires some previous studies.

First of all, a study of electrodes to perform measures was necessary. For this work, microelectrodes of platinum have been used. Some consideration on microelectrodes will be presented in chapter 3. In particular, advantages with respect to classical macroelectrodes will be highlighted, showing also the polishing procedure found during this thesis.

Redox mediators were of fundamental support in this work. Chapter 4 will be completely dedicated to them, by giving very large space to diffusion coefficient. This last has been demonstrated to be related to concentration of the redox mediator and could be thus used to evaluate the performance of the ion exchange membrane. The redox mediator used in this thesis work was potassium ferricyanide ($K_3Fe(CN)_6$). The choice of this compound was given by the fact that this redox mediator could be used in aqueous DSSC, it involved a redox reaction with one electron, it was reversible and it has been widely studied in literature.

Three techniques to calculate diffusion coefficient of a given solution have been

investigated: cyclic voltammetry, chronoamperometry and impedance spectroscopy. Results have been reported and discussed in order to determine the best method to be used in the final membrane characterization.

Chapter 5 will be devoted to ion exchange membranes. An overlook to what they are, to some commercial examples and to their employment in different devices will be given. Permselectivity, an intrinsic parameter of this kind of membranes, will be analysed and results for a 117 Nafion[®] membrane will be shown. For the studies of the membrane, an H cell has been conceived, designed and realized. It will be briefly presented, together with the choice of the reference electrode.

Always in this chapter, the produced H cell will be used to determine the goodness of the studied membrane, by checking the passage of potassium ferricyanide. In particular the cyclic voltammetry will be used, with the microelectrodes seen in chapter 3.

Finally, an active carbon electrode has been realized and studied. It has been used to determine the efficiency of ion exchange membrane, like in chapter 5. Results will be presented in chapter 6. Also in this chapter, the realized electrode was studied for a possible application for a supercapacitor.

Chapter 2

Energetic situation

The modern society is strongly based on energy consumption.

Nearly every day each one of us consumes a lot of energy in different ways. The most immediate examples can be: taking the car to go to work, turning on lights, using phones or domestic appliances. Anyway, there is also a more important and not immediately clear contribution. This one regards the energy consumption to produce some goods, especially in manufacturing raw materials (e.g. the heat to melt plastic needed for every day products) and in transport to the final consumer. The energy demand is in continuous growth with many consequences. Non-renewable sources, like oil or coal, are decreasing and running out, while greenhouse gases are continuously released in the air, contributing to global warming. An accurate control of emissions must be performed, concurrently with new and more eco-friendly ways of energy production.

In the following chapter the global situation will be analyzed, giving a brief summary of the data of consumption up to 2018. After that some new ideas will be presented, in particular taking the examples of DSSCs, supercapacitors and their integration.

2.1 Energy demand

The worldwide total energy consumption is growing day by day. As reported in [1], in 2018 the total energy used in the world was estimated to be of 14 282 Mtoe (megatonnes of oil equivalent, 1 Mtoe = 11.63 TWh)

This value should be compared to 5 519 Mtoe, which was the total energy consumption in 1971. In 47 years it increased of 160%. In 2018, the energy consumption of 1971, was nearly equated by the one of China alone.

Of the 14 282 Mtoe, around 32% came from oil, 27% from coal and 23% from natural gas; 5% was obtained from nuclear and 13.8% from renewable sources (most

of which from biofuels, around 9%, which cannot be defined as a real renewable source). Only 2% came from hydroelectric plants and less than 2% from other sources like solar or wind power. Also the division depending on sources has changed from 1971. Coal maintained nearly the same level, while oil fell from 44% to 32%. Natural gas increased of 7%, keeping the third position as consumed resource and nuclear gained its own portion of market (from 1% up to 5%). Renewable sources kept more or less the same values, taking a 2% from biofuels, but always remaining a marginal support.

A comparison between 1971 and 2018 data is better shown in figure 2.1.

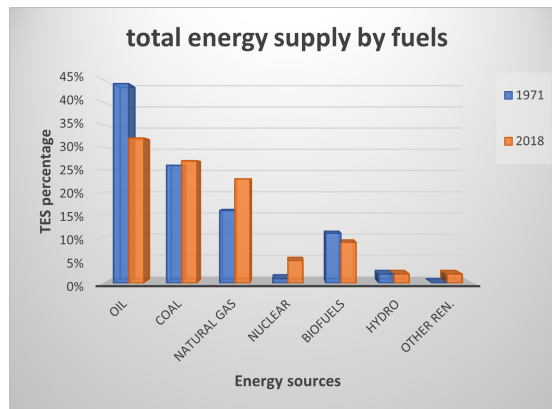


Figure 2.1: Total energy supply by sources, comparing 1971 with 2018 global demand. Data from [1].

However, non-renewable sources cannot continue to be the fundamental energy suppliers.

The reasons are for example the production of greenhouse gases, mainly carbon dioxide. These gases contribute to global warming, by absorbing infrared component of sunlight and releasing this energy by increasing temperature, so they must be reduced. One possibility to reduce the production of these gases is with the help of some CO₂ traps. However, these devices alone are not sufficient.

Furthermore, non-renewable sources, like coal and oil, have an inherent limited availability, so they will not be present for an infinite time. Due to these two main reasons, many researches have been conducted to improve efficiency and to reduce costs of renewable sources.

In tandem with this research, the politic world has taken a decision, by subscribing the Paris Agreement. During this occasion, the United Nations Framework Convention on Climate Change (UNFCCC), an act has been signed, taking decisions on climate change mitigation (in particular, on greenhouse gases reduction), climate change adaptation and finance. The act was signed in 2016 by 196 nations, in order

to control climate change and reduce the human impact due to energy consumption. In February 2020, the decisions should have started to work. 7 of the UNFCCC nations came out of the agreement (the most noticeable of which were Turkey and Iran). In July 2017 US president Donald Trump announced that also USA will withdraw from the Paris Agreement by the end of 2020.

This agreement made an important step, since it was understood that not only it was necessary to improve efficiency of energy production with renewable sources, but it was of fundamental relevance to also reduce consumption. This can be done in several ways, but one of the most efficient one is by improving energetic efficiency of new cars, vehicles, domestic appliances and all electric devices and discouraging the use of old ones. This can give an important hand in both reducing greenhouse emissions by old engines and to reduce also the energy demand.

However this interesting field is out of the scopes of this thesis, which is more oriented to improvement of devices for energy production from renewable sources, in particular, solar one.

2.2 Renewable energy sources

The possibilities to produce energy in this clean way are a lot.

Wind power plants are a reality in many countries, especially in the north Europe. The importance of wind power is affirmed today as the real renewable source for energy production. In fact, it has the advantage to be completely renewable, differently from biofuels or hydroelectric (many times used only as a storage of energy). According to this, many countries, have started a run towards eolic plants. For example, Denmark produces nearly 30% of its consumed energy from wind power. Portugal and Spain reached nearly 20% of energy production from wind. Germany arrived to a 10%.

The five principal producers of energy from wind are: China, United States of America, Germany, Spain and India.

In 2018 the total capacity of energy production arrived to 591GW, with an increase of 51.3GW (9.6% of previously installed capacity). In 2017 the increase was of 53.2GW. This rapid grow in this field confirmed the good expectations from this renewable source.

However, this resource is not present everywhere in the world, or better, it can't be used everywhere. In fact certain precise conditions must hold in order to harvest this energy. Wind must be constant for a reasonable amount of time and its velocity must be in a certain range of values (too high will damage plants, while too low will not put in rotation wind turbines).

Water is another renewable source and it can be used in many ways.

For example tidal: this kind of plants can harvest energy from tides in sea sides. It is a powerful kind of energy harvesting, but it can be obviously used only in some specific places (enough tide movement must be present and it is applicable only where seas are present).

Hydroelectric is confirmed from many years as the most used way to convert energy from water fall into electric energy. It represents the most widespread renewable source. Obviously it can't be applied everywhere, as requirements of rivers and falls are necessary. However, one of the most largely employed configuration for hydroelectric power plants is the one of saving energy. In fact, they can be composed by two dams. During day, when energy demand is high, water is made to flow from the upper to the lower one, producing electricity. During night, instead, water is repumped to the higher dam, consuming electricity. This cycle is obviously energetically unfavourable, however it allows supply at peak energy demands during days. The energy used during night can be the one produced by other sources like nuclear or eolic, which are in excess and are difficult to completely turn off.

Other new and interesting solutions of energy harvesting with water are based on capacitive mixing and reverse electrodialysis. These two techniques are still mainly at a research level, even if some plants are starting to work all along the world. They can produce energy thanks to salinity gradients in solutions (for example at interface of rivers entering in sea, or in water brine dispersion in rivers). These two last methods are however only at their beginning.

The last and most consolidated renewable energy is biofuels. This category contains all fuels which comes from biomass and not from materials formed during many years, like oil. The two most used biofuels are bioethanol and biodiesel (respectively formed from sugar fermentation of some wastes of plants and from transesterification of fats or oils). However, their main employment is as additive in fuels for vehicles and they are rarely used as main source of energy.

Always to the category of biomass and biofuels, there are all wood logs and pellets. Those are old and quite inefficient ways of producing energy, however they are still appealing due to low costs. Both biomass are generally employed only for heating. Biofuels are considered renewable also according to their "bio" nature: they produce energy starting from plants which have been grown and which have produced oxygen during their life cycle. Anyway, this is not really what a renewable source should be like. In fact, in order to work they need to burn and will produce carbon dioxide, known to be the most widespread greenhouse gas.

During last decades a new and more appealing solution in the field of biofuels has developed. It is the Microbial Fuel Cell. This electrochemical system harvests energy from metabolic path of bacteria in wastewater. It works thanks to redox reactions on proteins produced by certain bacteria. This system is nowadays an interesting solution in combination with wastewater treatment.

After all these possibilities there is the sun.

It has the advantage to be present everywhere on earth. It is free and available for everyone. Its energy would be totally renewable and with costs only connected to the generation system, without the need of transport of any fuel. Moreover, it offers the advantage to be suitable for off-grid applications. This last application is very good for some places which are difficult to reach with standard electric lines. Many unused areas on the planet can be dedicated to production of energy from sun.

The two main possibilities to harvest this kind of energy are: solar and photovoltaic. Solar energy is based on the heating of water, sometimes up to evaporation. In this case steam will spin a turbine producing electricity. The heating of water can be direct (the sun illuminates a water container) or through some other mediums (sun heats some liquids with high boiling temperature, which is conveyed to a water container where heat is released). Some solutions allow to store energy thanks to some particular liquids with very high heat capacities. Systems of lenses and mirrors can also be used in order to concentrate radiation and increase efficiency. Many solar plants are already diffused all along the world.

Solar energy is also very used in houses to heat water for domestic applications.

Photovoltaic energy, instead, consists in the direct transformation of solar radiation into electric energy. This reduces losses with respect to solar. Many harvesting solutions have been developed in this field and will be briefly analyzed in next section.

Energy from sun seems, thus, to be the most promising one, among renewable sources.

Since the power of sun registered on the earth during a year is of 120 000 TW, according with the fact that the global consumption is of around 15 TW per year, it seems to be the perfect choice for energy production.

The sun, however, has a big disadvantage with respect to fuels. It cannot guarantee a constant source of energy: clouds can cover it and during night no energy can be produced. This problem, in order to be solved, requires the employment of a storage system.

A summary of main advantages and disadvantages of every renewable source is shown in table 2.1.

Energy source	Advantages	Disadvantages
Biomass energy	<ul style="list-style-type: none"> • Abundant and renewable • Can be used to burn waste products 	<ul style="list-style-type: none"> • Burning biomass can result in air pollution • May not be cost effective
Geothermal energy	<ul style="list-style-type: none"> • Provides an unlimited supply of energy • Produces no air or water pollution 	<ul style="list-style-type: none"> • Start-up/development costs can be expensive • Maintenance costs, due to corrosion, can be a problem
Hydropower	<ul style="list-style-type: none"> • Abundant, clean, and safe • Easily stored in reservoirs • Relatively inexpensive way to produce electricity • Offers recreational benefits like boating, fishing, etc. 	<ul style="list-style-type: none"> • Can cause the flooding of surrounding communities and landscapes. • Dams have major ecological impacts on local hydrology. Can have a significant environmental impact • Can be used only where there is a water supply • Best sites for dams have already been developed
Marine energy	<ul style="list-style-type: none"> • Ideal for an island country • Captures energy that would otherwise not be collected 	<ul style="list-style-type: none"> • Construction can be costly • Opposed by some environmental groups as having a negative impact on wildlife • Takes up lots of space and difficult for shipping to move around
Solar energy	<ul style="list-style-type: none"> • Potentially infinite energy supply • Causes no air or water pollution 	<ul style="list-style-type: none"> • May not be cost effective • Storage and backup are necessary • Reliability depends on availability of sunlight
Wind energy	<ul style="list-style-type: none"> • Is a free source of energy • Produces no water or air pollution • Wind farms are relatively inexpensive to build • Land around wind farms can have other uses 	<ul style="list-style-type: none"> • Requires constant and significant amounts of wind • Wind farms require significant amounts of land • Can have a significant visual impact on landscapes • Need better ways to store energy

Table 2.1: Comparison and main differences between technology using renewable sources, from [2].

2.2.1 DSSC

Sun can be used in many ways. Apart for the previously cited solar energy, used to heat water, important considerations can be done on photovoltaic one. This is based in the conversion of solar radiation into electric energy, which represents a great advantage with respect to solar energy. The spectrum of solar emission is shown in figure 2.2. Higher energy can be harvested since most of it can be absorbed by photovoltaic cells. Therefore, proper choices must be done.

Historically photovoltaic solar cells have been divided in order of appearance. The first generation consisted of a Silicon panel (both monocrystalline and polycrystalline) and worked thanks to a p-n junction. Solar rays provided electron-hole generation which were separated at the interface of the two regions. Connections to an external circuit lead to a current flow through it. However, this technology (which has now an efficiency of more than 20%) has reached a limit. After this level, photovoltaic panels made of crystalline silicon are difficult to produce, quite expensive and their realization has many impacts on the environment, due to large temperatures employed in fabrication and they can't physically increase efficiency over a further limit.

So, many other solutions have been found through the years. One example was represented by thin film photovoltaic cells. They were the second generation of solar cells. They were made by using again silicon, but in an amorphous form which required lower temperatures to be managed. The advantages of thin films, were the low cost of fabrication (by having the possibility to be produced by

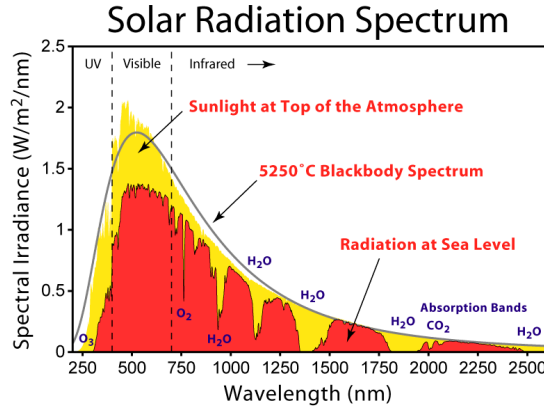


Figure 2.2: Spectrum of the solar radiation. This Figure was prepared by Robert A. Rohde as part of the Global Warming Art project.

roll printing), reduced CO₂ emission during production, reduced wastes of silicon, smarter applications (flexible cells, compared to the rigid ones of first generation), possibility to be printed on many materials or surfaces, possible multi-junction configurations (overlay of many layers with different absorption range, which can harvest larger sun spectrum), use in tandem with other new technologies like concentrators, intermediate bandgap solar cells, Si microspheres and semiconducting inks.

Other interesting solutions, born in same years as second generation cells, were the organic photovoltaics, which have good efficiency, low costs and flexibility. They were completely or partially made with polymeric materials.

Perovskites are very recent and seems to be the most promising technology to harvest solar energy. In fact, they show the highest efficiencies (after some p-n based photovoltaic cells like those based on gallium arsenide (GaAs), but which are really expensive and not viable for large distribution). At the moment, however, they present a very high disadvantage which has slowed their diffusion: the efficient Perovskites Solar Cells (PSCs) contain lead, which represents a risk for health, it is not abundant enough in nature to supply all world's request and moreover it is harmful for environment. For the moment, thus, employment of PSCs is still really limited and generally only found at research level.

Finally, a further solution is represented by DSSCs (Dye-Sensitized Solar Cells). DSSC, reported for the first time by Grätzel et al. [3], represent one of the most studied solutions for energy harvesting in integrated devices.

The working principle of a DSSC mimics the one of a leaf in the process of photosynthesis. In particular, a dye absorbs solar radiation, by exciting one of its electrons from HOMO to LUMO states. The electron can be thus transferred to the collector (generally made of high surface and proper bandgap materials, like

TiO₂ nanoparticles).

At this point the electrons can flow in the external circuit, powering the connected device. The closure of the circuit happens at the cathode, where the electrons reduce the oxidized form of the redox mediator. This last, then diffuses towards the photoanode, where the oxidation reaction will take place. This will regenerate the dye, leading it again to its standard state, ready for the absorption of a new photon.

However, not all photogenerated electrons follow this good path, due to losses caused by some undesired recombinations with either the oxidized form of the mediator, or with the dye itself, thus reducing efficiency.

The schematic representation of the working principle of a DSSC is reported in figure 2.3.

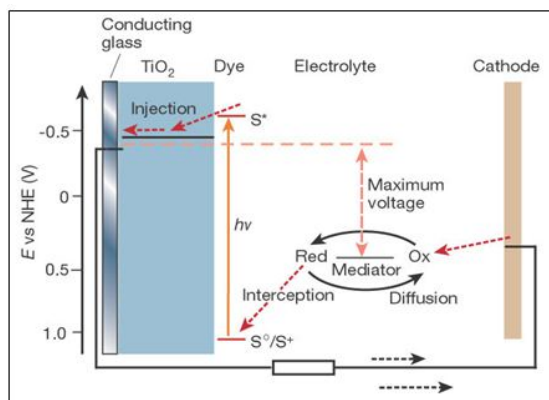


Figure 2.3: Working principle of a DSSC, from [4]

The advantages of DSSC are:

- the low cost of fabrication, considering that no particular processes are required;
- it is eco-friendly, meaning that it can be produced at low temperature and without the use of toxic substances or pollutants. Generally, the photoanode is easily recyclable;
- it has the unique property of good indoor efficiency, in the sense that it works well also with low illuminations, differently from all other solar cells;
- it allows flexible geometries.

However, two intrinsic problems of DSSC still limit its diffusion. First of all, the best DSSC up to now uses a liquid electrolyte. This is a problem, since the system can have leakages. Therefore it requires proper seals and must be refilled

with time. However, those problems can be solved by proper cell designs. The real disadvantage of this solar cell is its low efficiency when compared with other configurations (maximum reported efficiency are slightly above 10%).

So, generally, DSSCs seem to represent a good solution for the harvest of energy, giving the possibility to integrate it with storage devices. The research on this type of solar cell is in continuous evolution and produces every day new and better structures. In this work thesis, the choice of harvest device fell on a DSSC, relying on an aqueous based electrolyte containing the redox mediator $K_3Fe(CN)_6$. The reasons were the good possibility of its integration in an HS device, the sustainability of this process and the good indoor efficiency. Examples of DSSC using this redox mediator have also been found in literature [5] and [6].

Many combinations of energy harvesting from sun with supercapacitors have been developed during the years (not only DSSC), a summary of them can be found in [7].

2.3 Storage devices requirements

Obviously, in order to have an integrated device, not only the harvest system, but also the way of storing energy must be properly chosen.

The possibilities offered by literature are many. Some systems use potential energy of water, with the previously cited methodology with two dams. Other similar techniques rely on the same system, by storing potential energy and releasing it when needed. Also with a comparable principle there are some solar plants which keep heated liquids with high thermal capacity. In this way, the solar energy can be maintained for longer times.

Those systems are, however, affected by many intrinsic defects, like high leakages in the case of heat conservation in fluids and many problems of energy conversion (from mechanical/thermal up to electrical and viceversa). They are well suited only for particular cases, since they offer the advantage to be scalable up to very large levels, limited essentially only by spatial problems. Moreover, these methods can't be reduced for portable devices. Their use will, thus, remain confined to some buffer solutions for specific cases in high power plants.

Only harvest devices relying on electrical or electrochemical functions are practical for a little integrated device.

These devices have also higher efficiency and provides better energy conservation with time. They offer the advantage to store directly energy in form of electricity and don't need inefficient systems of conversion from one type to the other and back again.

Many types and configurations are present, each one with proper and peculiar characteristics, which make them more suitable for different applications.

Mainly, these types have been divided in three categories:

- *capacitors* are easy to produce and have high power density, but very low energy density. They are suitable only for some particular applications where current is needed only for period of little time. They are generally made in a solid form, with two metal plates as electrodes, containing a ceramic dielectric in between. Charges are stored on the two armatures, in an electrostatic manner. One inherent problem can be the broken of dielectric if high overpotentials are applied;
- *batteries* are an electrochemical solution. They have very large energy density, but low power density. They have also very low leakages. Example of photobatteries (integrated HS devices containing batteries) are reported in [8]. Generally batteries are of two types, redox flow batteries (not feasible for little devices) and Li-ion (the most widespread). The differences between these two examples are:
 - *Redox flow batteries (RFB)* are relatively new with respect to classical batteries. They work thanks to separate electrolytes with different valence stored in two different chambers. Electrolyte is divided in anolyte and catholyte. The flow puts in contact at an ion exchange membrane only a little portion, where a redox reaction happens. This will release chemical energy in the form of electricity. The storage part works simply by keeping separated the two electrolytes, previously charged with the reversible process. They are well suited for large applications, since they are very bulky and require pumping systems;
 - *Li-ion batteries (LIB)* are, instead, made generally of a liquid electrolyte containing a lithium salt, a cathode of an intercalated lithium material and an anode of graphite. They are the main solution for energy storage in portable electronic devices and electrical vehicles, but also very used in military field;
- *supercapacitors* can be based on many effects, like pseudocapacitance, electric double layer and with redox-aided electrolytes. Their performances can be evaluated through some techniques [9]. They are in between performances of batteries and capacitors and will be analyzed in the following subsection.

2.3.1 Supercapacitors

Supercapacitors are a family of devices which accumulates electrical energy according to two major processes: electrical double layer and pseudocapacitance.

Supercapacitors are distinguished from classical capacitors for their very high

values of capacitance. Differently from capacitors they are generally liquid devices, containing an electrolyte and only few of them are in a solid or quasi-solid state.

The structure of a supercapacitor is shown in figure 2.4. It can be seen that the

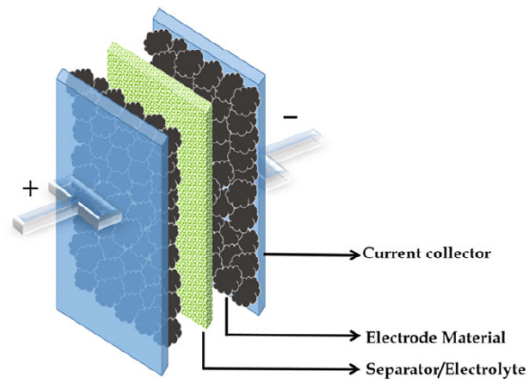


Figure 2.4: Components of a supercapacitor, from [10]

components [10] are:

- a liquid *electrolyte*, which holds the Helmholtz double layer, also called EDL (Electrical Double Layer);
- *electrode materials*, which have high surface area, in order to maximize EDL capacitance, or with faradaic properties to exploit pseudocapacitance [11];
- two *current collectors* covered with electrode materials;
- a *separator*, used to avoid the direct contact of electrodes, the one with the other;
- a *package*, to contain all other components. In general, due to the liquid nature of most of electrolytes, it must guarantee an hermetic sealing.

Supercapacitors are mainly used where rapid charge/discharge cycles are required (like regenerative braking and short-term energy storage).

They offer the advantage to be made with earth-abundant and non-toxic materials (mostly fabricated with carbon-based materials), differently from example with Li-ion batteries. These last, in fact, are based on Lithium, which has a limited availability.

Supercapacitors are non-hazardous, they can operate within a wide temperature range (typically between 40° and 85°C) and can tolerate over-abusing. These characteristics, however, also strongly depend on the materials from which the

supercapacitor is made. For example, an aqueous supercapacitor will work with little potentials (less than 1.2V vs. SHE, due to water stability) and will be eco-friendly, while others based on ionic liquids can operate with higher ones (more than 3V [12]), but can have some environmental impacts.

The main advantages of supercapacitors with respect to capacitors and/or batteries, are:

- high power rates;
- fast charge/discharge;
- good stability for many cycles.

However, one of the main drawback and limitation is the high rate of self-discharge [13], [14].

Supercapacitors have been explained in this little section, according to the proposals of this thesis work. In fact, the common choice for storage in integrated HS devices is the supercapacitor. Not only it has higher power densities than batteries and better energy density than a capacitor, but it also has a life cycle way better than the other two systems. This last property is very useful when considering a device made with a solar cell. In this last, in fact, due to the possible frequent variation of solar conditions (like passages of clouds), the switching between charge and discharge provides many cycles. It is faster than batteries, but providing more energy storage than a capacitor, it represents a very good compromise.

Moreover, many geometries are available and this helps its integration.

2.4 Integrated HS devices

Starting from 2004, with the work of Miyasaka and Murakami [15] and with a rapid increasing interest, integrated solutions for both harvest and storage of energy were studied. The reasons for this new idea were simple:

- need for off-grid solution;
- employment in compact devices;
- reduction of ohmic losses (they don't have connections with wires);
- possibility to have user-friendly devices.

The feature, in order to call "integrated" a certain harvest and storage device, is only one: both the functions of production and accumulation of energy must be performed by the same system. This allows one to be quite flexible with the inclusion

of devices in the family of integrated HS ones. In particular, some configurations with 4 electrodes can be defined also as integrated devices. This will not follow, however, the true idea behind the concept of integrated HS devices. This difference due to the number of electrodes will be better discussed later.

As previously stated, one of the advantages of integrated HS devices is the possibility to use them for off-grid solution. In fact, someone can imagine of an electrical user which is far kilometers from the electrical grid. It will need continuous and practical solutions in order to properly work. A simple photovoltaic panel would not be enough, since it won't be a continuous source. A system of batteries could be used, however they would need to be charged. Simply combining the photovoltaic panel with the battery is a good idea. From this, one could imagine to improve the system, up to reaching an integrated solution, where ohmic losses of connections will be reduced to the minimum.

By using integrated HS devices, also compact devices could improve performances. It is possible to have better and energy-autonomous sensors, which produce and store by themselves the electricity they require to work. Furthermore, even portable rechargeable devices are possible [16].

Some examples are sensors of temperature, air quality check, gas detection and many others. The ones which will benefit more from the integration of harvesting and storage would be those which works in remote regions, like a sensor that monitors the melting of polar ices, and those which must be miniaturized as much as possible, like sensors in phones.

With the increasing number of available integrated HS solutions, new ways of employment are opening. One of the more developed environments of application is the wearable electronics. This field consist in the study of technological solutions to have "energetic" clothes, tissues which, further than been sewn to have clothes, can also produce and store energy. This one can be then used for simple and smart applications, like charging phones, small torches or to power mp3 readers. The field of wearable electronics have greatly benefited from the HS devices in form of wires or ribbons. Some examples from literature can be found in [17], [18], [19].

2.4.1 Configurations

After having explained the features required for an integrated HS device and all the reasons for which they are studied, it is now the turn to compare and choose the final configuration. This final aspect will be the composition of an harvest device and a storage one.

As it can be easily deduced from previous sections, the final combination decided to be used for this thesis work is the one made of a DSSC and a supercapacitor. However it is mandatory to cite also some other configurations, which can offer

other advantages and limitations.

Many examples in literature are based on a combination of organic photovoltaic cells, silicon based cells and perovskite solar cells with supercapacitors, like [20], [18].

Studies using batteries have also been conducted [21], [8]. It has been easily noticed that the main limit lies in life cycle.

For this study, it has been decided to integrate DSSCs and supercapacitors. In particular, those based in aqueous solutions. The DSSC will work thanks to the redox couple $\text{K}_3\text{Fe}(\text{CN})_6/\text{K}_4\text{Fe}(\text{CN})_6$. This is an already existing and studied configuration [5]. The supercapacitor, instead will work with a KCl aqueous based electrolyte. In order to avoid redox shuttling in the supercapacitor part, an ion-exchange membrane is proposed. Thus, it is fundamental to check the good behaviour of the membrane, in order to be sure of the correct working of the device. Since this thesis work is mainly devoted to the characterization of the IEM, important factors have not been analyzed. In particular, those concerning DSSC and supercapacitor electrodes, in tandem with all packaging issues have not been seen. In the last section of this chapter (sec. 2.4.3) many literature works will be reported. In tables shown there, it will be possible to see how much these factors can affect device performances. For this reason, in a real device application, they will be of primary importance to be studied.

Once defined the right combination to be exploited, it is necessary to determine also other important factors. In fact, device performances strongly depends on geometrical parameters, other than the simple choice of device to be integrated. For example, taking two separate DSSC and supercapacitor and evaluating their performance, will not be the same as to consider the whole integrated device.

A geometrically relevant factor is the number of electrodes [22]. Three possibilities are available:

- **2** electrodes. This combination offers a complete integration. It requires easy circuit, but also implies low efficiency when the device is nearly charged;
- **3** electrodes. This configuration is the most used, because it offers the best compromise between 2 and 4. The efficiency of this kind of devices is the highest and most constant of the three. With this configuration, there is a semi-independent work of solar cell and storage device;
- **4** electrodes. This last structure doesn't provide a real integrated device in the real meaning. It is easy to assemble and it is mainly used in large Redox Flow Batteries or in high power applications.

Most of the existing devices are built in a 3-electrode configuration. As mentioned before this combination seems to have better efficiency performances (with respect to 2-electrode one) [23] and a good level of integration (with respect to 4-electrode

ones).

The differences between two and three electrodes has been graphically shown in figure 2.5.

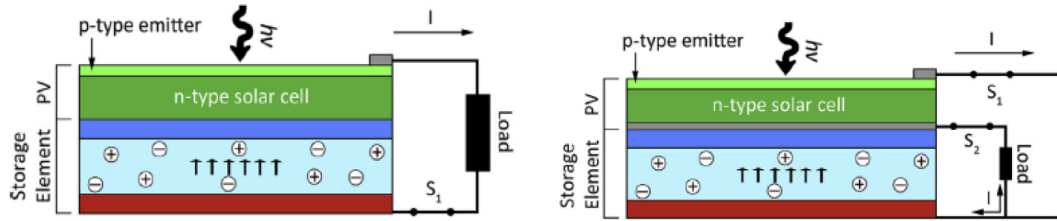


Figure 2.5: Comparison of the geometry of an integrated HS device according to the number of electrodes: A) 2 electrodes vs B) 3 electrodes; from [22].

The shape of the device also plays a fundamental role on HS device performances. The general classification of HS devices is done between planar and fiber-shaped ones, reported in figure 2.6.

Planar geometry, which is the most used has some features:

- easiest configuration to produce;
- highest efficiency;
- rigid structure, with limited or absent flexibility.

While the fiber-shaped configuration, which is more recent, has complementary characteristics:

- flexible;
- suitable to smart applications like wearable electronics;
- performances are not angle dependent (symmetrical geometry);
- lower efficiency and life cycle.

Resuming, planar devices are made of layers of materials which form electrodes, separators, collectors and electrolytes. They are easy to build, have the best conditions of working with higher efficiency and are also cheaper. On the other side they have a rigid or slightly flexible geometry, limiting their employment in certain applications. Fiber-shaped devices are, differently, very flexible and thus suitable for smart applications, like wearable electronics. Moreover, they don't suffer the

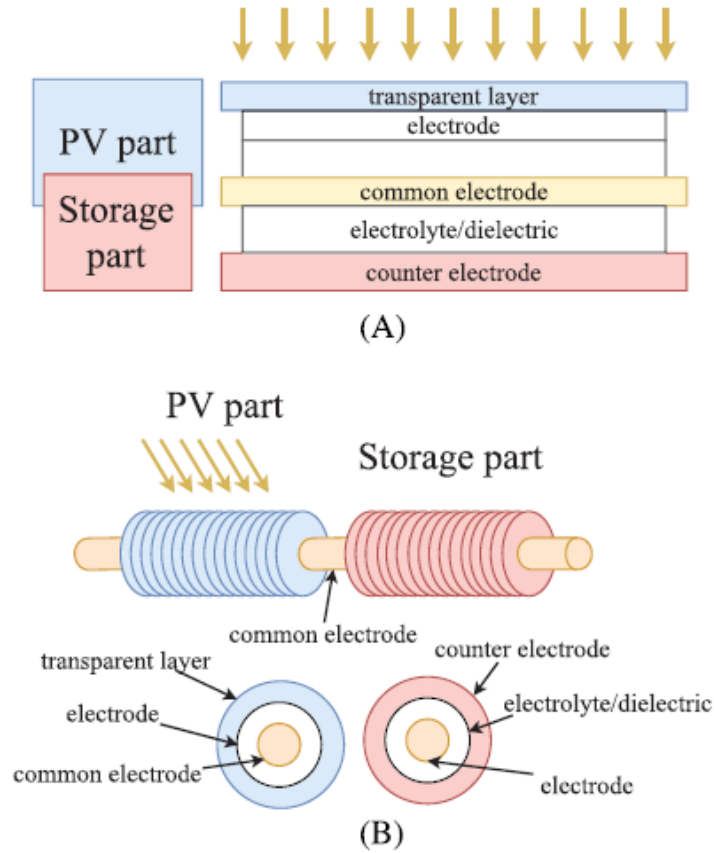


Figure 2.6: Comparison between two examples of the geometries: A) planar and B) fiber-shaped; from [24].

problem of the angle of incidence of light, due to their cylindrical shape. However, this configuration shows lower efficiency and even lower life cycle (every bending of these wires reduces performances).

For these reasons the study of HS devices is generally divided in two main geometries. Their feature have the advantage to be complementary, so it is possible to choose the right one for every application.

A further classification, similar to the one planar vs. fiber-shaped, is the one: planar vs flexible. In this other division, considered by [25], planar devices represent only those with a flat aspect and with no-flexibility. On the contrary, flexible ones contain all those which can be bent and continue to perform well (both if fiber-shaped or flat).

Many different configurations have been reported during the years ([24],[25]). Some with peculiar characteristics are described in section 2.4.3.

2.4.2 Parameters to evaluate

Integrated HS devices, in order to be compared the one with the other, should have some common parameters. The fact for which a particular section has been devoted to this, it is that they are a new class of devices and there isn't a common behaviour of the community yet. In particular, parameters should take into account both of the evaluation of the ability to produce energy and the one of storing it. In literature it is still not present a common standard, thus, sometimes, comparisons are hard to perform. In this work, 5 parameters have been chosen. This decision has been taken according to data availability (these parameters seemed to be the more used) and complete description of device. Namely, they are:

- *OPECSE*, or η_{tot} ;
- *open circuit voltage*, V_{OC} ;
- *solar cell efficiency*, η_{SC} ;
- *storage device capacity*, C ;
- *storage device efficiency*, η_S ;

Solar cell efficiency and open circuit voltage are parameters concerning the part of harvesting, while storage device capacity and efficiency take into account the part of storage. Since an accepted standard is not present, capacities can be normalized with respect to volume, mass or area. The probably best choice for integrated HS devices is the one which refers to area. This is due to the fact that the real interest in integration is the occupied space and that one talks of layers, so volume has low meaning. For this reason during this work, where it has been possible, capacities have been reported as F/cm^2 (or mF/cm^2).

OPECSE, which means Overall Photon-to-Electron Conversion and Storage Efficiency, represents an indication of performances of the HS device in the complete working. In particular, it represents the number of photons absorbed by the device, converted in electrons, stored and then released. It sounds complicate and in fact it is not so easy to define a quantification of the efficiency of an HS device, due to the ensemble of more integrated processes. The choice of considering OPECSE was done according to many literature works (as also confirmed in [26]). It can be calculated as

$$OPECSE = \frac{\frac{1}{2}CV^2}{GtS} \quad (2.1)$$

where C is the capacitance of the EDLC section, V is the maximum voltage achieved during photo-charge, G is the electromagnetic power density impinging

onto the solar cell, t is the photo-charging time and S is the PV surface. However, equation 2.1 is not always correct, especially when there is not a linear discharge of the device. For this reason, a common choice, performed by many authors, is to calculate OPECSE as the product of storage efficiency and photovoltaic efficiency. In the following, where available, this second approach will be used. V_{OC} represents the open circuit voltage of the solar cell. This value is generally lower than 1V, however it can be increased if working with ionic liquids instead of aqueous ones (but usually not eco-friendly materials). Also an example of high voltage HS device obtained with a 4 DSSC module will be reported after [27]. The solar cell efficiency is simply the factor of evaluation of a solar cell. It is obtained by dividing the energy impinging on the PV cell, by the energy produced. Storage device capacity is the capacity due to electric double layer or pseudocapacitance. It is used to evaluate the accumulation of charges in the device. Storage device efficiency, the last considered parameter, represents the fraction of energy which the device can give after being charged, with the charging energy. Sometimes it is substituted by Energetic efficiency, which has the same meaning. Coulombic efficiency, rarely used, is based on the same concept, but applied to charge stored, instead of energy. These 5 parameters have been chosen to evaluate and compare different HS device performances. However it is important to mention that, in a real application, many other factors should be taken into account. For example some device characteristics are present and of relevant impact on the possibility to physically realize the project: cost, life cycle, power density, energy density, flexibility, environmental impact and many others. These parameters should be evaluated for a real application, but in this work they have not been considered.

2.4.3 Reviews

In this section a review with many examples of integrated HS devices is provided. The first integrated HS device appeared in 2004 with the work of Miyasaka and Murakami [15]. They reported an open circuit voltage of 0.45V, a capacity of 0.69 F/cm² and a coulombic efficiency of 59%. OPECSE wasn't calculated and the value of photovoltaic efficiency considered (32%) was evaluated at the optical absorption peak, so it is not suitable for a comparison.

An example of all-solid-state device has been given in [28]. Solid-state means that the electrolyte is not in a liquid form. This provided the advantage of no leakages and eliminated the requirements for a perfectly sealed structure and the need of a refilling. The electrolyte here used was in a gel form and used a sulfur based mediator for the DSSC part. The electrodes of the storing part were made up of

MWCNT (multi-wall carbon nanotubes), which are cheap, easy to produce and offer a quite good conductance. Photovoltaic efficiency was 6.1%, open circuit voltage was 0.75V. The capacity was of 48 F/g, coulombic efficiency was 84% and OPECSE 5.12%. Even if solid-state, the device was found to be stretchable for around 100 times.

The focus of the work was on the electrodes. It has been found that adding PANI to MWCNT an increase of capacity (up to 208 F/g) was reached, trading off in OPECSE (reduced to 2.31%).

One of the most efficient devices in fiber shaped form is reported in [17]. It consisted of DSSCs with TiO₂ nanotubes electrodes, in series with supercapacitors based on PEDOT-MS. The capacity was of 251.2 mF/cm², efficiency 69.9%, open circuit voltage was 0.74V and photovoltaic efficiency was 6.9%. The OPECSE was 5.1%, the best value for a wire photocapacitor based on DSSC and supercapacitor. Moreover, the strength of this device also relied in its high life cycle, when it was bent, a fundamental property for applications in wearable electronics.

Generally the open circuit voltage has values in the range 0.7-0.8V. This is due to intrinsic limits of DSSCs, especially when the electrolyte is aqueous. A solution was found in the work [27], where it was demonstrated the possibility of inserting 4 solar cells in series. The so obtained open circuit voltage was 2.45V, really higher than in other considered cases. Other parameters were of the same order of magnitude of other cases. Capacity was 233 mF/cm². Photovoltaic efficiency was 2.25% and OPECSE depended on the voltage at which one was working (0.41% at 2.45V and 1.83% at 1.63V).

An interesting solution to built easily an integrated device of harvest and storage has been presented in [29]. It consisted in the deposition of a polymeric material, which, opportunely modified, could work as fluorinated barrier or as electrolyte. The device showed an open circuit voltage of 0.67V, a photovoltaic efficiency of 4.33%, coulombic of 86%, leading to an OPECSE of 3.72%. These values were comparable to many other devices, but it offered the advantage of a solid-state and easy solution.

In order to perform a simple but powerful comparison, even a case based on perovskites solar cell has been reported [18]. It had a fiber shaped geometry and an open circuit voltage of 0.96V, a capacity of 145.15 mF/cm², efficiencies of photovoltaic and storage parts were respectively of 10.41% and 67%. Due to the high efficiency of the solar part, the OPECSE was 6.97%. This value is higher than any other one reported up to 2020, for what concerns fiber shaped devices with DSSC. Moreover it is also larger than the most of planar cases (again with DSSC). This showed the potential of employment of perovskites in future solar cells and in turn maybe also in integrated HS devices. However, at the moment, their use is still strongly limited by their content of lead.

All these previously cited devices have been also summarized in table 2.2, with

their main parameters.

Further summaries of integrated HS devices can be found in [24] and [25]. Classi-

ref.	V_{oc} (V)	η_{sc} (%)	C (F/cm ²)	η_s (%)	η_{tot} (%)
[15]	0.45	59	0.69	/	/
[28]	0.75	6.1	48* (208*)	84	5.12 (2.31)
[17]	0.74	7.3	0.251	69.9	5.1
[27]	2.45	2.25	0.233	/	0.41-1.83
[29]	0.67	4.33	/	86	3.72
[18]	0.96	10.41	0.145	67	6.97

Table 2.2: Summary of some integrated HS devices. V_{oc} stands for open circuit potential, η_{sc} for photovoltaic efficiency, C for capacity, η_s for storage efficiency and η_{tot} for OPECSE. (*expressed in F/g)

fications of devices were done according to the geometry, respectively planar vs. fiber-shaped or planar vs. flexible.

Chapter 3

Microelectrodes

For this thesis work the choice of working electrode fell on platinum microelectrodes. In particular the three electrodes had a diameter of the platinum disk of 10, 20 and 50 μm respectively.

The three electrodes were all from MetrOhm. They were designed by sealing small diameter platinum wires in glass and polished to mirror finish. Reasons for which they have been preferred is reported in the first section. A comparison with usual "macroelectrodes" is performed, putting in light advantages and major differences. The second section of this chapter is devoted to explain the procedures adopted in order to polish these electrodes. In fact, due to the reduced dimension of the platinum surface with the solution, even small defects on it could have large effects.



Figure 3.1: Microelectrodes used during the thesis work

3.1 Differences with respect to macroelectrodes

The choice of microelectrodes for this thesis work had some peculiar reasons. In fact, those kinds of electrodes, which differ from classical disk-shaped platinum electrode only for the diameter, have some intrinsic characteristics directly connected to their small surface.

Referring to [30] one can find immediately some fundamental differences. First of all, is the diffusion regime in which the electrode works. By considering to have a microdisk electrode (like in this thesis work), concentration of analyte follows the Fick's second law (here in cylindrical coordinates)

$$\frac{\partial c}{\partial t} = D \frac{\partial^2 c}{\partial r^2} + \frac{D}{r} \frac{\partial c}{\partial r} + D \frac{\partial^2 c}{\partial z^2} \quad (3.1)$$

where z is the perpendicular distance from the electrode surface and r is a radial coordinate from the centre of the disc. The following boundary conditions are required:

$$\begin{aligned} t < 0 & \quad \text{all } r, z & \quad c = c^* \\ t \geq 0 & \quad z = 0, r < r_e & \quad c = 0 \\ t \geq 0 & \quad z \rightarrow \infty \text{ all } r & \quad c = c^* \\ t \geq 0 & \quad r \rightarrow \infty \text{ all } z & \quad c = c^* \end{aligned}$$

where t , is the time, and r_e represents the radius of electrode. The solution of eq. 3.1 was calculated by [31].

A transient behaviour is found, with a limiting current value for long times. The flux at every radius from the center of the electrode is given by

$$j = \frac{2}{\pi} \frac{c^* D}{\sqrt{r_e^2 - r^2}} \quad (3.2)$$

The equation seems to predict an infinite flux at the edges of the microelectrode, which is obviously nonphysical. However, the diffusion is really determined by the edges of the disk and in particular by its perimeter. In fact, the limiting current value is proportional to the radius (circumference is $2\pi r_e$).

The full current behaviour with respect to time has been calculated again by [31] and provides

$$I = 4nFc^*Dr_e f(\tau) \quad (3.3)$$

where the function $f(\tau)$ is

$$f(\tau) = \begin{cases} \frac{\pi}{4\tau} \frac{1}{2} \frac{\pi}{4} + 0.094\tau^{\frac{1}{2}} + \dots & \text{for } \tau < 1 \\ 1 + 0.71835\tau^{-\frac{1}{2}} + 0.005626\tau^{-\frac{3}{2}} - 0.00646\tau^{-\frac{5}{2}} + \dots & \text{for } \tau > 1 \end{cases} \quad (3.4)$$

τ represents a dimensionless time and is calculated as

$$\tau = \frac{4Dt}{r_e^2} \quad (3.5)$$

For short times the Cottrell behaviour is obtained (see eq. 4.7), while for long times the limiting current value is recovered (see eq. 4.3).

From previous equation it can be found that, for short times, the diffusion is planar. This is justified by the fact that only a very thin region in the solution contributes to mass transport, meaning that diffusion region is small compared to the electrode surface.

The decrease in current value slows as time goes by, arriving to a steady state situation. In this case the diffusion layer, approximates the hemispherical one. This is due to the fact that the diffusion layer goes out of the electrode edges, enlarging and introducing a radial contribution.

The great advantage to work with microelectrodes is the fact that steady state is reached in very few time, differently from macroelectrodes. In fact, as can be seen in 3.5, τ is inversely proportional to the square of electrode radius. An idea of the difference of times can be acquired from table 3.1, where times corresponding to $\tau = 1$ are reported. From these values, one can have an idea of what short times region (nearly values divided by 10) or large times region (nearly values multiplied by 10) really means. The cases reported are the ones for electrodes of diameter 10, 20, 50 μm (microelectrodes) and 3 mm (a macroelectrode, used as comparison). The considered specie is $\text{K}_3\text{Fe}(\text{CN})_6$ and the used value for diffusion coefficient is the one obtained from cyclic voltammetry (see next chapter).

electrode diameter	10 μm	20 μm	50 μm	3 mm
time for which $\tau=1$	6.94 ms	27.78 ms	173.61 ms	625 s

Table 3.1: Times for which the dimensionless time is equal to one. The diffusion coefficient here used is $9.1 \cdot 10^{-6} \text{cm}^2/\text{s}$.

The importance to reach steady state in very few time, is the fact that thermal convection starts to give noticeable contributions after 60 seconds. Thus, after this time, previous model won't work with the same degree of reliability and sometimes will not be valid at all (see for e.g. behaviour of macroelectrode in next chapter).

One further great advantage to use microelectrodes is the fact that, having a really small surface, even low concentration on the electrode surface can give appreciable contribution. This allows for more sensitive measurements. This implies the fact that also very small currents will be used, having possible problems of noise or of

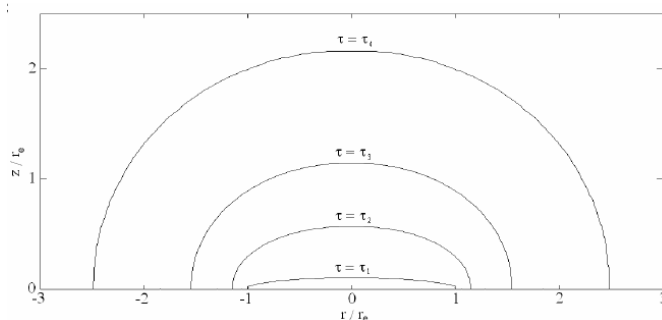


Figure 3.2: Behaviour of diffusion layer at different times, on the surface of a microdisc electrode. From [30]

external contributions. This situation can be easily solved by working in a Faraday cage.

Microelectrodes have also advantages in terms of iR drop. In fact, even if resistance increases linearly by reducing dimensions, the currents (proportional to the area of the electrode) decrease quadratically. So, overall, the iR drop also decrease in a linear way, making it often negligible (see chapter 6 of [32]).

Some disadvantages in using microelectrodes are also present. First of all, the impact of impurities and surface defects play a dominant role. The problem, thus, is connected to the polishing of the electrode. The common procedure, in fact is not sufficient to provide good results. Moreover, the impossibility of use the technique called flame-annealed reduces goodness of results [33].

Flame-annealing consists in the positioning of electrode over a burning flame of butane, in order to rearrange platinum surface atoms. This allows to have very good level of polishing, up to a mirror level. Due to the extremely small and fragile nature of microelectrodes, however, this methodology can't be applied to them.

The effect of this impossibility, immediately provides an increase of double layer currents, which will modify the expected behaviour of Pt in H_2SO_4 (see next section). Furthermore, also peaks in hydrogen adsorption-desorption region and in the oxygen one, are not completely defined as for macroelectrodes.

Having a rough surface will lead to the increase of the electroactive area, which in turn will provide higher currents. For this reason, particular attention must be paid when polishing their surface.

A further problem of the small dimension of microelectrodes is the rapid contamination of the surface.

However, all these problems can be overcome by having a proper polishing procedure. After that, once the microelectrode is mirror cleaned, all advantages like low iR drop contribution, high sensitivity and easy working in steady state region, can be exploited.

3.2 Polishing procedures

In order to have reliable results, a procedure of polishing must be produced. Based on works [33], [34], [35] and [36], some common aspects have been detected. In particular, the two fundamental steps are the cleaning with polishing pad and the electrochemical polishing. Due to the small microelectrode nature, flame annealing was not a possible technique.

The procedure adopted to polish microelectrodes consisted in few simple steps:

- sonication;
- surface abrasion;
- 2 sonications;
- N₂ bubbling in 0.5M H₂SO₄ solution;
- electrochemical polishing;
- sonication.

The process of sonication consisted in an ultrasound bath at 59 kHz for 1 minute. This allowed particulate residuals on electrode surface to be removed. The sonication was generally performed in simple deionized water, without heating. Only in the steps where two sonications are indicated, there was a change in the immersing liquid. A solution 3:1 of deionized water and ethanol was used for the first of the two baths, while in the second the usual deionized water was employed. The need for two sonications after surface abrasion and before electrochemical polishing was found to be fundamental in order to get better results (as can be seen in figure 3.3). Before and after each sonication step, abundant rinsing with deionized water was necessary.

The available polishing pads consisted in three abrasive papers made of SiC with different graininess and other two pads of alumina and diamond. The three abrasive papers, with a roughness of 30, 10 and 7 μm , have been used only when large defects on the electrode surface were encountered. For example, the microelectrode with diameter of 20 μm showed a scratch all along the surface, crossing the platinum tip. This lead unavoidably in affecting measurement results. However, thanks to many steps of polishing with different abrasive papers, the electrode was restored and brought to a clean and flat surface.

The diamond and alumina pads consisted in two little pieces of slightly rough soft papers. They had to be pretreated by placing 2 droplets of colloidal solutions

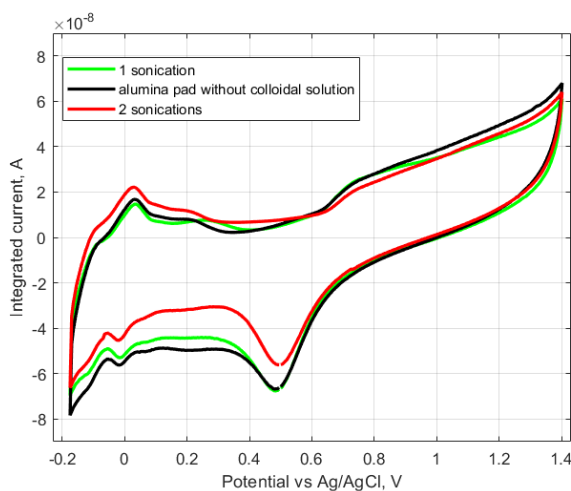


Figure 3.3: Different conditions of sonication after surface abrasion (comparison between 1 and 2 steps of sonication and with bare polishing with clean alumina pad).

followed by 5 droplets of deionized water. The two colloidal solutions, from ALS Co. Ltd as polishing pads, contained respectively 1 μm diamonds and 50 nm alumina nanoparticles.

The previously presented cleaning procedure showed a step called "surface abrasion". This step consisted in softly scrape the electrode on the proper polishing pad (or abrasive paper), by drawing an infinite for 5 minutes. The procedure, as indicated, represents one cycle of polish. In order to have a complete cleaning, different cycles must be performed.

After many tries with different combinations, the best sequence was found to be: one cycle with diamond pad and then two with alumina ones. Abrasive papers were used only when large defects, generally in forms of bubbles or scratches, were found. In order to check these large defects an optical microscope with a magnification of 6x was used. Better checks could be done with a Scanning Electron Microscope (SEM), however the sample chamber of the one present at Politecnico of Torino was not large enough for the electrode.

The electrochemical polishing allowed for a very fine cleaning of electrode surface and, moreover, it offered a good and simple way to check the level of roughness. It consisted in a cyclic voltammetry at high scan rate in a solution of 0.5M H_2SO_4 . The solution was frequently changed during experiments, nearly every two days, in order to have always comparable and good data. The apparatus for this electrochemical polishing consisted in a glass conical-shaped cell with an electrode holder which allowed the insertion of working electrode (the microelectrode under study), counter

electrode (a platinum rod) and reference electrode (an Ag/AgCl electrode filled with 3M KCl of HANNA Instruments). A N_2 bubbler was also present. Experiments were performed in a Faraday cage, in order to avoid noise from external sources. In fact, the recorded currents were of the order of nA, comparable to those induced in the wires when a message to a phone in the chamber was received.

During electrochemical polishing a CV (cyclic voltammetry) plot was recorded. Some peaks could be observed, according to effects of hydrogen and oxygen (in particular when one of the two was generated, or with adsorption and desorption). The expected behaviour was the one of figure 3.4, from [37]. The limits for the working windows were the ones of water, due to oxygen (positive potentials) and hydrogen (negative potentials) evolutions.

In order to have a confirm of the right potential windows to use and to check with

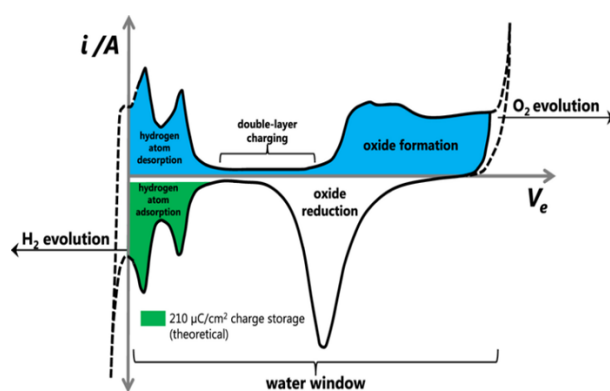


Figure 3.4: Behaviour of the CV when polishing electrodes in 0.5M H_2SO_4 , highlighting the causes of different peaks. From [37].

the used electrodes, many voltage ranges have been explored. Different combination in the window $-0.25V \div +1.7V$ have been tried. The range which was found to be the best was $-0.17V \div +1.4V$, where little evolutions of oxygen and hydrogen were present. The choice was due to the fact that it allowed to work without having large peaks of oxygen and hydrogen evolution, while always having a good behaviour, comparable to the one of figure 3.4. For fastest measurements, also the range $-0.17V \div +1.1V$ was used. It offered a quicker way to check the behaviour, providing also very small EDL currents. However, it is important to say that results obtained with the two methods cannot be compared the one with the other, since both the elements of evaluation strongly depend on the used potential window.

Two ways of understanding the level of polish were used.

First of all, the electric double layer current contribution had to be low. In figure 3.4 this current is the one in the negative region between peaks of oxide reduction and hydrogen atom absorption. This value, which should be theoretically equal to 0nA, must be low with respect to peaks height.

The second parameter of interest is the roughness factor [36], [35]. This number represents the level of polishing, by looking at the charge of absorbed hydrogen atoms. It can be calculated as

$$R_f = \frac{A_g}{ESA} \quad (3.6)$$

where A_g is the geometrical area ($A_g = \pi r^2$) and ESA is the electroactive surface area, obtained from

$$ESA = \frac{q_+}{q_{ML}} \quad (3.7)$$

In this expression, q_{ML} represents the charge stored in one monolayer of adsorbed hydrogen, it has been experimentally found to be $210 \frac{\mu C}{cm^2}$. The desorbed charge q_+ instead, can be obtained as the integral with respect to time of current in hydrogen atom desorption region minus EDL one.

Theoretical value of a perfectly flat surface is 1, meaning that the geometrical area perfectly equals the electroactive one. In reality, this value can't be reached. For convention, it has been decided to consider as sufficiently good surfaces, the ones with roughness factors lower than 5. General results for the electrode with the developed procedure gave R_f with values between 2 and 3.

An example of the CV obtained after polishing steps with the microelectrode of diameter $10 \mu m$ is shown in figure 3.5.

A little parenthesis should be opened to talk about currents considered during the

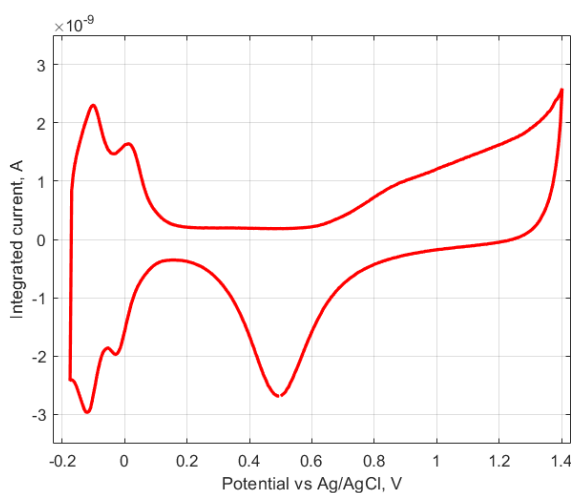


Figure 3.5: CV behaviour of $10 \mu m$ microelectrode after a complete polishing procedure.

cyclic voltammetry. In fact, as can be also seen in figure 3.5, the current reported

on y axis was an "integrated current". This is due to the fact that the imposed voltage was not a perfect linear ramp signal, but a staircase. At each step, the current had a decreasing behaviour and thus a lower total value is recorded when using staircase profile instead than a linear one. The Autolab instrument had a function of integration which took into account this effect and tended to balance it [38].

According to these, all CV profiles were recorded as integrated current versus potential. However, as it was found experimentally, integrated current was not suited to determine roughness factor, since providing values often lower than 1 (physically impossible situation). This effect could be due to the fact that integrated current also included in large part EDL contributions, increasing thus the area below the CV line in the hydrogen desorption region. For this reason, integrated current was used to check EDL values, while normal current to evaluate roughness factor. The procedure has been considered as good only when satisfying both conditions.

Nitrogen was of fundamental relevance for electrochemical polishing. In fact, as previously cited, a step of N_2 bubbling in solution was required. This operation was necessary before every electrochemical polish and should last for a time of more than 10 minutes for each 10 mL of solution. In this work, according to cell dimensions and the need to immerse correctly the three electrodes, 50 mL of 0.5M H_2SO_4 were used. Thus, 1 hour of N_2 bubbling was required.

After this step, nitrogen continued to be important. In fact, as long as mea-

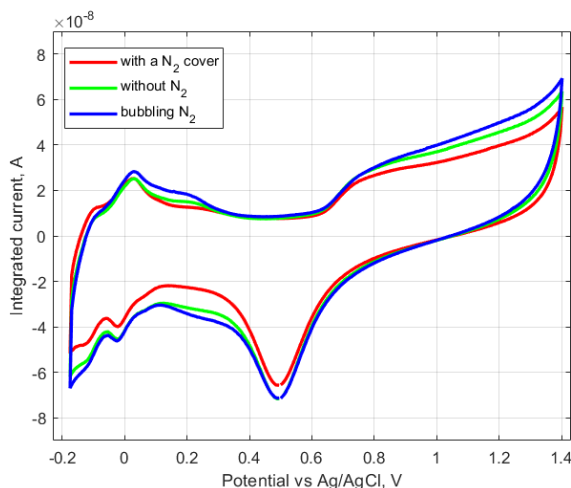


Figure 3.6: Comparison of different conditions during electrochemical polishing.

surements were carried out, the passage of current produced oxygen. This could be removed with the help of a blow of N_2 . However, if bubbling it again in the solution, higher and noisy responses were obtained, due to convective motions in

the solution. For this reason, new solutions were explored. It has been found that keeping a cover of N₂ blowing over the solution worked quite well. The comparison can be seen in figure 3.6.

Finally it must be also said that measurements of electrochemical polishing were performed for many cycles. Stabilization was reached in average after 50 cycles. As convention it was decided to perform 100 cycles, taking data from the 99th. Measurements were performed at 28°C ($\pm 1^\circ\text{C}$).

The procedure defined in this chapter is the one used before every other measurement. From now on, when talking of polishing of electrodes, it will be referred to this procedure. In particular, if not differently and specifically written, the sequence adopted was of one polishing with diamond pad and two with alumina ones.

Chapter 4

Redox mediators

Redox mediators are substances which can undergo reversible oxido-reduction reactions. They offer many advantages like the one of having a tabulated formal potential at which reaction happens. During this work thesis the potassium ferricyanide has been used. This compound has a reversible reaction with potassium ferrocyanide, which involves one electrode. It has the advantage to be widely studied in literature.

In particular, the need of using a redox mediator came from the purpose to determine ion exchange membranes effective working for future use in integrated HS devices. The relation between concentration and diffusion coefficient has been used. Three techniques have been decided to be used for the evaluation. In the following a theoretical introduction on redox mediators and diffusion coefficients will be given. After that, results obtained with cyclic voltammetry, chronoamperometry and impedance spectroscopy will be discussed.

4.1 Diffusion coefficient of $\text{K}_3\text{Fe}(\text{CN})_6$

Diffusion coefficient is a parameter which takes into account the ease of an ion to move in a solution. Better than this first definition it will be to specify that it is only referred to a kind of motion: diffusion.

This is a process for which an entity (ions in this case) moves only due to a gradient of concentration. In fact, as for many other factors, also differences in concentration of a solution represents a non-equilibrium situation.

Diffusion depends both on the element which has to move and on the medium. As already said, this process can be described through a diffusion coefficient, a value with dimensions of $[L^2/t]$. In particular, for this thesis work, the adopted units of measure of the diffusion coefficient were $\frac{\text{cm}^2}{\text{s}}$.

In general, diffusion coefficient depends directly on kinetic energy of moving particle and inversely on its radius and to medium viscosity. This is also provided by Stokes-Einstein relation

$$D = \frac{k_B T}{6\pi r \mu} \quad (4.1)$$

where k_B is the Boltzmann constant, T the temperature, r the particle radius and μ the viscosity of the medium.

Temperature played also an important role in the evaluation of the diffusion coefficient.

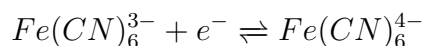
In particular, it has been experimentally seen in literature that an Arrhenius relation seems to well fit this behaviour

$$D = D_0 \cdot \exp\left(-\frac{E_A}{RT}\right) \quad (4.2)$$

It would have been interesting to also see in laboratory this behaviour with temperature. However, due to a lack of time this was not possible. During this work all measurements were performed at room temperature. This implies that no perfect control was possible and little mismatches for different days were possible. The major observation on temperatures is that there were mainly two situations. In fact, all measurements were performed at $25 \pm 1^\circ\text{C}$, except those marked in the following with a blue star *, which were done at $20 \pm 1^\circ\text{C}$.

The reason to determine diffusion coefficient was the possibility to use it to discover concentration of an unknown solution. This method was really simple and useful. It could, however, be used only with redox mediators, according to the need of investigate reversible processes at precise potentials.

The reaction investigated during this work was



In next sections it will be presented how to connect diffusion coefficient to current or impedance with different techniques.

The expected theoretical value of the diffusion coefficient was $7.17 \cdot 10^{-6} \text{cm}^2/\text{s}$, according to [39].

In the following, after having defined and explained the employed setup, the three techniques used will be presented. These methods to define diffusion coefficients of ions in a solution have been widely studied (see [40]) and used in literature. The need to study three different techniques was done in order to find which one was the best, in order to use it for future works. The "best" was here indicating the method which allowed for a larger agreement of results (that technique with the lowest variability of obtained diffusion coefficients).

4.1.1 Setup

The setup used to determine the coefficient diffusion of $\text{K}_3\text{Fe}(\text{CN})_6$ was the same for each of the three methods used.

First of all, the measurements were all performed in a Faraday cage. This allowed to avoid noise from the ambient, which was of noticeable relevance with ranges of currents normally detected. This first observation was a direct effect of using microelectrodes, as previously cited, since currents were directly proportional to electrode radius.

The cell used for measurements was a glass one, with a conical shape. On the top of it a plastic plug, with 5 holes was placed. This support had the function of electrode holder and was tightly fixed on the top of the cell by a mechanism, which avoided sliding of it. The cell was the same used for the electrochemical polishing of microelectrodes.



Figure 4.1: Apparatus used to perform measurements of diffusion coefficient of $\text{K}_3\text{Fe}(\text{CN})_6$.

A glassy N_2 blower was inserted through one of the holes in plug. The importance of this blow will be discussed and analyzed in detail in next sections. Measurements were performed in a three electrode configuration (working, counter and reference).

The working electrodes were the three microelectrodes. Measurements were repeated for all of them, in order to compare values. This comparison allowed to check if some measurement was failed due to electrode surface problems. Moreover it also allowed to find which one was the best. These microelectrodes consisted in a platinum wire fixed in a glass rod. They won't be explained here, since already treated in chapter 3.

Sometimes also a platinum macroelectrode (radius = 1.5mm) was used as working electrode. The reason was to compare differences in working of micro and macro electrodes.

The counter electrode was a simple platinum rod. The reasons of the choice were: a very large surface, to avoid charging effects, a very good conductance of the material and also the low reactivity of platinum.

Finally, the reference electrode was a Ag/AgCl wire immersed in 3M KCl. This reference provided an open circuit potential versus SHE of 197mV. This value was used when comparing with formal potentials. The regenerative solution of this electrode (3M KCl) was changed once a week. This allowed to keep a constant potential and to remove eventual impurities which could have permeated the membrane. Some considerations on reference electrodes will be performed in next chapter, in section 5.4, due to the fact of using different ones.

The electrodes were all connected to the potentiostat/galvanostat, which was a Multi Autolab Cabinet of MetrOhm. The program used on PC to interface with the instrument was Nova 2.1.

A photo of the assembled apparatus inside Faraday cage could be seen in figure 4.1. In order to see effects of different concentration of $K_3Fe(CN)_6$ and of supporting electrolyte, different solutions have been used. In particular, they will be sometimes referred with a number in the following of this work, according to:

- **sol2** : 7.5mM $K_3Fe(CN)_6$ + 0.5M KCl;
- **sol3** : 7.5mM $K_3Fe(CN)_6$ + 0.05M KCl;
- **sol4** : 7.5mM $K_3Fe(CN)_6$ + 0.005M KCl;
- **sol5** : 7.5mM $K_3Fe(CN)_6$;
- **sol6** : 10mM $K_3Fe(CN)_6$ + 0.5M KCl;
- **sol7** : 20mM $K_3Fe(CN)_6$ + 0.5M KCl;

The presence of KCl in the solution was that of supporting electrolyte and its importance will be explained later. In general only charged molecules were affected by the adding of supporting electrolyte. The iR drop, due to low conductive solutions, made profiles of CV to shift towards cathodic potentials.

The solutions were all brought to $\text{pH} = 3$. This was done because at this pH , the salt had its maximum solubility. This condition was reached by adding HCl and verifying it with litmus papers.

4.1.2 Cyclic voltammetry

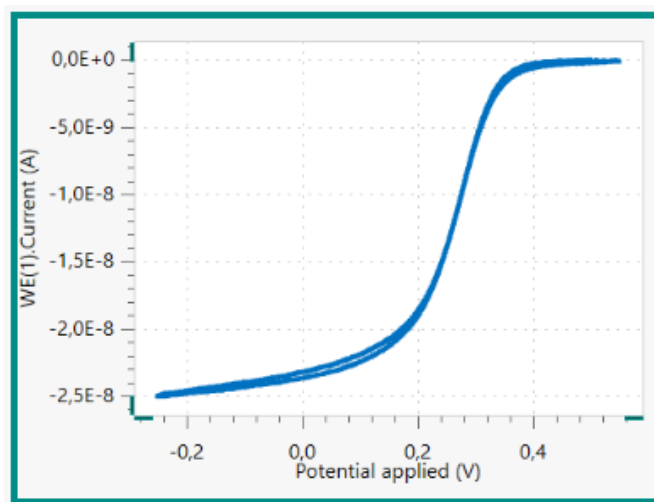


Figure 4.2: Example of cyclic voltammetry for solution 3, recorded with $20\mu\text{m}$ diameter electrode, as seen in Nova 2.1.

The first analyzed method was Cyclic Voltammetry (CV). This technique consisted in imposing a linearly increasing potential signal to the solution and to record how current changed in consequence.

Many similar studies of cyclic voltammetry has been done in the past, for example for triiodide/iodide couple detection in ionic liquids for DSSC like [41], [42], [43], for the study of microelectrodes array [44], for ferrocene and hexacyanoferrate diffusion coefficients in ionic liquids [45] or for different electrodes used in reverse electrolysis [46].

The case considered was the one adopting microelectrodes, which allowed determination of diffusion coefficient (according to [39]) starting from limiting current.

The steps adopted to perform CV were the followings:

- Bubbling N_2 in the solution for 1 hour;
- Polishing of microelectrode;
- Immersion of electrodes and moving up of the N_2 blow;

- Performing cyclic voltammetry at a scan rate of 50mV/s for n^* cycles;
- Performing cyclic voltammetry at a scan rate of 5mV/s for 3 cycles (data were extracted from the last cycle);
- Polishing of microelectrode.

The step of CV at 50mV/s was used to allow to the surface of electrode to stabilize in the solution, in order to get correct data. The number of cycles (n^*) was different depending on the concentration of supporting electrolyte (10, 5, 5 and 0, for concentrations of KCl of 0M, 0.005M, 0.05M and 0.5M).

The cyclic voltammetry consisted in imposing a staircase potential in the window $-0.25V \div +0.55V$. Thanks to the fact that microelectrodes were used, a sigmoidal behaviour appeared (as can be seen in figure 4.2). The plateau at higher currents was the so called limiting current and was proportional to the diffusion coefficient. The transition between the two plateaux happened at the formal potential of the redox mediator.

Limiting current was provided by the formula

$$i_L = 4nDFca \quad (4.3)$$

where n was the number of electrons involved in the reaction (in this case one), D the diffusion coefficient, F the Faraday constant (96 485 As/mol), c the concentration of the redox mediator and a the radius of microelectrode.

By reversing this equation, one could easily get the diffusion coefficient. During the work of this thesis, in order to have a standard procedure for all measurements, the exact value of limiting current has been chosen to be the average of those currents when potential is lower than 90% of minimum used value (-0.25V).

Cyclic voltammetry also offered an immediate and easy way to find if the reaction was reversible or not.

$$E = E_{\frac{1}{2}} + \frac{RT}{nF} \ln \frac{i}{i_L - i} \quad (4.4)$$

In fact, since the relation 4.4 is valid only for reversible reactions, by plotting potential versus $\ln \left(\frac{i}{i_L - i} \right)$, one should observe a linear behaviour (like in figure 4.3).

Moreover, the slope should be equal to 59.2mV, since only one electron was involved in the reaction. This fact has been proved and used to detect between good and wrong measurements. Measurements were considered as valid only when the reaction resulted to be reversible (slope=59±2mV).

Data manipulation has been done with Matlab.

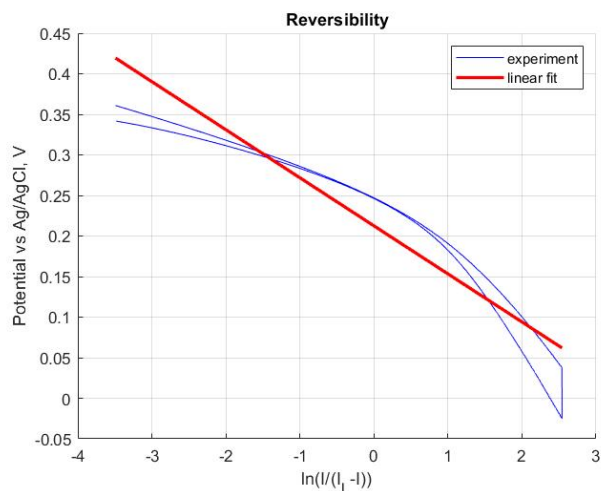


Figure 4.3: Reversibility of reaction in solution 3, recorded with $20\mu\text{m}$ diameter electrode.

4.1.3 CV results

The first quantities to be reported were the limiting currents. These values, in fact, have been taken from the sigmoidal behaviour of cyclic voltammetry profiles. They have been reported in table 4.1 for solutions 2, 3, 4 and 5. From the table it was possible to observe the differences between electrodes with diameter of $10\mu\text{m}$, $20\mu\text{m}$, $50\mu\text{m}$ and 3mm (macroelectrode).

KCl concentration	$10\mu\text{m}$	$20\mu\text{m}$	$50\mu\text{m}$	3mm
0.5M	12.62	26.93	68.71	18 059
0.05M	12.97	27.47	68.83	16 733
0.005M	13.18	26.46	66.76	18 043
0M	9.93	26.07	71.40	19 443

Table 4.1: Limiting current [nA] values, reported versus KCl concentration (solutions 2, 3, 4 and 5). Comparison between the three different microelectrodes and macroelectrode has been presented.

From those values of currents, it was possible to obtain diffusion coefficients for every combination of solution and electrode. The calculus has been done by

reversing equation 4.3. The so-obtained diffusion coefficients have been listed in 4.2.

KCl concentration	10 μm	20 μm	50 μm	3 mm
0.5M	8.72	9.30	9.49	207.98
0.05M	8.96	9.49	9.51	192.70
0.005M	9.10	9.14	9.23	207.79
0M	6.87	9.01	9.87	223.91

Table 4.2: Diffusion coefficients [$10^{-6}\text{cm}^2/\text{s}$] calculated, reported versus KCl concentration (solutions 2, 3, 4 and 5). Comparison between the three different microelectrodes and macroelectrode has been presented.

Some observations on obtained results have been immediately performed. First of all it was clear that great discrepancies were evident between micro and macro electrodes. The diffusion coefficients for macroelectrode were nearly 20 times larger than those for microelectrodes. For this reason one could immediately say that this model didn't work for large electrodes. However, values for 3mm electrode were not so different the one with the other. This meant that a correlation between the recorded currents and diffusion coefficients really existed also for macroelectrodes. However, a different model should have been adopted for it. In particular, the Randles-Sevcik equation, based on peak heights evaluation could be a good idea (see chapter 11 of [32]).

The reason of this difference could be also found in CV plots, where it was immediate the different behaviour. In picture 4.4 the comparison between 10 μm , 20 μm , 50 μm microelectrodes and 3mm macroelectrode has been shown.

The relevant difference in the shape obtained while performing cyclic voltammetry was the presence of peaks. Those peaks, respectively anodic and cathodic ones, were centered at the formal potential of the reaction. In this case the half-wave potentials have been reported after, in table 4.3. From the peaks it was possible to have some information about the reaction. First of all, since as previously stated they were centered at the formal potential, it could have been understood which reaction was happening.

Second and last, also information of concentration of the redox mediator could be extracted. In particular, this quantity was directly proportional to peak height. The presence of peaks was connected to the different distribution of the diffusion layer. This one was not constant for macroelectrodes, as it was instead in microelectrodes or in stirred conditions (see section 3.1).

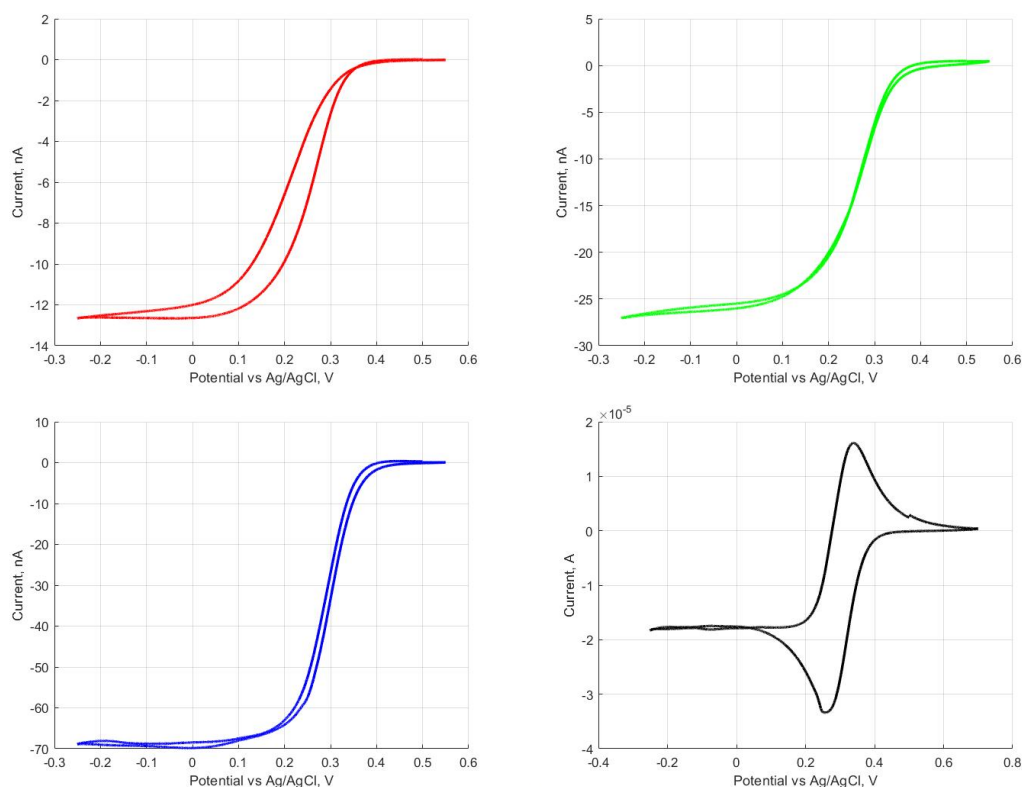


Figure 4.4: Comparison between a) $10\mu\text{m}$, b) $20\mu\text{m}$, c) $50\mu\text{m}$ microelectrodes and d) 3mm macroelectrode, when used to analyze solution 2.

The size of microelectrodes, played instead a role only in the values of current, being it directly proportional to radius. This has been proved and could be seen in figure 4.5. The shape remained the same and only values of limiting current were different. When calculating diffusion coefficient, since dividing current by radius, similar D values were obtained.

One important consideration on results could also be performed. The effect of supporting electrolyte couldn't be neglected. In fact, by looking at table 4.2 one immediately saw that the case with no KCl had the worst agreement of results. It gave a variation of 30.4% (considering only microelectrodes), which was not suitable to define a good procedure.

The value of variation was instead lower in the other three cases (8.11%, 5.78% and 1.4% respectively). Those values were always a little over-estimated, due to an effective area of the $50\mu\text{m}$ electrode, slightly larger than the theoretical one. The presence of KCl, in fact, had the role to:

- increase solution conductivity;

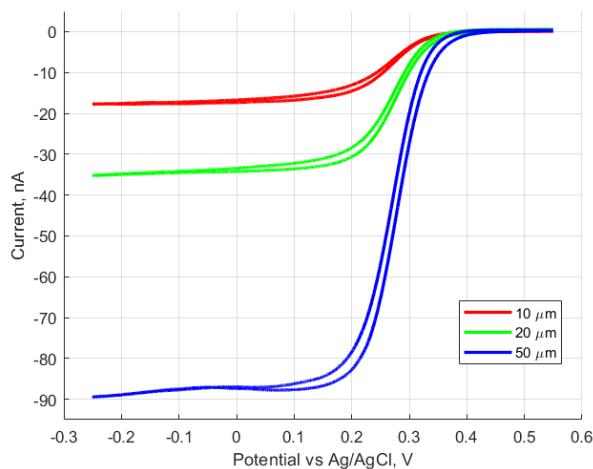


Figure 4.5: Comparison of the results for the three microelectrodes in solution 6 (10mM $K_3Fe(CN)_6$ + 0.5M KCl).

- reduce mass transport from migration (thus maximizing impact on diffusion, which was the one of interest);
- reduce dimension of electrical double layer;
- increase ionic strength, thus facilitating electron kinetic transfer.

Thus, a balancing between too much and too few KCl had to be used, this was also the reason for which no saturated solution was employed.

Low KCl concentrations also lead to slightly lower slope of CVs, since the potential of the reaction started to move toward cathodic potentials due to reduced ionic conductivity.

Furthermore this supporting electrolyte concentration variation provided another really important effect. The time employed by cyclic voltammetry to reach stability increased as long as concentration was reduced. This was taken into account with a modification of the initial procedure, inserting certain CV cycles at higher scan rates (50mV/s) in order to reach equilibrium and then measurements have been done.

An idea of the effect of KCl on cyclic voltammetry could be given by looking at plots of figure 4.6.

The major implication of using more cycles to stabilize, apart from taking more time, had one intrinsic problem. As long as the measurement was performed a sort of gel of $K_3Fe(CN)_6$ was formed over the electrode surface. This obviously provided a reduction of recorded currents, thus to an underestimation of diffusion coefficients. The smallest microelectrode has been found to be the one to suffer

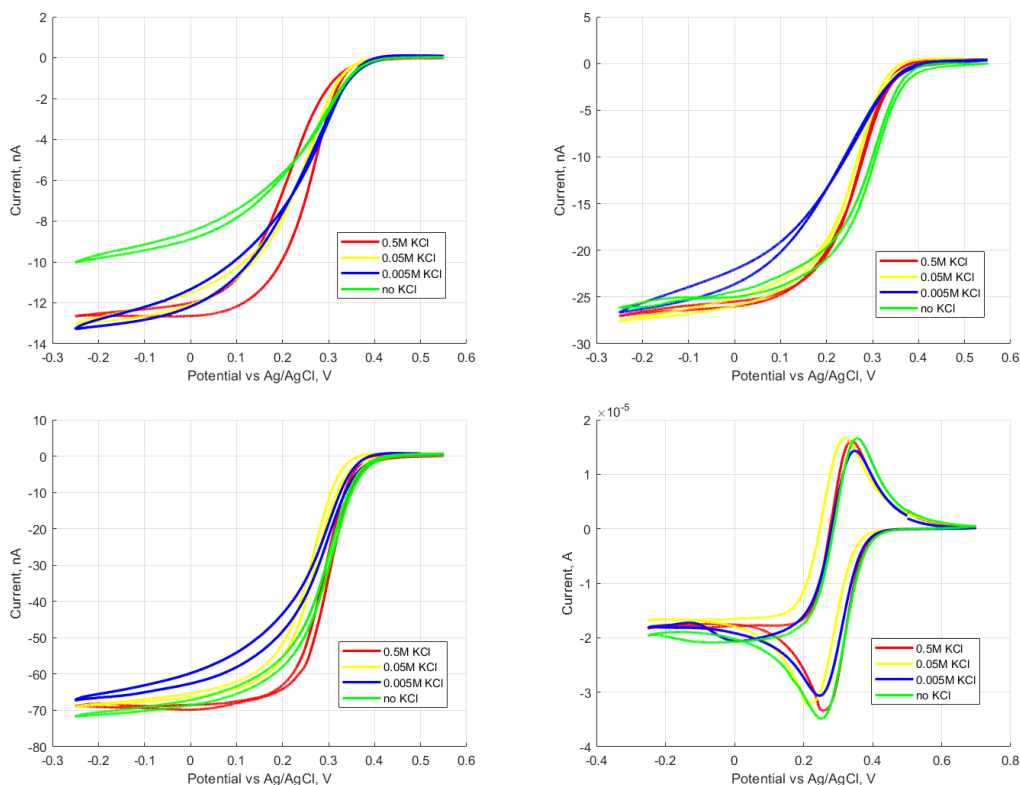


Figure 4.6: Effect of KCl variation on the $10\mu\text{m}$, $20\mu\text{m}$, $50\mu\text{m}$ and 3mm electrodes.

the most of this effect.

In figure 4.7, it has been reported the case of CV in solution 5 (no KCl) with the smallest microelectrode compared to the same electrode in solution 2 (0.5M KCl). The first immediate observation was the need to perform more cycles, in order to reach the correct behaviour and results closer to the expected ones.

Moreover it was necessary to mention that the real value, which was expected, was never reached because the born of the gelation, reduced limiting current.

In figure 4.8 it has been also shown the importance of stabilization even for a larger electrode ($20\mu\text{m}$ of diameter). As it could be seen from these two plots, without stabilization it wasn't obtained the correct sigmoidal behaviour. In particular, the plateau at the limiting current was not present and substituted with a slowly decreasing ramp.

Some words must be still spent about the scan rate used for the measurements. This parameter, in principle, didn't explicitly appear in the equation of the limiting current or in the one of diffusion coefficient, so at a first glance it could seem to be not relevant. However, this was not what was observed. In fact, it seemed to play a fundamental role. The reason of the importance of it was that increasing

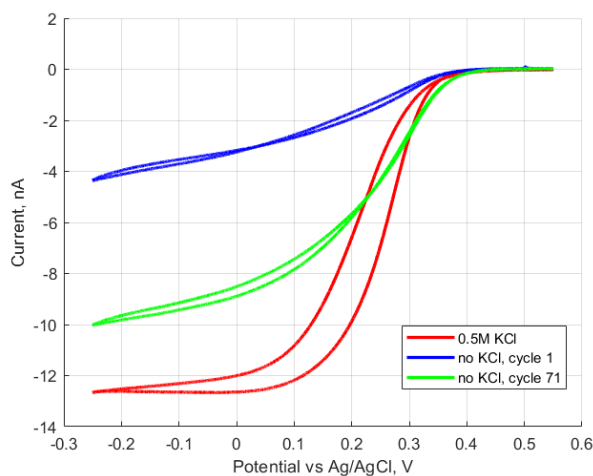


Figure 4.7: Comparison between 1st and 71st cycles in solution 5 (no KCl) and solution 2 (0.5M KCl), with 10 μ m microelectrode.

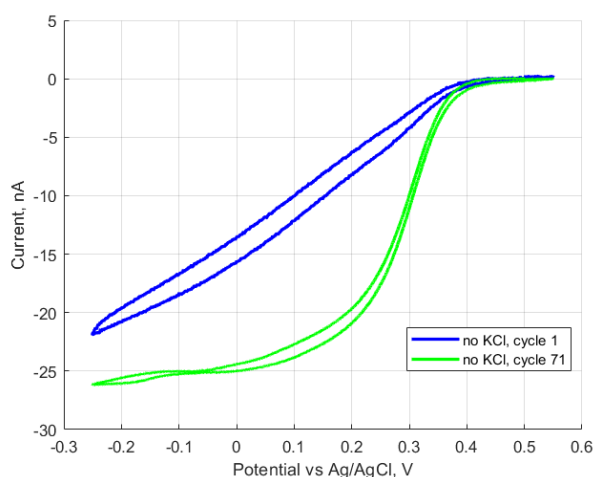


Figure 4.8: Effect of performing many cycles in a solution without supporting electrolyte for 20 μ m microelectrode.

the scan rate provided the diffusion layer to be no more constant. In this way, the diffusion profile passed from hemispherical to planar, due to the passage from the steady state condition to the Cottrell region.

This effect was reflected back in the behaviour of current versus potential of the CV. The most important and immediately visible consideration was on the appearance of two separate peaks and in the opening of an area between the currents of anodic and cathodic reactions.

The effect of various scan rates on the experiment could be seen in figure 4.9. Macroelectrode seemed to have the most dramatic change.

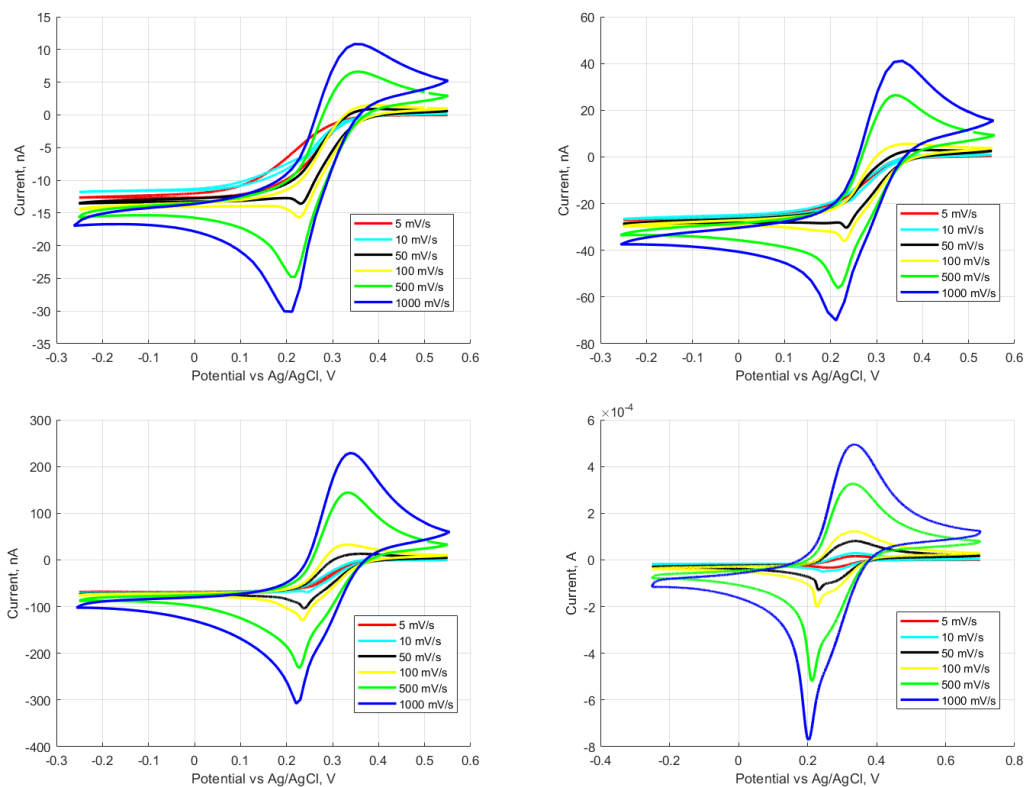


Figure 4.9: Effect of different scan rates on the $10\mu\text{m}$, $20\mu\text{m}$, $50\mu\text{m}$ and 3mm electrodes, in solution 2.

Then, as long as electrode diameter was reduced, the effect of scan rate was gradually less important. The reason was quite obvious.

As long as microelectrode dimensions were reduced, the time to reach steady state was also reduced as r_e^2 . This provided that smallest microelectrode could work in steady state conditions also for higher scan rates. In fact, as could be seen in figure 4.9, only for scan rates higher than $\nu=100\text{mV/s}$, distortions of the sigmoidal behaviour started to appear. Differently, the largest microelectrode showed appreciable deformations also for $\nu=50\text{mV/s}$.

Starting from this observation on scan rates, it has been possible to say that macroelectrodes were largely affected by variation of it, while for microelectrodes this was less marked and reduction in diameter helped in keeping good insensibility to scan rate.

However, the combination of different scan rates and variation of supporting electrolyte could have new effects. The most relevant result, showed in figure 4.10,

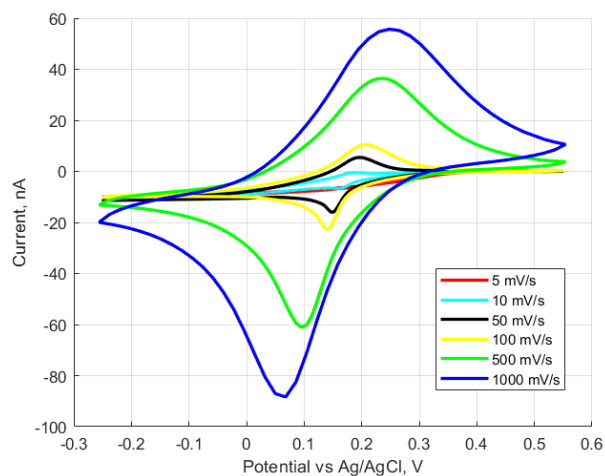


Figure 4.10: Effect of different scan rate on smallest microelectrode ($10\ \mu\text{m}$) in solution 5 (no supporting electrolyte).

was that with low KCl concentrations (or not at all), dramatic effects of scan rate could be observed also for the smallest microelectrode.

This could be probably imputed to the stabilization time required and to the lower ionic conductivity of the solution. In fact, the solution could be modeled as a resistance in parallel to a capacitance. If the value of resistance increased (e.g. reducing supporting electrolyte), the time constant ($\tau = R \cdot C$) also increased. This would have led to a slower response time and to an hemispherical-like diffusion behaviour.

It has been obvious, thus, that the effect of scan rate for macroelectrode in low

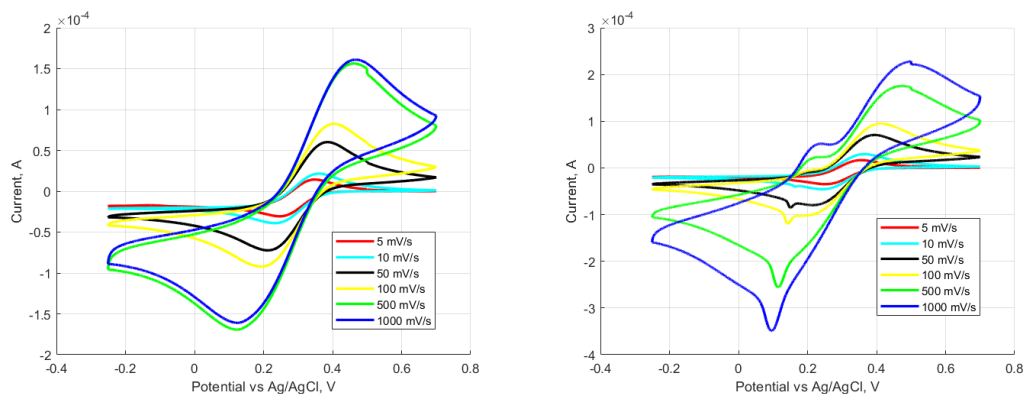


Figure 4.11: Effect of scan rate on measurements when using 3mm macroelectrode. CV obtained in solutions with a) 0.005M KCl, b) no KCl.

concentrated solutions was dramatically incident on results (see figure 4.11). In the case of solution 5 it was also possible to see the effect of oxygen impurity (like the one described in the following). In fact, by using higher currents, also O_2 formation was improved.

During measurements, a strange behaviour has been observed for solution 5 when using smallest microelectrode. Two peaks, respectively in cathodic and anodic oriented path, appeared in the sigmoidal behaviour of the cyclic voltammetry. They were centered to a potential of 0.18V vs. Ag/AgCl. Due to the double and symmetrical nature of those two peaks, they were supposed to be originated from a redox reversible reaction (ORR due to oxygen dissolved in solution).

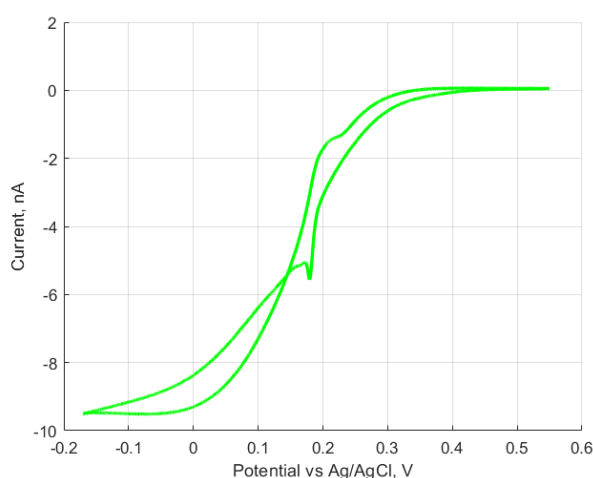
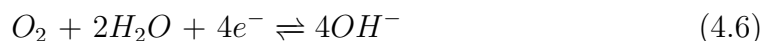


Figure 4.12: CV plot obtained in solution 5, with smallest microelectrode. A double peak could be observed, due to an impurity in the solution.

According to Randles-Sevcik equation

$$i_p = (2.69 \cdot 10^5) n^{\frac{3}{2}} F^{\frac{3}{2}} A D^{\frac{1}{2}} \nu^{\frac{1}{2}} c \quad (4.5)$$

(D of oxygen in water was $2.42 \cdot 10^{-5} cm^2/s$) and the possible reaction, which was found in table 18.1 of [32]:



the concentration of oxygen in solution was of 0.95nM. The impurity was, thus, oxygen. This problem was known and it was the reason for which bubbling of nitrogen before measurements was necessary. In the found case, probably this step was not sufficient to remove all O_2 from solution (maybe many experiments have

been conducted before and the usual procedure was not sufficient to clean the solution). The problem have been easily solved by bubbling N_2 for another hour. After that, everything returned to the expected behaviour. The effect of impurity on CV has been represented in figure 4.12.

In order to solve this problem, one could taught why bubbling of nitrogen was

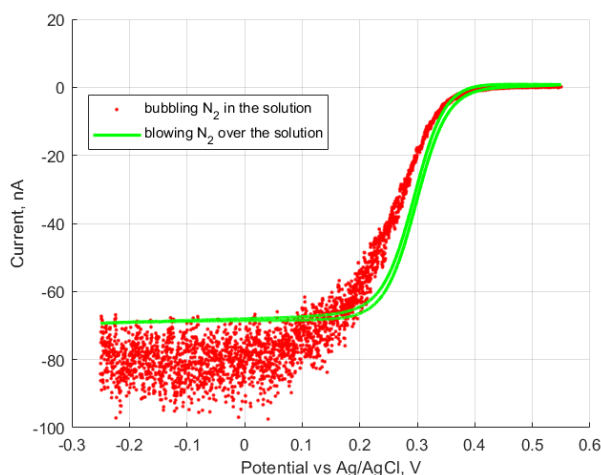


Figure 4.13: Effect of bubbling N_2 in the solution while performing cyclic voltammetry. It could be observed an increase in limiting current and the introduction of noise.

performed only before measurements and not also during. In fact, while measurements were running only a N_2 cover was maintained over the solution. The reason was simple and could be seen in figure 4.13.

The presence of continuous bubbling in solution, produced convection, thus the mass transport was no longer diffusion controlled. Formulas used up to now only considered the diffusion limited region and could not take into account convective contributions. This would have produced, unavoidably, to variations of limiting currents recorded and thus also of calculated diffusion coefficients. Furthermore also a lot of noise was introduced in the signal, thus making all measurement to be more complicated to be manipulated.

Thanks to equation 4.4, it has been also possible to calculate the half-wave potential ($E_{\frac{1}{2}}$). For definition the $E_{\frac{1}{2}}$ was the potential when the current was equal to half of the limiting one. For reversible reactions, like the one analyzed in this work, the half-wave potential was equal to the formal potential. This was the value of potential at which the reaction was happening.

In table 4.3 values of half-wave potential, calculated by reversing eq. 4.4, have been reported.

$E_{\frac{1}{2}} [mV]$	10 μm	20 μm	50 μm	3 mm
0.5M	220.30	229.75	271.65	224.15
0.05M	209.89	213.97	203.50	210.53
0.005M	219.27	201.03	218.48	204.49
0M	185.23	247.12	235.81	207.41

Table 4.3: Half-wave potentials calculated, reported versus KCl concentration (solutions 2, 3, 4 and 5). Comparison between the three different microelectrodes and macroelectrode has been presented.

By comparing all these values, the average one which was calculated was $E_{\frac{1}{2}} = 218.91$. All cases agreed quite well, except those with no supporting electrolyte (especially the smallest microelectrode as previously mentioned) and the 50 μm microelectrode in solution 2. Interestingly, also good agreement was obtained with the 3mm macroelectrode, thus equation 4.4 seemed to work also for it.

The obtained value was reported to pH=0 and then referred to SHE potential (as previously done in the case of impurity in solution 4). The formal potential obtained after those passages was: $E_0 = 0.356V$. This value agreed quite well with the theoretical one reported in [32] ($E_0 = 0.361V$).

Due to the found problem of gelation for long measurements in solutions with low KCl concentrations, two long time analyses have also been done. In the next experiments, those used to characterize ion exchange membranes, solutions with 0.5M KCl concentrations will be used (according to found better behaviour). For this reason, long time measurements have been performed in those kind of solutions. In fact, using low concentrated solutions would have only produced too much underestimated results, not useful for the purpose of this thesis work.

Two cases were considered. First of all, the microelectrode with diameter 20 μm was tested in solution 2 (7.5mM $\text{K}_3\text{Fe}(\text{CN})_6$ + 0.5M KCl). The measurement has been run for 3 hours (40 cycles at scan rate of 5mV/s).

The second case analyzed was under more severe conditions. The smallest microelectrode (10 μm of diameter) was checked. The smallest microelectrode was probably the one which suffered the most of any effect connected to large times of measurement. Moreover it was also the electrode which showed the largest problem of gelation.

10 μm microelectrode was analyzed in solution 7 (20mM $\text{K}_3\text{Fe}(\text{CN})_6$ + 0.5M KCl). The experiment was carried out for 7.5 hours (60 cycles).

Results of both experiments have been shown in figure 4.14. The first experiment

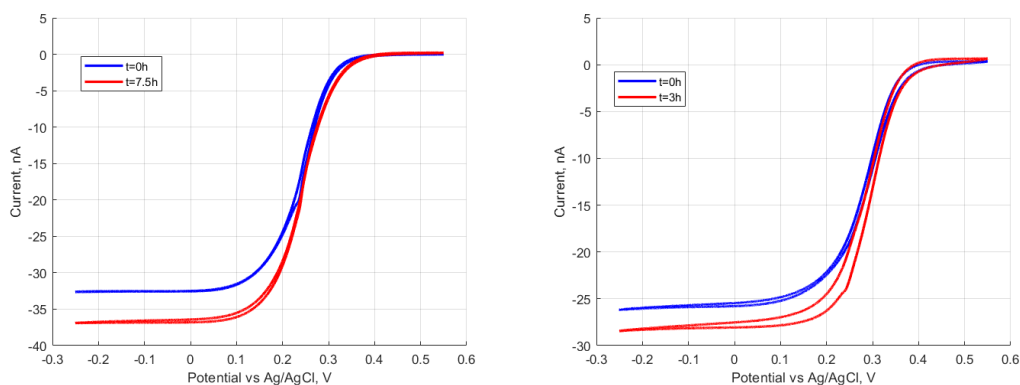


Figure 4.14: Results of measurements performed for: **a)** $10\mu\text{m}$ microelectrode in solution 7 for 7.5h and **b)** $20\mu\text{m}$ microelectrode in solution 2 for 3h.

($20\mu\text{m}$ microelectrode in solution 2 for 3h) lead to a limiting current in final cycle equal to 108% of the initial one. The second experiment ($10\mu\text{m}$ microelectrode in solution 7 for 7.5h) instead had a limiting current in the last cycle equal to 112% to the initial one.

The increase of limiting current with time was quite counter-intuitive, in fact, due to the effect of gelation, lower values would have been expected. However, it was possible that thanks to the presence of KCl in high concentration, gelation was avoided. According to this, long number of cycles for surface stabilization were necessary only for low KCl concentrations.

The increase in current was probably due to the oxygen evolution with time and to deposition of salt crystals on the electrode surface, increasing thus electroactive area. This would have added a further contribution to limiting current value. The growth of value was proportionally constant with time for both the experiments (around 2.67% more every hour).

This effect should be taken into account if measurements will be carried out for long times. The importance of this evaluation was also connected to the fact that measurements performed in characterizing ion exchange membranes were all performed without the N_2 bubbling pretreatment, due to the shape of used cell.

4.1.4 Chronoamperometry

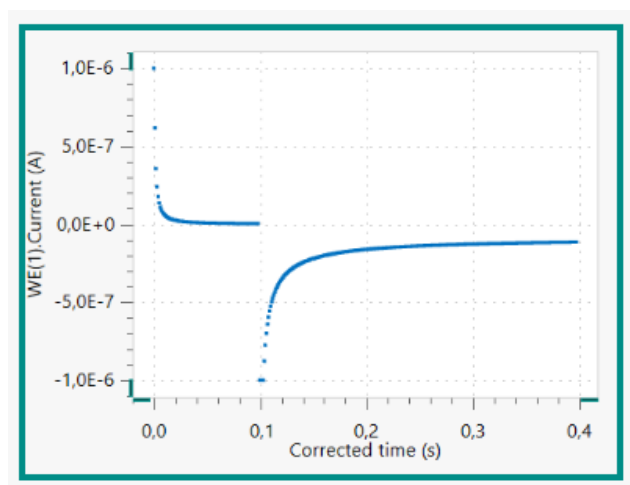


Figure 4.15: Example of chronoamperometry for solution 3, recorded with $10\mu\text{m}$ diameter electrode, as seen in Nova 2.1.

ChronoAmperometry (CA) was the second technique used to investigate diffusion coefficient of the $\text{K}_3\text{Fe}(\text{CN})_6$ solutions [39], [47], [48] and [49].

This methodology had the advantage to be really faster than cyclic voltammetry. Less than a second was employed. This was again an advantage connected to little electrode dimensions.

The procedure employed for CA analysis was:

- Bubbling N_2 in the solution for 30 minutes;
- Polishing of microelectrode;
- Immersion of electrodes and moving up of the N_2 blow;
- Performing direct chronoamperometry;
- Performing reverse chronoamperometry;
- Polishing of microelectrode.

As previously said for CV, N_2 bubbling was necessary to reduce oxygen impurities. With this technique, since really quicker, times to wait between different experiment (when blowing N_2) were reduced to 30 minutes.

The polishing procedure was the one described in chapter 3.

Chronoamperometry consisted in applying two step of potential, while recording

current. The first potential was 0.5V, at the theoretical open circuit potential and it was held for 0.1s. The second one, instead was -0.22V, where the limiting current was observed and it was kept constant for 0.3s.

A double decreasing behaviour was observed. This two decreasing curves represented Cottrell contribution of current. From a physical point of view, this fact could be described as the charge of the electric double layer formed at interface of electrodes with solution. By analysing this curve one could connect again current to diffusion coefficient. The complete description of current in chronoamperometry experiments was:

$$i = \left(\frac{8}{\pi^2} \right) \frac{nFAc\sqrt{D}}{\sqrt{\pi t}} + 4nDfa \quad (4.7)$$

where A was the area of electrode surface and c the concentration of analyte.

The second term, as could be easily seen, was the same used for cyclic voltammetry, being the limiting current. For large times, in fact, all contributions from capacitive effects vanished and so what remained was the faradaic part alone.

In chronoamperometry, however, it was of more interest the first part. This one, with the decreasing behaviour, was strongly time dependent. In particular, a relation $i \propto t^{-\frac{1}{2}}$ held. This relation could also be checked in order to see if the reaction was reversible. During this work, it has also been done and an example has been shown in figure 4.16.

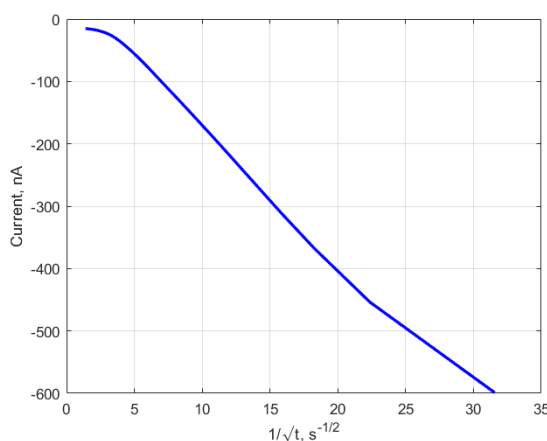


Figure 4.16: The linear behaviour of current with respect to the inverse of square root of time. The case was solution 2, analyzed with $10\mu\text{m}$ diameter electrode.

From the Cottrell term it was also possible to connect current to diffusion coefficient. By reversing the equation it was possible to calculate D . Results will

be shown in next section.

After having performed this type of chronoamperometry, which was called "direct", also the "reverse" one was done. In reverse chronoamperometry the two steps of potential were changed in order. In this way it was firstly applied -0.22V for 0.3s and then 0.5V for 0.3s. From this reversed sequence it was possible to compare results for normal reaction (reduction) with the opposite one (oxidation). Also results for this methodology will be reported and discussed.

4.1.5 CA results

The diffusion coefficients obtained from chronoamperometry were calculated by using eq. 4.7. The results have been shown and summarized in table 4.4.

KCl concentration	10 μm	20 μm	50 μm	3 mm
0.5M	323.10	32.51	17.14	14.41
0.05M	17.45	22.40	15.83	11.58
0.005M	52.38	11.72	40.70	17.25
0M	548.89	623.76	23.15	23.92

Table 4.4: Diffusion coefficients [$10^{-6}\text{cm}^2/\text{s}$] of $\text{K}_3\text{Fe}(\text{CN})_6$ obtained from chronoamperometry by using Cottrell equation.

The first thing which was possible to note from table 4.4, was that this method was not a good one in order to determine the diffusion coefficient. Results, in fact were widely in disagreement the one with the other and moreover, no one of them was similar to the theoretical one, or with the one obtained from cyclic voltammetry.

In particular, it seemed that the diffusion coefficient has been overestimated for each case. The fit has been done on Matlab, by reversing eq. 4.7. The agreement of fits seemed good for every plot, however the proportionality with the diffusion coefficient was not respected. The relation current versus reverse of the square root of time, anyway, has been verified (see figure 4.16).

The quality of results could be slightly improved by considering only current values after 100 ms (as suggested by [39]). The reason was that since in the first times of measure current varied very rapidly with time, it was possible that little mismatches occurred. The improved results have been reported in table 4.5.

KCl concentration	10 μm	20 μm	50 μm	3 mm
0.5M	58.83	28.15	13.76	13.45
0.05M	11.80	21.59	12.46	11.35
0.005M	8.19	10.18	6.13	17.97
0M	81.17	110.28	18.39	22.61

Table 4.5: Diffusion coefficients [$10^{-6}\text{cm}^2/\text{s}$] of $\text{K}_3\text{Fe}(\text{CN})_6$ obtained from chronoamperometry by using Cottrell equation with corrections.

Anyway, even with corrections, values didn't have a large and good consistence. A new and better model should be thus adopted.

The Shoup-Szabo one has been chosen. It consisted in a new and more complete model. In fact, it considered the whole behaviour of current, by didn't having a distinction between the two current regions depending on time. The equation [50] was thus valid in general and with the form:

$$i = 4nFDcr \cdot \left(0.7854 + 0.4431\tau^{-\frac{1}{2}} + 0.2146\exp(-0.7823\tau^{-\frac{1}{2}})\right) \quad (4.8)$$

where τ was a corrected time and was calculated as

$$\tau = \frac{Dt}{r^2} \quad (4.9)$$

This new equation has been used to fit data obtained from chronoamperometry. Values of diffusion coefficient have been reported in table 4.6. One note should be made: in the equation τ has been calculated using diffusion coefficients obtained from cyclic voltammetry. Better results would have been obtained by using proper iterative methods.

KCl concentration	10 μm	20 μm	50 μm	3 mm
0.5M	7.28	4.07	5.79	9.09
0.05M	2.34	3.88	5.58	7.93
0.005M	2.51	2.87	7.14	8.47
0M	7.56	20.12	6.74	11.72

Table 4.6: Diffusion coefficients [$10^{-6}\text{cm}^2/\text{s}$] of $\text{K}_3\text{Fe}(\text{CN})_6$ obtained from chronoamperometry by using Shoup-Szabo equation.

Results obtained with the new model seemed to be quite better. In fact, the order of magnitude was correct. However, great discrepancies between different measurements were still encountered. In general, it was observed that the values obtained with this technique were underestimating real ones. Interestingly, the macroelectrode seemed to behave better with this model, giving diffusion coefficient more similar to the real ones.

Results could have been improved by using a correct iterative way of calculation, by inserting diffusion coefficients in the formula of τ and by considering values of current after 100ms, in order to avoid strange values due to the rapid variation of current [39]. Diffusion coefficients obtained with these corrections have been shown in table 4.7.

KCl concentration	10 μm	20 μm	50 μm	3 mm
0.5M	9.91	9.36	8.37	8.87
0.05M	7.90	8.97	8.07	7.82
0.005M	5.46	7.59	7.33	10.24
0M	6.15	13.40	9.33	13.01

Table 4.7: Diffusion coefficients [$10^{-6}\text{cm}^2/\text{s}$] of $\text{K}_3\text{Fe}(\text{CN})_6$ obtained from chronoamperometry by using Shoup-Szabo equation with corrected calculations.

By using the corrections, it was possible to improve the quality of results. Values found in this way were more similar to those obtained in cyclic voltammetry. In general they were also quite consistent and in agreement the one with the other (apart for the case 20 μm microelectrode in solution 5).

As for every method used up to now, the solution 5 was the one with the largest variability, due to reduced stabilization. The reduced values of diffusion coefficients obtained when working with low concentrations of supporting electrolyte could be connected with the low ionic conductance, which in turn reduced values of recorded currents.

When using corrections a quite strange effect arose, the macroelectrode reduced its confidence, due to the fact that this model was developed mainly to work with very small electrodes.

The mean value of diffusion coefficient for microelectrodes was of $9.21 \cdot 10^{-6}\text{cm}^2/\text{s}$ when considering only solution 2 (the most accurate one) and of $8.40 \cdot 10^{-6}\text{cm}^2/\text{s}$ in general (excluding microelectrode with diameter 20 μm in solution 5, which was too different from the others).

A further proof that this approximation was better than the one made by using Cottrell equation, could be seen in figure 4.17.

Anyway, although the verified improvement in using this approach, also with the

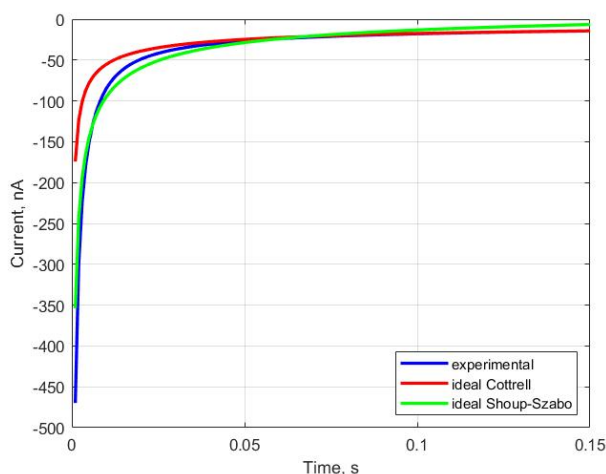


Figure 4.17: Comparison of current fits with Cottrell equation and Shoup-Szabo one. measurement performed with 20 μm microelectrode in solution 2.

corrections, this method was not satisfactory enough. For this reason, chronoamperometry has not been chosen as a candidate to determine the diffusion coefficient of $\text{K}_3\text{Fe}(\text{CN})_6$.

For sake of completeness, chronoamperometries for every experiment were also performed in reverse mode. This implied to perform the measurements by inverting the two steps of potential. In this way, the diffusion coefficient examined was the one of $\text{K}_4\text{Fe}(\text{CN})_6$. Values have been reported in 4.8.

According to the previously found better consistence of Shoup-Szabo results with respect to Cottrell ones, values in reverse mode were calculated with the best method only.

KCl concentration	10 μm	20 μm	50 μm	3 mm
0.5M	6.96	7.19	8.49	0.45
0.05M	5.62	1.22	1.75	1.66
0.005M	1.90	1.10	5.07	0.85
0M	4.91	8.40	9.52	1.80

Table 4.8: Diffusion coefficients [$10^{-6}\text{cm}^2/\text{s}$] of $\text{K}_4\text{Fe}(\text{CN})_6$ obtained from chronoamperometry in reverse mode, by using Shoup-Szabo equation with corrections.

Interestingly the variability of results in this mode seemed to be increased. Again, a great consistency was not present, so values obtained in this way should not be considered.

Anyway, an observation could still be made: reverse values of diffusion coefficients were generally lower than the direct ones, implying a lower mobility of $\text{K}_4\text{Fe}(\text{CN})_6$. A simple and new idea has been proposed and here reported.

Chronoamperometry could be used to register limiting current values. In this way, the time varying part had no more meaning and only the steady state one had. Starting from limiting currents, the same equation used in cyclic voltammetry could be used.

Values of currents obtained in this way have been reported in table 4.9 and respective diffusion coefficients in table 4.10.

KCl concentration	10 μm	20 μm	50 μm	3 mm
0.5M	12.78	26.57	65.28	15 528
0.05M	10.19	20.99*	62.63	14 102
0.005M	9.97*	20.07*	56.90*	12 538*

Table 4.9: Limiting current [nA] values obtained from chronoamperometry for 2 minutes, reported versus KCl concentration (solutions 2, 3, 4 and 5). Comparison between the three different microelectrodes and macroelectrode has been presented.

KCl concentration	10 μm	20 μm	50 μm	3 mm
0.5M	8.83	9.18	9.02	35.76
0.05M	8.47	7.25*	8.65	32.48
0.005M	6.89*	6.93*	7.86*	28.88*

Table 4.10: Diffusion coefficients [$10^{-6}\text{cm}^2/\text{s}$] of $\text{K}_3\text{Fe}(\text{CN})_6$ obtained from chronoamperometry, evaluating limiting current (values of table 4.9)

Results obtained with this method seemed to be quite good. In fact a good level of agreement has been reached between different measurements.

Before analyzing data, however, a little note had to be reminded. Since it wasn't possible to control the temperature in the laboratory, some changes has occurred. A reduction in temperature seemed to be significant for data handling. For this reason a choice has been done. Values obtained in the first part were all collected at higher temperatures, while seconds at around 20°C . This lasts were marked with a blue star.

The mean value of diffusion coefficient calculated at 25°C was $8.83 \cdot 10^{-6}\text{cm}^2/\text{s}$, while at low temperature it was $7.23 \cdot 10^{-6}\text{cm}^2/\text{s}$. However, by simply recording laboratory temperature and deciding which of the two values to use, would simply solve the problem.

Those two values were lower than those get from cyclic voltammetry. A possible reason could be that, since low times were required, also less oxygen contributions were present. According to this lower values of current were recorded.

Anyway, they seemed to be consisted and the idea resulted to be quite good, offering an easy and fast way to determine diffusion coefficients. One limitation was offered by the fact it was not possible or easy to determine if currents were recorded exactly on the limiting one plateaux. This method could be used as a fast and good solution to check and verify measurements obtained from different techniques.

4.1.6 Impedance spectroscopy

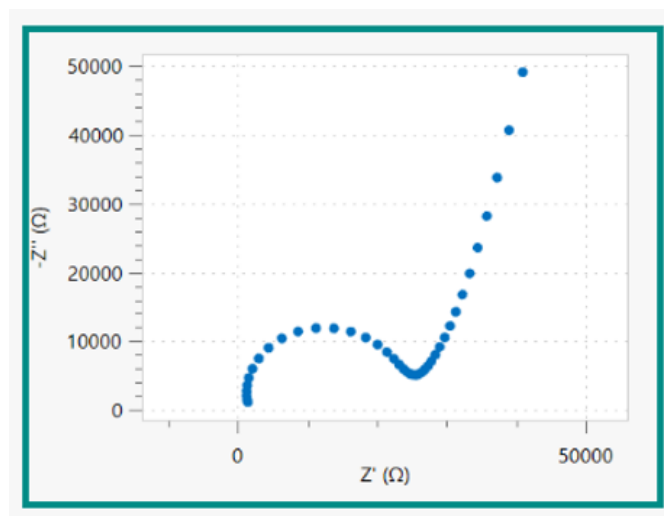


Figure 4.18: Example of impedance spectroscopy for solution 2, recorded with 20 μm diameter electrode. Nyquist plot as seen in Nova 2.1.

An impedance spectroscopy has been used in this work. In particular, a frequency response analysis (FRA) have been chosen.

This technique consisted in imposing a constant bias voltage, with superimposed an AC signal with lower modulus. The response in current will also be a constant current with superimposed an AC one. By considering the ratio of voltage and current, it was possible to have the impedance for every frequency.

What was obtained was the Nyquist plot, like the one presented in figure 4.18. This plot had on x axis the real component of impedance (resistance) and on the y axis, minus the imaginary component. The general behaviour was similar to the one of previous picture: a part similar to a semicircle at high frequency and a linear rapidly increasing one at low frequency. From this plot many parameters could be extracted, like equivalent series resistance and capacitance of the double layer. However, according to the purpose of this thesis work, the Warburg element was computed.

This component could be used to determine the diffusion coefficient [51], [52], [53] and [54].

Another plot of usefulness which could be extracted by a FRA measurement was the Bode one, where modulus and phase of impedance were reported versus frequency. Bode plot of 4.18 was reported in 4.19. This kind of plot has been also useful to better find Warburg element.

This parameter was represented by a constant phase element, with a phase of 45° ,

meaning that real and imaginary parts of impedance grew in the same way. During experiments it was possible to detect Warburg impedance. This value had the advantage to be connected to diffusion coefficient through the relation:

$$Z_W = \frac{A_W}{\sqrt{\omega}} + \frac{A_W}{j\sqrt{\omega}} \quad (4.10)$$

where $\omega = 2\pi f$ represented frequency effect, j was the imaginary coefficient and A_W was the Warburg constant. This last could be computed as:

$$A_W = \frac{RT}{AF^2n^2c\sqrt{2D}} \quad (4.11)$$

By taking the impedance at the frequency for which phase had a constant maximum, it was possible to get Z_W . Then, by reversing equations 4.10 and 4.11, the diffusion coefficient was calculated.

The DC voltage at which measurements were performed was equal to the formal potential of the redox reaction of the couple $K_3Fe(CN)_6 \rightleftharpoons K_4Fe(CN)_6$. The reason was to work where the reaction was more reversible and it will be better explained in next section. A comparison between measurements with different bias voltage will also be presented.

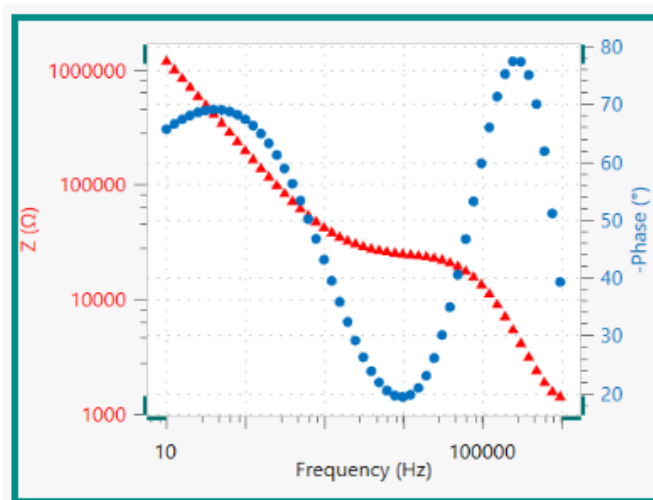


Figure 4.19: Example of impedance spectroscopy for solution 2, recorded with $20\mu\text{m}$ diameter electrode. Bode plot as seen in Nova 2.1.

Lissajous plot has also been used to check the right current range, in order to improve measurement results.

4.1.7 FRA results

The first important aspect, when dealing with impedance spectroscopy, was to perform the measurement at the right potential. In fact, as it was found, this one had a large effect on the shape of the Nyquist plot obtained and thus, in turn, also on the diffusion coefficient calculated from the impedance value. In figure 4.20, it is shown the effect of different bias voltage applied during the measurements.

As one could easily see, the effect was really dramatic, leading to really high

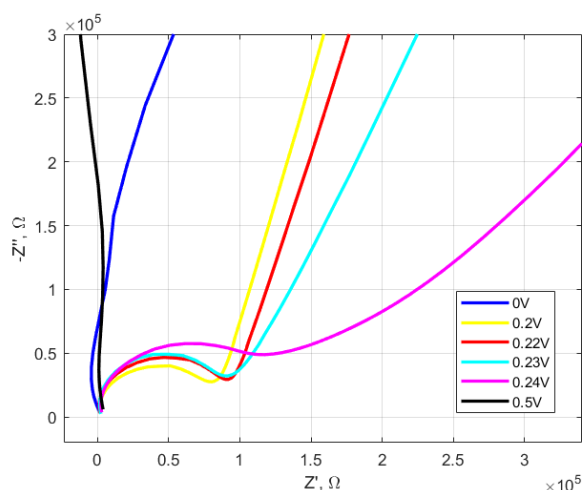


Figure 4.20: Comparison of FRA results when using different bias voltage. Solution 2 analyzed with 10 μm microelectrode.

results variations. The good choice was found to be at 220mV, the potential at which the reaction happened and where it was found that the behaviour of CV was the most linear. According to this, all measurements reported for FRA technique have been performed using this bias potential.

In table 4.11 the diffusion coefficients, calculated by reversing equations 4.10 and 4.11, have been reported.

KCl concentration	10 μm	20 μm	50 μm	3 mm
0.5M	8.73	8.34	2.54	$4.6 \cdot 10^{-5}$
0.05M	3.06*	5.91*	1.79*	$3.6 \cdot 10^{-5*}$
0.005M	0.75*	1.42*	7.11*	$5.7 \cdot 10^{-5*}$

Table 4.11: Diffusion coefficients [$10^{-6} \text{cm}^2/\text{s}$] of $\text{K}_3\text{Fe}(\text{CN})_6$ obtained from electrochemical impedance spectroscopy. *The blue star * represents again measurements performed at lower temperatures.*

The first thing that one could immediately see, it was that the model was certainly not suited for macroelectrodes, giving results wrong of 5 orders of magnitude. Microelectrodes, instead suffered of large variability, even if keeping the correct order of magnitude. It was interesting to observe that every result was underestimating the expectations.

The reason of the possible mismatches in values was found. It was due to the fact that microelectrodes provided regions with constant phase (those were Warburg element should have been computed) which were really narrow. For this reason, even small variations of the analyzed frequency lead to great discrepancies.

It was possible to adjust data manually, by looking at the right frequency case by case and comparing values obtained from Warburg. However, since the final goal was to define a procedure to determine an unknown concentration, it has been decided to adopt a common procedure. It consisted in the use of the Matlab software to found frequencies for which the derivative of phase was zero (regions of maximums or minimums).

By having this procedure, it was possible to have a standard method, even if results were not really consistent. A graphical explanation of the error reason has been shown in figure 4.21. In this plot, the phase vs frequency has been reported with an orange line. A blue dashed line represented the theoretical diffusion coefficient value (that obtained from CV). Finally, blue circles corresponded to the diffusion coefficients calculated at every sampled frequency, as they were in a constant phase region.

As it could be seen in the figure, the constant phase region at high frequency was really narrow, but it was placed in region which gave values in the correspondence of the true value of diffusion coefficient. The case reported was that of 10 μm microelectrode in solution 2, which showed the best agreement. Interestingly, not only the phase maximum at high frequency lead to correct diffusion coefficients, but also the minimum and maximum at lower ones.

For this reason, it has been decided that, even if the method was correct, it was

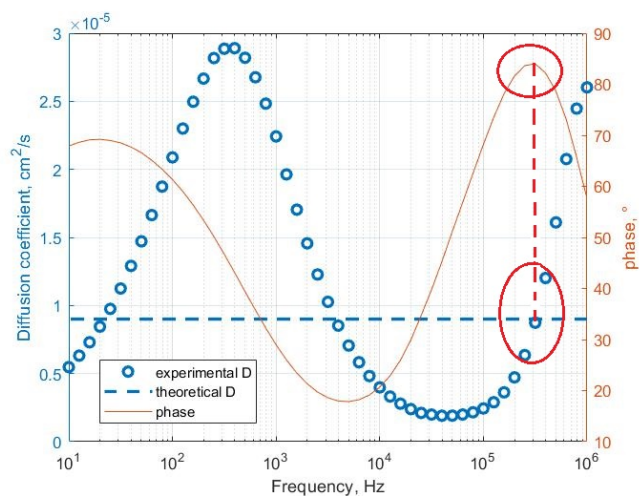


Figure 4.21: Graphical explanation of why the EIS method didn't offer a good solution to evaluate diffusion coefficient. The coefficient has been calculated for every frequency, but the correct value is in the phase constant regions alone. Small errors on frequency can determine very large effects on diffusion coefficient.

not suited to be used in tandem with microelectrodes for this kind of analysis. The effect of microelectrode radius has been analyzed briefly and a graphical comparison could be performed by looking at figure 4.22.

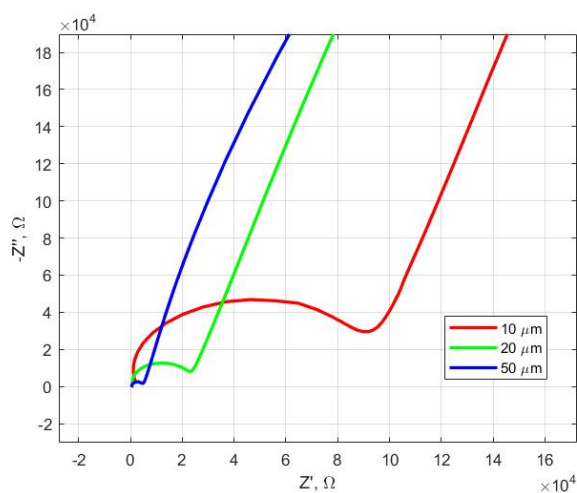


Figure 4.22: Zoom of the Nyquist plots for the three microelectrodes in solution 2 (7.5mM $K_3Fe(CN)_6$ and 0.5M KCl at pH=3, in order to perform a comparison at high frequencies.

The main variation was connected to the different capacitance and resistance values observed.

A further element to analyze was the effect of supporting electrolyte. This last, in fact had the roles previously described in cyclic voltammetry section. Immediately, the different ionic conductivity could have been seen, with really different resistances between the case when a lot of electrolyte was present and the one with the lowest concentration. Even the capacitance, due to the formation of an electrical double layer, was strongly affected by the different KCl concentration.

In figure 4.23, the comparison was quite intuitive.

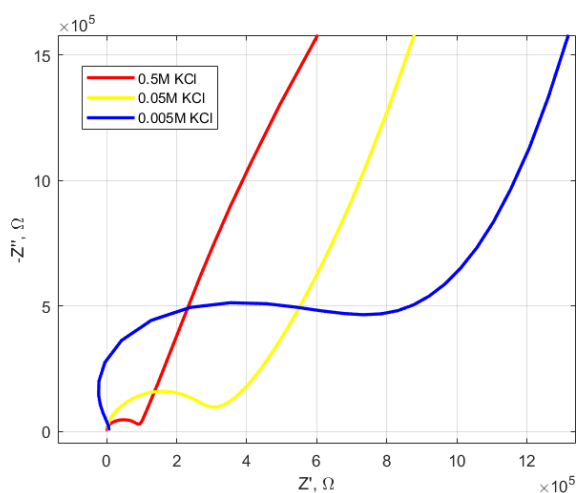


Figure 4.23: Effect of different concentration of supporting electrolyte on impedance spectroscopy measurements. Results for 10 μm microelectrode.

For a final consideration, also the role played by the nitrogen was studied. In particular, this has been done in order to look if it was necessary also with this kind of fast measurement, to blow it over the solution.

Results (figure 4.24) showed that the main effect was appreciable only for low frequency. A possible explanation of that, could be that since in this frequency range the time employed to perform analysis was higher, then also the effect of oxygen production was more relevant.

For this reason, it has been decided to keep to procedure containing N_2 steps, even if reducing the time of bubbling (being more interested to the high frequency region behaviour).

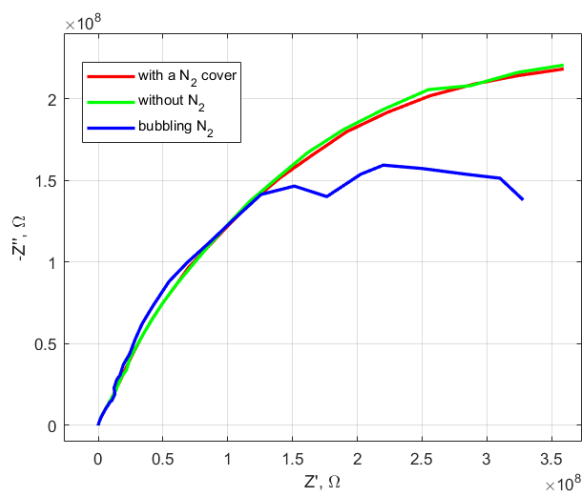


Figure 4.24: Effect of absence of nitrogen cover. measurements with 20 μm microelectrode in solution 7 (20mM $\text{K}_3\text{Fe}(\text{CN})_6$ and 0.5M KCl at pH=3).

4.2 Calibration with different concentration

The great power of determining diffusion coefficient was that it could be easily referred to concentration. This was the real goal of this kind of measurements.

In fact, in the final measurements, used to characterize the membrane, it was of interest to find the quantity of ions passed through a membrane. This passage, would lead unavoidably to a variation of concentration of the solution without analyte. Thus, by having a proper method to find this concentration would allow to determine membrane efficiency.

During measurements in cyclic voltammetry, it was shown that currents were linearly proportional to concentration, while diffusion coefficient remained constant. In this way, calibration was possible. For chronoamperometry a similar relation was holding, but connected to the current behaviour in time. In impedance spectroscopy the parameter of interest, instead, was the impedance, in particular that referred to the Warburg element.

In this section results for the three methods have been reported. The calibration has been performed by considering solutions with a constant supporting electrolyte concentration (0.5M KCl) and three different concentrations of redox mediator (7.5mM, 10mM and 20mM $\text{K}_3\text{Fe}(\text{CN})_6$), obviously all at pH=3.

Plots of this, in combination with results, will be provided in the following.

4.2.1 CV results

In cyclic voltammetry the relation of interest was the one providing that the limiting current was directly proportional to concentration. For this reason 3 different redox mediator concentrations have been investigated. The values of limiting currents have been reported in table 4.12.

concentration	10 μm	20 μm	50 μm	3 mm
7.5mM	12.62	26.93	68.71	18 059
10mM	17.70	35.15	89.33	22 125
20mM	36.05	69.26	179.22	46 289

Table 4.12: Limiting current values [nA], reported versus redox mediator concentration (solutions 2, 6 and 7). Comparison between the three different microelectrodes and macroelectrode has been presented.

In order to complete the tests to record diffusion coefficients, limiting current values have been used to determine this ones. They have been reported in table 4.13. To say that this method was good enough to perform concentration evaluation it was necessary that variability of results should have been the lowest possible.

concentration	10 μm	20 μm	50 μm	3 mm
7.5mM	8.72	9.30	9.49	207.98
10mM	9.18	9.11	9.26	38.22
20mM	9.34	8.97	9.29	39.98

Table 4.13: Diffusion coefficients [$10^{-6}cm^2/s$] calculated, reported versus redox mediator concentration (solutions 2, 6 and 7). Comparison between the three different microelectrodes and macroelectrode has been presented.

Good agreement of diffusion coefficient values has been found. Comments on obtained plots and results were similar to those reported in the first part of this chapter, so they won't be repeated (effect of nitrogen, oxygen production, effect of radius and differences with macroelectrode). The mean value recovered from microelectrodes was of $9.18 \cdot 10^{-6}cm^2/s$. In particular, since in the last part when

characterizing ion exchange membranes only one of them would have been used, the mean values for each of them has been calculated. The smallest microelectrode lead to a diffusion coefficient of $9.08 \cdot 10^{-6} \text{cm}^2/\text{s}$, the $20 \mu\text{m}$ gave $9.13 \cdot 10^{-6} \text{cm}^2/\text{s}$ and the largest ($50 \mu\text{m}$ of diameter) provided $9.35 \cdot 10^{-6} \text{cm}^2/\text{s}$.

A further proof of the goodness of the results has been also checked graphically by making calibration plots. They were simple plots provided for each microelectrode, where the limiting currents have been reported versus concentration. In order to be right, a linear relation should have held between the two quantities. This has been proofed and reported in plots of figure 4.25.

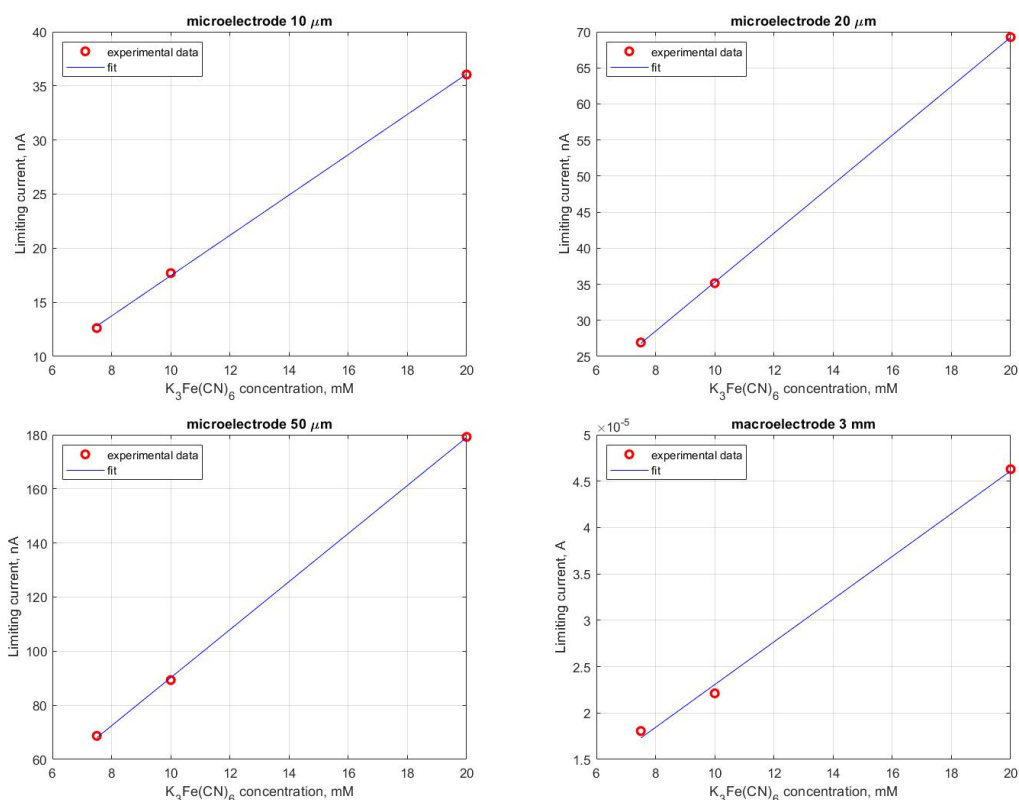


Figure 4.25: Calibration plot of CV results for the four electrodes (with diameters of $10\mu\text{m}$, $20\mu\text{m}$, $50\mu\text{m}$ and 3mm). Limiting current versus concentration.

4.2.2 CA results

In chronoamperometry the relation of concentration with current is maintained. However, by didn't having a certain value for every case, it was not possible to show any calibration plot.

What has been done, instead, it was to calculate the diffusion coefficients with the corrected version of the Shoup-Szabo model.

concentration	10 μm	20 μm	50 μm	3 mm
7.5mM	9.91	9.36	8.37	8.87
10mM	7.84*	6.42*	8.19*	7.50*
20mM	7.02*	6.24*	7.22*	8.43*

Table 4.14: Diffusion coefficients [$10^{-6}\text{cm}^2/\text{s}$] calculated, reported versus redox mediator concentration (solutions 2, 6 and 7). Comparison between the three different microelectrodes and macroelectrode has been presented.

Variation between results determined the level of goodness of the method. As could be seen in table 4.14 the disagreement between results was still quite high. The method approached real values, but large variations between different cases didn't allowed to use this technique.

It should be also mentioned that, in agreement with expectations, results marked with the blue star were lower, according to the holding relation of diffusion coefficient with temperature (see eq. 4.2).

Since the idea to use limiting current values obtained in 2 minutes in chronoamperometry was before proposed, results for this method have been also computed and reported.

In table 4.15 values of limiting currents have been reported.

concentration	10 μm	20 μm	50 μm	3 mm
7.5mM	12.78	26.57	65.28	15 528
10mM	15.59*	30.09*	76.92*	15 106*
20mM	32.13*	62.17*	155.20*	45 578*

Table 4.15: Limiting current [nA] values obtained from chronoamperometry for 2 minutes, reported versus redox mediator concentration (solutions 2, 6 and 7). Comparison between the three different microelectrodes and macroelectrode has been presented.

By using this method, considering limiting currents, the calibration plots were

again possible to be drawn. In fact they have been reported in figure 4.26. From the values of limiting currents, instead, diffusion coefficients have been determined. A good agreement of results were expected. They have been reported in table 4.16.

Results of diffusion coefficients when considering the limiting current in chronoamperometry were quite good, by having a consistence.

Obviously, the difference of temperature played a non negligible effect.

However, considering values in the right temperature range, two distinct diffusion coefficients could be available. In particular, they were $9.01 \cdot 10^{-6} \text{cm}^2/\text{s}$ for 25°C and $8.05 \cdot 10^{-6} \text{cm}^2/\text{s}$ for around 20°C . This variation consisted in a 11% reduction of value when decreasing of 5°C the temperature.

The method was found to be good and very useful to determine diffusion coefficients.

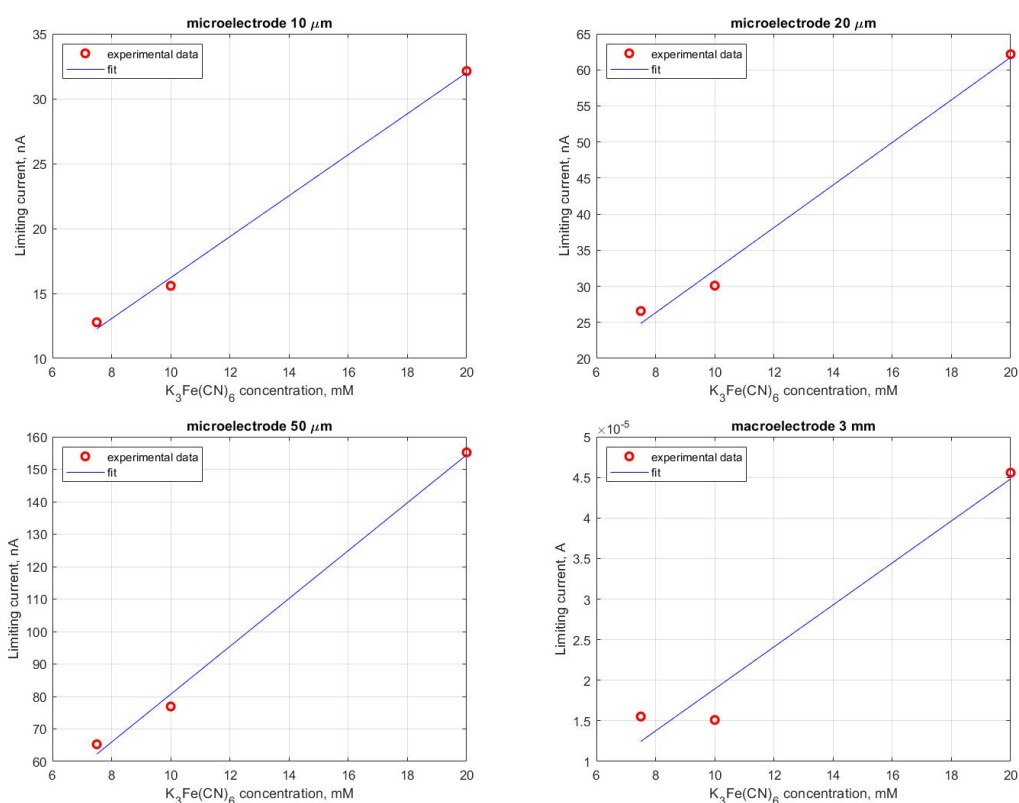


Figure 4.26: Calibration plot of CA results for the four electrodes (with diameters of $10\mu\text{m}$, $20\mu\text{m}$, $50\mu\text{m}$ and 3 mm). Limiting current versus concentration.

concentration	10 μm	20 μm	50 μm	3 mm
7.5mM	8.83	9.18	9.02	35.76
10mM	8.08*	7.80*	7.97*	26.09*
20mM	8.33*	8.05*	8.04*	39.37*

Table 4.16: Diffusion coefficients [$10^{-6}\text{cm}^2/\text{s}$] calculated, reported versus redox mediator concentration (solutions 2, 6 and 7). Comparison between the three different microelectrodes and macroelectrode has been presented.

4.2.3 FRA results

Impedance spectroscopy, differently from cyclic voltammetry or chronoamperometry, was not connected to the study of current. This, again, didn't allowed to define any calibration plot.

It was, instead, possible to get values of diffusion coefficient, relating as previously stated to the Warburg element. Diffusion coefficients for the various cases have been summarized in table 4.17.

concentration	10 μm	20 μm	50 μm	3 mm
7.5mM	8.73	8.34	2.54	$4.6 \cdot 10^{-5}$
10mM	7.65*	3.27*	1.06*	$8.1 \cdot 10^{-6*}$
20mM	2.87*	1.80*	0.31*	$8.6 \cdot 10^{-6*}$

Table 4.17: Diffusion coefficients [$10^{-6}\text{cm}^2/\text{s}$] calculated, reported versus redox mediator concentration (solutions 2, 6 and 7). Comparison between the three different microelectrodes and macroelectrode has been presented.

Large variations between calculated diffusion coefficients were again present, due to the problems cited previously. Effect of temperature have been still seen. In any case it was not possible to give much value to those results, according to their large variability.

As already mentioned and intuited, this method was not able to be used for concentration determination.

4.3 Comparison between the three techniques

In order to properly conclude this chapter some comparison and observations must be done. The reasons for which three different microelectrodes were employed for measurements were essentially two.

First of all, results could be checked, verifying if obtained values were due to real effects or just problems of some electrode. In fact, the major issues which could affect measurements and thus providing different diffusion coefficients were:

- 1) wrong analyte concentration;
- 2) radius of electrode different from the nominal one;
- 3) temperature different from the one of tabulated values (25°C);
- 4) further current contributions, like the one due to oxygen impurities.

This four possible sources of error should have been avoided and solutions to check their presence were required. Errors in analyte concentration were solved by producing different solutions and by checking them all. Problem of electrode real dimension has been considered by comparing three different electrodes and by controlling agreement of results. Temperature effect was unavoidable, but certain agreement has been tried to be obtained. In particular, measurements were all performed at around 25°C except a certain group at 20°C ca. However, they were all reliable, having only a constant shift of values. Finally, currents due to impurities, depending on the fact that the major one was oxygen, were solved by bubbling N₂ in solution before every measurement and keeping a constant nitrogen cover while measuring.

The second reason to use three different electrodes was that the "best electrode" had to be chosen. In principle the choice should be the smallest one, which in turn should allow for higher sensitivity. However, the sensitivity was not the only requirement taken into consideration when deciding which one to use. The two electrodes with the more agreement of results have been found to be those with diameter of 10 μm and 20 μm.

However, in order to define which one to use for next measurements, the choice has fallen on the 20 μm one, because it better resisted to high number of cycles and had no problems of gelation (fig. 4.27), when working at low supporting electrolyte concentrations. According to this, a tradeoff has been made: a little reduction in sensitivity has been accepted in order to avoid eventual problems of gelation.

Furthermore, the largest microelectrode, gave results higher of about 3-4% with respect to other two cases. The cause of this was probably a not perfectly perpendicular surface with respect to Pt wire. This provided an elliptical electrode

surface, with an equivalent larger radius, producing thus higher results and thus was not suited for this application.

Also the three used techniques have been compared. In fact, the reason for which

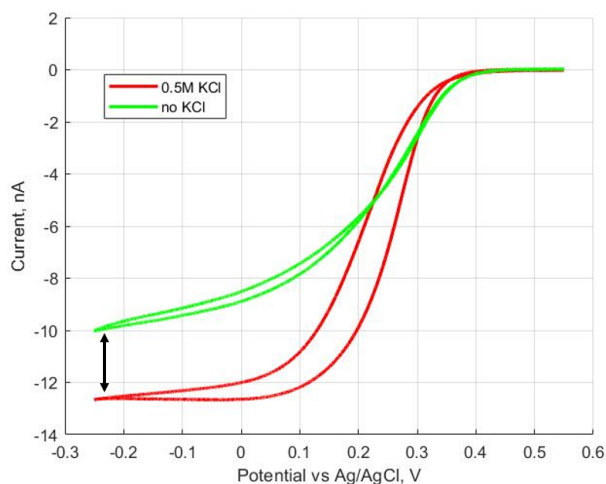


Figure 4.27: Results of the effect of gelation on smallest microelectrode. Comparison between solutions 2 and 5 (0.5M KCl and 0M KCl respectively). Gelation provided the shift in limiting current value).

cyclic voltammetry, chronoamperometry and impedance spectroscopy have been studied, was to determine which one offered better results and reliability.

The characteristics of the three methodologies were quite different. First of all, chronoamperometry and impedance spectroscopy were way faster than cyclic voltammetry. In fact, less than a second was used to acquire CA plot, while 2-3 minutes were used for FRA. Differently, for CV, times varying from 30 up to 80 minutes were employed.

CA and CV, both offered an immediate and simple way to see if reaction was reversible (in CA by plotting current versus one over square root of time and in CV versus $\ln\left(\frac{i}{i_L-i}\right)$). CV and impedance spectroscopy, allowed for an immediate evaluation of the situation. In fact, a certain behaviour was expected (fig. 4.2 and 4.18) and could be checked while measuring. In chronoamperometry it wasn't so easy to understand it only by visual inspection.

Finally, the last and the most important characteristic was result agreement. The method which guaranteed more continuity between the three used ones was cyclic voltammetry. Maximum results variations were of 8.3% (comparing $50\mu\text{m}$ with $10\mu\text{m}$ diameter electrodes). For this value the case with no supporting electrolyte wasn't considered, since quite different from the average of other measurements (problems with smallest electrode, having variations with respect to the largest one

of 30.4%).

This good value, was way better than those for other methodology. Even the corrected Shoup-Szabo model made in chronoamperometry didn't allow similar confidence (15.6%). Similar results were instead get when dealing with determination of limiting current in chronoamperometry.

For all this reasons, the final choice fall on an idea. The measurements to check unknown concentrations were done with cyclic voltammetry, in tandem with recording limiting current of chronoamperometry during 2 minutes of experiment.

In this way, eventual measurement mismatches due to errors in procedures could be found and easily solved.

Chapter 5

Ion exchange membranes

Ion Exchange Membranes (IEMs), are a group of membranes which selectively allow the passage of certain ions, according to their charge. Many types of them exist and continuous research is done daily in this field.

During this thesis work, a Nafion[®] 117 membrane, a sulfonated tetrafluoroethylene based fluoropolymer-copolymer from DuPont, was used. This is a commercial Proton Exchange Membrane, commonly used since many years.

The study of this membrane has been done in agreement with the idea to integrate a DSSC containing a redox mediator ($K_3Fe(CN)_6$) with a supercapacitor using an aqueous electrolyte of KCl. The need for a PEM was consistent with the need to avoid redox shuttling. In this chapter, an introduction on IEMs and their employment will be given. Even procedures used to activate the membrane will be shown, in union with description of the used reference electrodes and the designed H cell used in the last part of the thesis work.

The studied membrane will be analysed, by giving information on its permselectivity in different electrolytes. Finally, the ability of Nafion[®] 117 membrane to confine the redox mediator will be reported. Considerations will be performed on the possibility to use this membrane in the integrated HS device.

5.1 Theory

After having explained the importance and need of realise an integrated HS device [55], some practical facts must be seen to start the project.

DSSC and some supercapacitors are based on redox reactions. In DSSC those reactions happen in the electrolyte and are used as a sort of electron carrier. In fact, by varying their valence number, they can take or restore electrons at the two electrodes. This allows the cell to work. Supercapacitors can be based on the electric

double layer effect. However their performances can be improved by employing redox mediators, both for using pseudocapacitance and active electrolytes [56]. They substantially store charges by varying the valence number of some atoms. These charges are then released when an external circuit is connected to the supercapacitor.

When one tries to integrate a DSSC with a supercapacitor, one of the first problems encountered is the problem of redox shuttling. It consists in the leakage of ions between the two parts of harvest and storage. These, in turn, will cause the discharge of the supercapacitor. Moreover secondary and sometimes dramatic effects may happen (for example iodine, used in DSSC, can corrode electrodes of the supercapacitor).

In order to avoid this problem the idea which immediately comes to mind is to

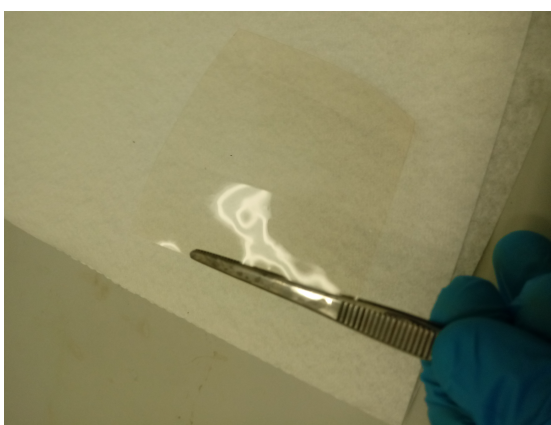


Figure 5.1: Nafion[®] 117 membrane.

use ion-exchange membranes. They consist of materials which allows the passage of ions with a determined charge. As the used membrane was a polymeric one, from now on, the focus will be on polymeric IEMs.

In particular, some active sites are present on main chains of the polymeric matrix. Only ions with the opposite charge can pass through the membrane (the so-called counter-ions). Co-ions will be blocked, instead. The ability of a membrane to allow the passage of counter-ions while repealing co-ions, is represented by the permselectivity.

Ion-exchange membranes have been widely used in microbial fuel cells (MFC), redox-flow batteries (RFB and especially VRFB) and electro dialysis (ED). Here they are employed to avoid the passage of ions, in order to reduce shuttling, or in the case of ED for separate salts from a solution. Examples of their use in MFC are reported in [57], where a Nafion[®] membrane is used. This one is one of the most used, since it offers very good results and has been produced for many years. It is a proton-exchange membrane, but cations can easily permeate it. For years it

represented a standard in ion-exchange membranes and it still has a dominating role.

However MFCs based on proton-exchange membrane suffer of undesired cations passages between the two separate chambers of catholyte and anolyte. In order to reduce and maybe eliminate this problem also anion-exchange membranes were studied [58]. AEM offer the advantage to block cations like Na^+ and Cu^{2+} . However H^+ can still pass, due to its very small dimension. Anions can freely move, but are generally not present or non-problematic. In conclusion the device can work better using AEM instead of PEM. The only limit which still reduce this configuration is that this kind of membranes still have low permselectivity.

An analogue speech can be done where redox reactions at cathode and anode must be kept separate. Also here AEMs seem to lead to better result. Some cases of membranes used in RFB have been reported in [59], [60], [61] and [62]. Advances in membranes for redox flow batteries could be found summarized in [63].

By looking at interesting results for MFC and RFB it appeared to be quite obvious to apply the technology of ion-exchange membranes also to REHES (Redox aided Electrolyte Hybrid Energy Storage [64], [65]) devices. Many works showed the positive effect of IEM in REHES devices, demonstrating that redox shuttling can be reduced with a consequent reduction of leakages and performance improvement [66] and [67].

Due to these results it appears interesting and useful to characterize new IEMs for the development of newer and better integrated HS devices. Many parameters could be evaluated in order to characterize Ion Exchange Membranes.

First of all, the water uptake can be considered. It is defined as the amount of water which can be absorbed by the polymer. The formula to calculate this factor is

$$W_u = \frac{m_{swollen} - m_{dry}}{m_{dry}} \quad (5.1)$$

The two values m_{dry} and $m_{swollen}$ are simply obtained by measuring the weight of the membrane before and after immersion in water. This factor has a relevant impact on the working of the membrane, since a good one should have no water uptake. In this thesis work this has also been evaluated and very good results have been found and shown in sec. 5.5.1.

One other important parameter, probably the most signifying one, is permselectivity. This factor takes into account how much a membrane can discriminate between co-ions and counter-ions. It will be treated in more detail in section 5.5.

The work of this thesis fixed as the focus the characterization of this kind of membrane, using mainly diffusion coefficient evaluation as better explained later.

5.2 Activation

Before using, membrane must be activated. This process has been done in order to remove impurities and activate sites with desired ions.

The used procedure consisted in some steps, similar to those followed by [68], where a Nafion[®] 115 was used.

First of all, the membrane was rinsed with deionized water. After that it was placed in a solution of hydrogen peroxide (3% in weight). This was heated to 80°C for one hour.

After this step, again a rinsing with deionized water and a second bath in 1M HCl at 80°C for one hour were performed. After a further rinsing step, the last bath in the 1M solution of the desired salt was done. A final rinsing with deionized water gave the activated membrane.

The passage in H₂O₂ solution was fundamental in order to remove larger impurities. In fact, it was possible to notice that the membrane was of a light yellow before the bath and completely transparent after that. HCl, thanks to its acid nature, allowed the activation of sites.

The final bath allowed functionalization of sites with the desired ions, in this work Li⁺, Na⁺ and K⁺.

Membranes obtained in this way were able to be used in experiments. They were stored in a plastic Petri dish, in dark. The only step required before its use was the rinsing of the membrane with deionized water with the subsequent drying.

5.3 H cell

Ion exchange membranes have been characterized in an appropriate container, called H cell. For the part of permselectivity determination, a cell already present in laboratory was used. This was quite large, with a total volume of 50mL. It allowed the insertion of two Ag/AgCl reference electrodes, needed for the measurements (see later in section 5.5).

For the second part (concentration determination with cyclic voltammetry), instead, a new and smaller H cell has been used.

This device has been designed and projected thanks to SolidWorks[®]. In order to have a good cell, some issues have been considered:

- Little chambers volume, to minimize necessary amount of solutions;
- Lateral transparent windows, useful to verify internal situation (like electrode positioning, presence of bubbles and eventual leakages between the two chambers);

- Correct dimensions of vertical pipes, to hold electrodes;
- Little opening between the two chambers, to minimize both membrane area and force due to osmotic pressure;
- Internal conical shape, to reduce trapping of bubbles on the membrane.

According to these, the layout of figure 5.2 was obtained.

Following the design step, the two halves of the final cell were printed in 3D in the

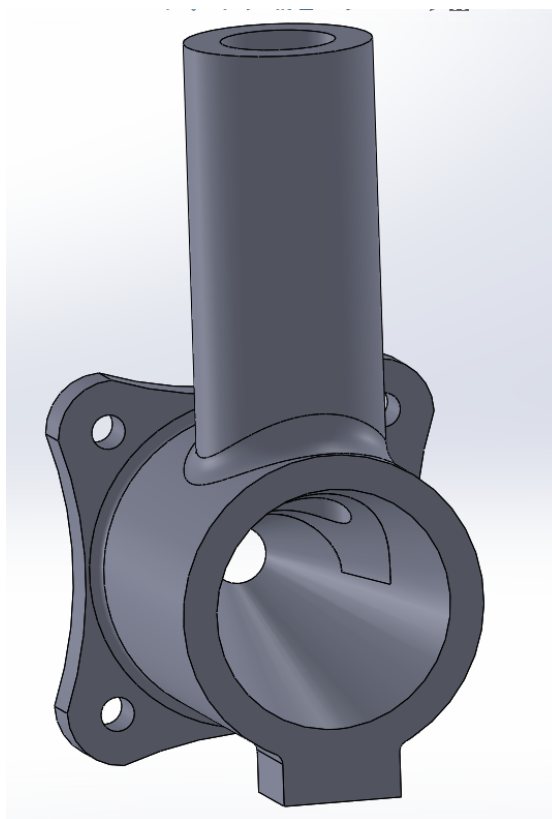


Figure 5.2: Design of the half-cell

Politecnico laboratory of Chivasso at Chilab. After the removal of sacrificial layers and an accurate polishing, the structure still presented two open windows. Those were closed by sealing with two pieces of PMMA. The used glue was a mixture 20:1 (in weight) of SYLGARD™ 184 silicone elastomer base and SYLGARD™ 184 silicone elastomer curing agent. A step of curing was required, by placing the two half cells on an hot-plate at 80°C for 24 hours.

The last thing necessary to have a working cell, was to produce some elastomeric rings, used to seal the two half cells, avoiding leakages and fall off of the membrane

in between. These gaskets have been produced with the same mixture used to glue the lateral windows. The silicone elastomer was placed in a circular mold on an heated hot-plate at 80°C for 2 hours.

The H cell could be assembled by placing membrane on the gasket and inserting these two in between the two parts of the cell. Then it was all closed tightly by using four screws and nuts.

The resulting assembled cell had a total capacity of 13mL.

The final H cell has been shown in figure 5.3.



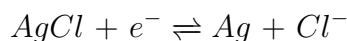
Figure 5.3: View of the completed H cell

5.4 Reference electrode

A brief comment on the reference electrode has been thought to be necessary.

First of all, it must be said that reference electrode have the peculiar ability to keep their potential constant. This is possible thanks to redox reactions which maintain the potential in equilibrium.

In an Ag/AgCl reference, the reaction



governs the working of the electrode. The potential is calculated as [32]:

$$E_{Ag|AgCl} = E_{Ag|AgCl}^0 - \frac{RT}{F} \ln a_{Cl} \quad (5.2)$$

remembering that $E_{Ag|AgCl}^0 = 0.222V$ vs NHE (25°C). The potential will depend thus mainly on the redox reaction potential and also on the filling electrolyte used. The Ag/AgCl reference electrode used in this work was filled with 3M KCl. The

structure of electrode was of a silver wire covered with silver chloride immersed in a 3M KCl solution. This was contained in the glass cover and worked thanks to a wide membrane on the lateral section of the electrode. It was a HI3148B of HANNA instruments.

The initial choice for reference electrode was this one. This was in fact used for all the first part of measurements, those concerning diffusion coefficient calculation. However, in order to conform to the requirements for a little H cell, a smaller one has been preferred in the second part. This led to some variations between results obtained during the first part of the work and the final in the H cell when testing membranes.

This wasn't a problem, since the only found variation was in the open circuit potential (OCP) of the reference electrodes. This variation was found to be stable and it was measured before every experiment. This shift in potential was of around 700mV.

By adding this difference to the usual values used with macroelectrodes, consistent results were obtained and therefore the new reference electrode was considered as good and reliable.

This new possibility for measurements consisted in a platinum rod.

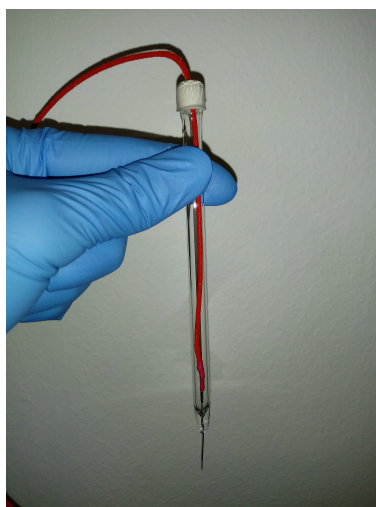


Figure 5.4: Aspect of the platinum wire used as pseudo-reference.

This was a pseudo-reference electrode. Differently from classical electrodes, a Pt rod can't reach stabilization with thermodynamic equilibrium. This is due to the lack of a common ion at the interface of the two phases [69], [70].

Further disadvantages of pseudo-references are their polarizable nature and the fact that they work in a limited range of conditions like pH or temperature.

However pseudo-references also offer some peculiar advantages. In particular, they

are generally very simple (like the previously mentioned platinum rod, fig. 5.4) and can be directly immersed in electrolyte solutions. They don't show liquid junction potentials and even the ohmic resistance is really small. Furthermore, pseudo-reference electrodes have the great advantage to not contaminate the solution with molecules or ions.

The potential of pseudo-references can be easily determined by inserting it in the desired solution and then, thanks to a reference electrode, a comparison can be performed. New measurements must adjust the reference potential according to this.

For the part of permselectivity determination, instead, a further Ag/AgCl reference electrode filled with 3M KCl was used in couple with the one previously mentioned. This other Ag/AgCl reference electrode was from MetrOhm.

This little note on reference electrodes was necessary in order to understand different potential windows used in experiments.

5.5 Permselectivity

Since the mission of Ion Exchange Membranes is to discriminate between ions and co-ions, the testing of this ability is necessary. In particular, in order to compare performances, an adequate parameter should be used.

It is the case of permselectivity. It has been defined by IUPAC in 1993 as "*A term used to define the preferential permeation of certain ionic species through ion-exchange membranes*" [71].

Permselectivity can be determined by measuring the potential which is developed between two solutions of the same electrolyte, but with different concentrations, separated by the investigated membrane. A good solution can be to use KCl solutions, since potassium and chloride ions have similar mobilities [72]. Instead, the use of sodium chloride can give potentials when two different concentrations are put in contact, also without an ion exchange membrane in between. This is due to the large difference in sodium and chloride ions.

The potential between the two solutions separated by the membrane must be measured by two identical electrodes. In particular, they must have the same potential, in order to avoid further contributions in the reading. If electrodes don't have the same potential two possible solutions are available. First of all, electrodes can be switched from one solution to the other in the middle of the measurement and then get the average, or by calculating the open circuit potential between both when no membrane is present.

An electric potential arises across the interface of an ion exchange membrane when exposed to a gradient of ionic concentration. The potential which originates is

called the Donnan one and can be calculated as

$$E_{Don} = \bar{\Psi} - \Psi = \frac{1}{z_i F} \left[RT \ln \frac{a_i}{\bar{a}_i} - (\bar{P} - P) V_i \right] \quad (5.3)$$

where Ψ is the permselectivity, z_i represents charge number of ion i , a_i is the activity of ion i , P is the pressure and V_i is the volume of ion i . The letters marked with an over bar represent properties of membrane, while those without are referred to the solution.

Applying electroneutrality to the Donnan potential equation will give the Donnan membrane equilibrium equation (see eq(3) in [73]).

The permselectivity of a membrane can be calculated as the degree at which it excludes co-ions. It can be obtained from

$$\Psi = 1 - \frac{\bar{t}_m}{t_m} \quad (5.4)$$

where t_m represents the transport number of counter-ions. A perfect membrane would have a permselectivity of 1, meaning that no co-ions can pass through it.

By measuring potential at interface of two solutions with different salt concentration separated by an ion exchange membrane, it is possible to determine transport numbers. From these, then one can get the permselectivity value.

In this thesis work a similar, but slightly different method has been used [74].

The formula of permselectivity thus used was

$$\alpha = \frac{\frac{E_{mem}}{E_{mem-ideal}} + 1 - 2t_g}{2t_c} \quad (5.5)$$

where t_g and t_c are the transport numbers of counter-ions and co-ions, respectively. They can be calculated as

$$t_g = \frac{|z_+|D_+}{|z_+|D_+ + |z_-|D_-}$$

$$t_c = \frac{|z_-|D_-}{|z_+|D_+ + |z_-|D_-}$$

where D_- and D_+ represents diffusion coefficients of anions and cations respectively. Their values were taken from [75]. Further information and notes could be found in [76].

E_{mem} is the potential previously determined starting from the measured one minus the two contributions references and junctions at their interfaces.

Eq. 5.5 gives the apparent permselectivity calculated from the measured potentials. This method is a quite accurate approximation of the permselectivity of the

measurement as it takes into account also ion mobilities. This technique is more centered on the study of junction potentials at interfaces between two solutions with different electrolyte concentration.

This is important since reference electrodes were filled with a 3M KCl solution, so different mobility of ions played a role also at the junction with solution.

First of all, the potential between the two solutions was measured. The obtained value was the sum of many contributions:

$$E_{measured} = E_{mem} + \Delta E_{ref} + \Delta E_j \quad (5.6)$$

where E_{mem} is the real potential on the membrane, the one which should have been obtained in order to calculate permselectivity.

ΔE_{ref} represents the potential difference between both electrodes. It was measured before every experiment, by simply inserting the electrodes in the 0.5M solution used for the measurements. This value represented a non-ideally working electrode, since their potentials can be considered equals.

ΔE_j , instead, takes into account the contribution of the potential that arises at the interface between the electrode and the electrolyte. It is calculated through the corrected Henderson equation

$$E_j = \frac{\sum_i \frac{|z_i|u_i}{z_i} [a_i(2) - a_i(1)]}{\sum_i |z_i|u_i [a_i(2) - a_i(1)]} \frac{RT}{F} \ln \frac{\sum_i |z_i|u_i a_i(1)}{\sum_i |z_i|u_i a_i(2)} \quad (5.7)$$

where u_i stands for mobility of ion i (in $m^2 \cdot V^{-1} \cdot s^{-1}$) and a_i is the activity of ion i . The two variables 1 and 2 were referred to the solution which was considered. For convention, always according to [74], solution 1 was the one which filled the electrode, while solution 2 corresponded to the electrolyte.

Once the contributions of both E_j and E_{ref} are considered, the real potential on the membrane are obtained. This one could be easily used to calculate the permselectivity.

The evaluation of the permselectivity obtained in this way, was connected to the evaluation of the potential with the theoretical one ($E_{mem-ideal}$). This last could be mathematically derived from the Nernst equation

$$E_{mem-ideal} = -\frac{RT}{z_g F} \ln \frac{a_{0.5}}{a_{0.1}} \quad (5.8)$$

where a is the activity of the salt (in this work, three cases were considered: LiCl, NaCl and KCl) and subscript referred to its concentration.

So, resuming all the work done to measure permselectivity, the steps are:

- determine potential between two solutions with different concentration (0.5M and 0.1M) separated by the membrane (Nafion[®] 117 with different activation salt);

- subtract from this value contributions determined by reference electrodes and their interfaces;
- calculate the theoretical value of the potential for the analysed case;
- calculate permselectivity with eq. 5.5.

Results were produced by considering not only the four possible activation (HCl, LiCl, NaCl and KCl), but also three different electrolytes. All measurements were performed by inserting in a side of the H cell the solution less concentrated (0.1M) and in the other the more concentrated one (0.5M). The area between the two chambers, completely covered by the ion exchange membrane was circular, with a diameter of 5mm. The H cell for this characterization was larger than the realized one, with a total volume of around 50mL. The larger dimension allowed for the use of good Ag/AgCl electrodes. The setup has been shown in figure 5.5.

In order to minimize contaminations between different measurements, the adopted

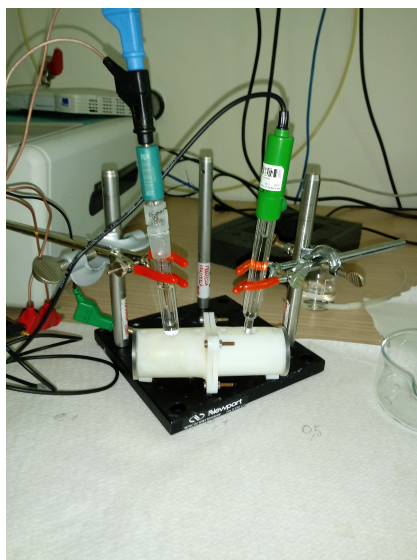


Figure 5.5: Setup used to measure permselectivity of the Nafion[®] 117 membrane.

sequence of experiments consisted in studying before every combination for a certain electrolyte and only after, passing to the new one. When electrolyte was changed, great attention has been paid in washing the H cell. Also in order to minimize possible contaminations or variations of concentrations, one chamber of the cell was completely dedicated to the 0.5M solution and the other to the 0.1M one.

In next section, the studied cases will be reported with results. Comparisons will be performed with the different combinations of electrolyte and activated membrane.

5.5.1 Results

Permselectivity of Nafion[®] 117 membranes was calculated given its importance for possible applications on its integration in a harvest and storage device.

As previously seen, the membrane had to be activated in order to exploit its functions. However, different types of activation were possible. One of the goals of this part was also to find which one of them worked better in the case of this work thesis: a KCl containing solution.

Values of permselectivity, calculated according to the procedure explained in previous section (from [74], by using eq. 5.5), have been reported in table 5.1.

salt of electrolyte	HCl activ.	LiCl activ.	NaCl activ.	KCl activ.
LiCl	77.11%	86.15%	82.49%	88.16%
NaCl	95.34%	94.45%	94.93%	100.15%
KCl	97.45%	99.24%	98.62%	98.77%

Table 5.1: Values of permselectivity obtained for the various combinations of membrane activation (columns) and electrolytes (rows).

From the previous results, a direct relation between cation size and permselectivity can be observed, apart from the case of NaCl as electrolyte and the membrane activated with KCl.

This size exclusion comes from the fact that the bigger the ions, the easier for the membrane to block them. Also it is worth to notice that the membrane activated with HCl didn't show proper performances with LiCl as electrolyte.

Some further notes should also be reported. In fact, since available data for ion diffusion coefficients and activity coefficients were not always present, two important approximations in calculations have been done. First of all, the diffusion coefficients were considered equal to those in infinite dilution (see table 5.2). This first approximation lead to an error in results estimated in less than 1%.

Li ⁺	Na ⁺	K ⁺	Cl ⁻
1.029	1.334	1.957	2.032

Table 5.2: Values of ion diffusion coefficients [$10^{-5}cm^2s^{-1}$] (in infinite dilution conditions) for all electrolytes considered. Values from [75].

The second relevant choice, was instead performed in the evaluation of the junction potentials. In fact, due to the lack of data with right concentrations, the adopted standard was to use mobility values in infinite dilution. This approximation, also found in [74], was proved to lead in variations of E_j of less than 0.4mV. This, in turn, implied an error on permselectivity of around 1%.

These notes on approximations were necessary, in order to justify the value for the combination NaCl electrolyte with KCl activated membrane which showed a permselectivity value of 100.15% (which was obviously a non physical condition). This data should be interpreted, thus, as a small overestimation of a high performance membrane.

Also the variations due to approximations seemed to justify another observed case with NaCl electrolyte. By looking at the table of permselectivity values, it can be noticed that HCl activation seemed to be the worst one. Only for NaCl it was not valid. Nevertheless, this small variations in results (less than 1% in the previous case) can be attributed to those approximations.

In general, the electrolyte containing KCl was the one, giving the higher values of permselectivity. In average, for this electrolyte case, the permselectivity was of 98.52%, with also a very small variation of results (1.8%).

This was particularly important, since the studied solution containing the redox mediator of this thesis work ($\text{K}_3\text{Fe}(\text{CN})_6$) used always KCl as supporting electrolyte. The fact that high and slightly variable permselectivities were obtained for this electrolyte, showed good prospects for the use of Nafion[®] in this project: an integrated HS device made of an aqueous based DSSC with electrolyte containing the studied redox mediator, in combination with a supercapacitor using KCl.

This was a preliminary and necessary condition, however, in order to be sufficient, also the passage of $\text{Fe}(\text{CN})_6^{3-}$ ions should be evaluated. Results have been reported in next section.

On the other side, the effect of osmotic pressure was appreciable. In fact, at the end of each measurement (around 2-3 hours), the membrane presented a deformed surface (see photo shown in figure 5.6). This consideration, lead to no practical effects on measurements and didn't represent a problem in studied cases. However, during the realization of a real device it should be considered, especially if large devices or big chambers are present (leading to membrane break). During measurements, no one of the studied membranes broken or produced leakages, confirming expected high mechanical performances of Nafion[®] 117.

Water uptake represents an important parameter for ion exchange membranes. It should be the lowest possible, meaning a perfect hydrophobicity. IEMs, in fact, should allow the passage only to certain ions, but those with opposite charge and solvent should not pass. If water uptake is high, it means that water can pass through.

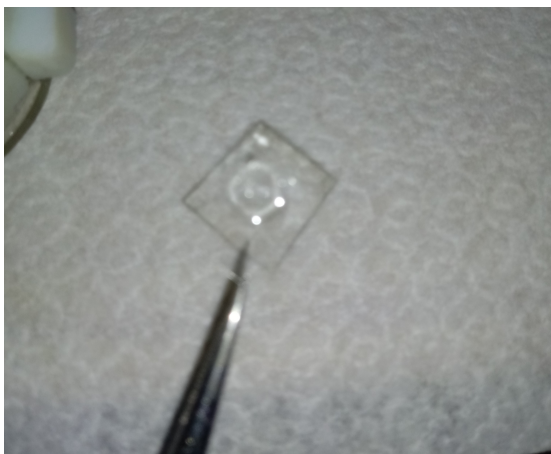


Figure 5.6: Effect of osmotic pressure on the membrane.

For sake of curiosity the water uptake of a piece of Nafion[®] 117 membrane activated with LiCl was studied when immersed in a 0.5M KCl solution. The mass of the membrane was collected in the dry state (after 24 hours in oven at 60°C) and in wet condition. In order to check if time played a role in the value of the water uptake, two measurements were performed: the first after 1 hour of immersion and the second after 24 hours.

The values of mass were $m_{dry} = 39.2\text{mg}$ in dry state, $m_{wet1} = 40.1\text{mg}$ after 1 hour of immersion and $m_{wet2} = 40.3\text{mg}$ after 24 hours.

The corresponding results of water uptake were of $w_1 = 0.023$ and $w_{24} = 0.028$. Considering that the uncertainty of the weight scale was of 0.1mg , the variation in one day was quite contained and the value didn't vary appreciably with time. Those two values (calculated with eq. 5.1) implied a good membrane, with small water uptake.

5.6 Determination of redox mediator concentration variations

The second method of characterization of the ion exchange membrane was that through evaluation of diffusion coefficient. In particular, results obtained in chapter 4 have been exploited, in order to evaluate membrane performances.

The idea consisted in putting the membrane in between of the designed H cell to separate a solution containing the redox mediator and one not. The solution containing redox mediator had a concentration of 20 mM $\text{K}_3\text{Fe}(\text{CN})_6$. Both solutions, instead, contained 0.5M KCl.

The studied membrane was again a Nafion[®] 117 one. After the results of permselectivity, according to the use of the electrolyte, the choice of activation fell on the one with LiCl. A further possibility, not considered in this work, was that of using the membrane activated with KCl, in order to reduce contaminations from Li⁺ ions. However, the choice has been taken only according to permselectivity values. The role of the membrane was that of keeping confined the redox mediator. The tests were necessary in order to determine if this particular PEM was suited for the use in an integrated HS device.

The adopted setup consisted in three electrode measurements, where the 20 μm microelectrode has been used as working one, according to results and analysis of chapter 4. Both counter and reference electrodes were platinum rods, those defined previously and with different dimensions (bigger and smaller respectively). The choice was consistent with the need of compact solutions.

The initial idea was of using both cyclic voltammetry and chronoamperometry (in the experiment of limiting current evaluation alone). However, as will be seen in the next subsection, this has not been done. Reasons will be explained later.

In the following, results will be shown and discussed.

5.6.1 Results

After having assembled the setup, measurements of both cyclic voltammetry and chronoamperometry were made. The idea was that of recovering limiting current values and starting from them to find also concentration of redox mediator. A perfect membrane would have led to zero concentration, since working electrode was placed in the chamber without $\text{K}_3\text{Fe}(\text{CN})_6$. A not good membrane, instead would have produced noticeable signals, revealing the passage of ions.

What has been immediately seen was that no ions passed through the membrane, according to the fact that no concentration variation was detected. Measurements have been repeated every 12 hours, keeping always the setup sealed at the best of the possibility, in order to avoid evaporation or problems of capillarity.

The total time considered for the whole experiment was of five days. During all this period no redox mediator concentration has been found in the second chamber. Results obtained at the end of the test could be seen in figure 5.7.

As could be seen in the figure, no variation of the profile was present at around -0.45V, where the redox reaction took place. This meant that no analyte had passed through the membrane during the 5 days. In order to have an idea of what would have meant to have no membrane was also represented. The profile of the CV in the same setup, but where no membrane was inserted was also shown.

The concentration on the solution where redox mediator was present was of 20mM.

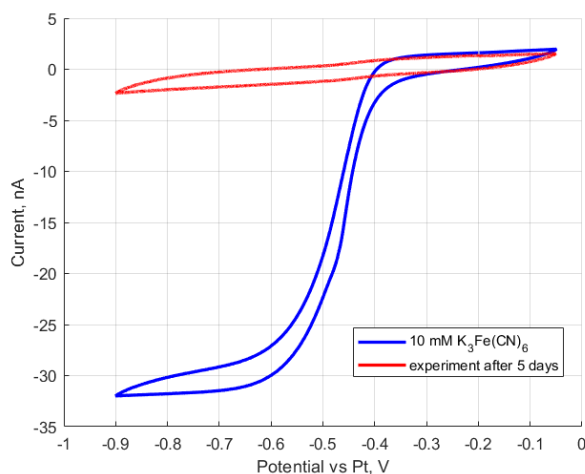


Figure 5.7: Cyclic voltammetry comparison between results obtained after five days and the case of redox mediator on both sides of the cell.

This in turn, lead to a concentration of 10 mM in the whole cell, when the membrane wasn't inserted. Obviously a very different profile would have been obtained, as can be seen.

Always according to the figure 5.7, it was quite immediate the reason for which chronoamperometry was not a reliable method, in particular, referring to the case of analyzing only its limiting current value.

In fact, due to the ohmic resistance of both water and membrane, according to a capacitive effect due to the interface of microelectrode with solution, the value of current at 0.8V was not zero. From CV the cause of this value was clear, but referring only on chronoamperometry, this would have lead to errors and possible mismatches. In fact, if considering values of current obtained (around 2 nA), would have produced concentrations of 0.6 mM. This would have been wrong.

According to that, the chronoamperometry was not used to evaluate performances of the membrane.

After having looked at results of the previously described plots, the possibilities were 2. First, the experiment was correct and the studied membrane had a very good behaviour, making it very suitable for an employment in integrated HS devices. Anyway, a second possible explanation was that the experiment had some intrinsic problems which lead to these results.

In order to confute this second eventuality, a further proof has been provided. The same experiment has been performed, but a little change has been done. The membrane has been perforated with a needle, with a diameter of 0.7mm. The pressure between the two compartments had also effect on the membrane, reducing

thus the hole. In this way, the expectations were of having a little passage of ions with time between the hole in the membrane.

Results for these measurements has been reported in figure 5.8.

As could be seen, large variations between measurements performed at different

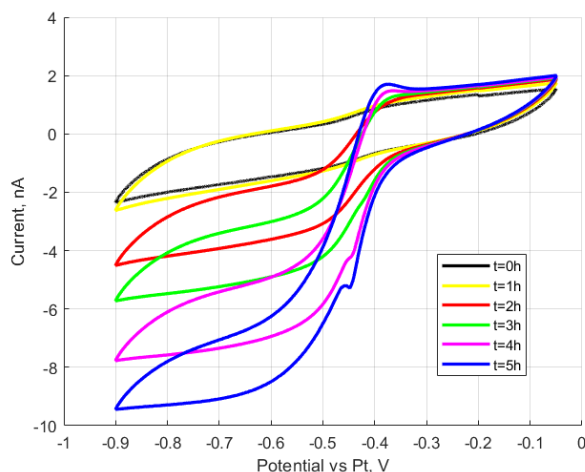


Figure 5.8: Evolution with time of CV results for a broken membrane.

times were really appreciable. Furthermore, also the colour of the solution (which at the beginning was transparent, when containing only 0.5M KCl) turned to a slight yellow with time.

This time evolution of the passage of redox mediator has been thus evaluated as the variation of concentration. Results have been presented in table 5.3 and graphically shown in figure 5.9 to highlight the linear variation with respect to time.

time (h)	0	1	2	3	4	5
concentration (mM)	0.00	0.29	0.81	1.26	1.74	2.27

Table 5.3: Concentrations of $K_3Fe(CN)_6$ in the chamber of the H cell, reported in function of time when membrane has been broken.

To better understand the entity of the redox mediator concentration variation, in figure 5.10, the evolution with time has been compared with a case with no IEM, thus with a concentration of $K_3Fe(CN)_6$ of 10 mM.

This final check provided that the broken membrane allowed the passage of ions, while the integer one didn't. In this way, it has been proofed that the Nafion[®] 117 membrane activated with LiCl, was a good one, with really high performances and

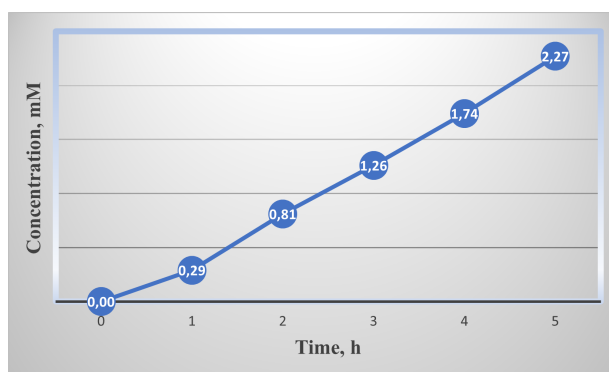


Figure 5.9: Concentrations of $K_3Fe(CN)_6$ in the chamber of the H cell, reported in function of time when membrane has been broken.

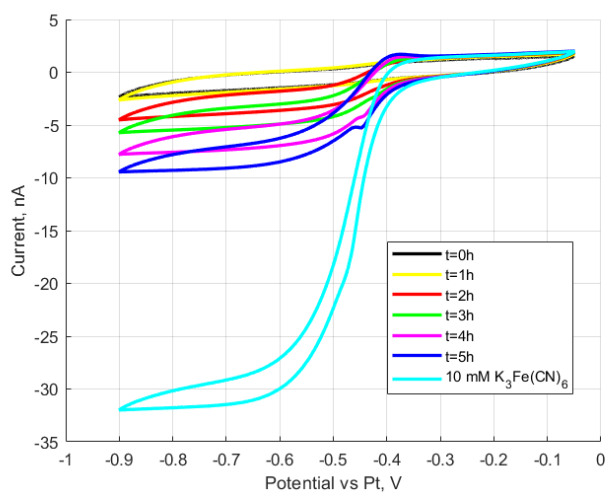


Figure 5.10: Evolution with time of CV results for a broken membrane compared with the case of no Nafion[®] present.

efficiencies. This in turn, would make it to be the perfect choice in the integration of a DSSC containing $K_3Fe(CN)_6$, with a supercapacitor.

Chapter 6

Carbon electrodes for supercapacitor

The final part of this thesis work was devoted to the realization and characterization of an active carbon electrode. This component showed a supercapacitive effect. Many different tries have been done, varying slurry composition, until a satisfactory level was reached.

The redox shuttling effect in presence of $K_3Fe(CN)_6$ was also found and demonstrated. This confirmed the need of using a good IEM, like the one analysed in previous chapter.

For a quick and easy check, also a glassy carbon electrode has been studied, having the advantage to be already realized and with known behaviour. It offered a simple and fast way to take confidence with measurements, before passing to the fabricated electrode.

Finally also a supercapacitor has been realized, by using electrodes with one of the studied slurries. Its performances have been evaluated, both in normal working conditions and simulating a leakage of redox mediator.

In the following the procedures used to build electrodes and results will be presented.

6.1 Realization of electrodes

Three different slurries have been employed in this thesis work. In particular, each one of them had some peculiar characteristics which allowed their employment only in certain configurations. In the following both lists of components ratios and methods of electrode realization have been shown.

The first electrode has been realized starting by the slurry preparation. The composition was:

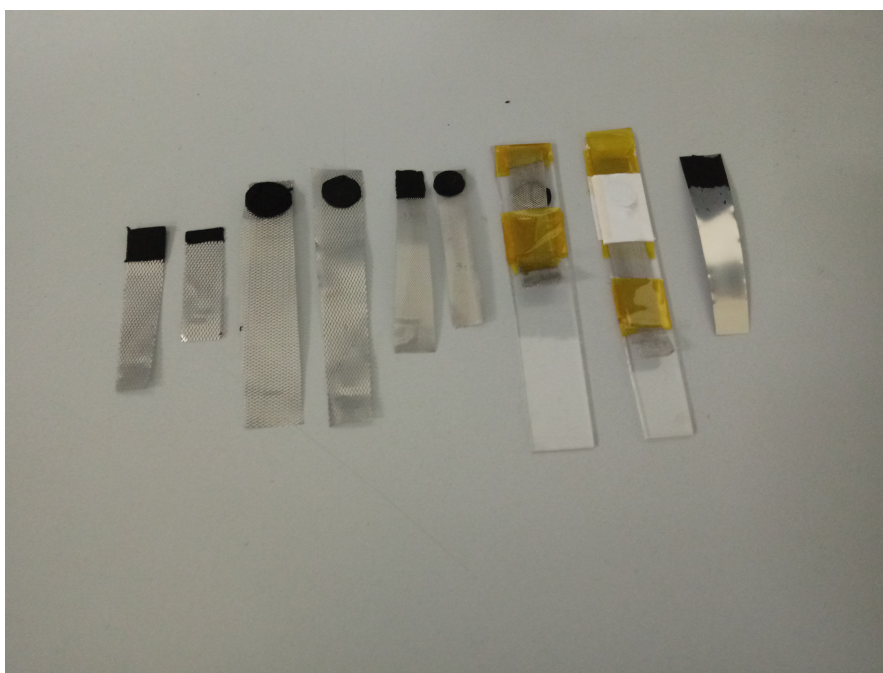


Figure 6.1: Some of the carbon-based electrodes produced for the simulation of a supercapacitor working in aqueous solution (from left to right: slurry 1 on steel grid, again on steel grid, but in a narrower region, pressed as disc on Ti grid, dropcasted on Ti grid, rolled on Ti grid, as disc pressed between two Ti grids on a glass, pressed on a Ti grid over a glass, thanks to a thin paper and slurry 2 deposited on steel foil).

- 85% Kuraray active carbon for super-capacitor electrode, model YP-50F;
- 10% TIMICAL SUPER C45 for applications as conductive additive for lithium-ion batteries (carbon black);
- 5% Polytetrafluoroethylene preparation (PTFE)*.

*considering 60% dispersion in water. Percentages were referred to proportions in weight.

The active carbon had the important role of providing a good wide surface of the electrode, in order to enable double layer capacitance effect. The conductive additive was obviously used to improve conductivity of the electrode. Finally PTFE had the role of binder.

After having weighted the three components to have a final active mass of 1g (0.85g active carbon, 0.10g black carbon and 0.083g PTFE solution), around 20 mL of ethanol were added. The beaker containing the mixture, was covered all around with a thermal cloth, made of two layers of paper and one of aluminium sheet.

Then the beaker has been placed on an heater, inserting a magnetic stirrer, under chemical hood. The temperature was held at 60°C for one hour and then raised to 80°C, until most of ethanol was evaporated. The reason of inserting ethanol was that PTFE started to soften, also according to heating. Stirring allowed an homogeneous mixing, while heating made ethanol to evaporate. In this way, PTFE could well act as binder. The final result was a soft slurry, with an elastic consistence.

After the production, the slurry had to be incorporated in the electrode structure. For this electrode, the supporting metal chosen was titanium. In particular, a Ti grid was used.

The incorporation of slurry in the metal grid has been performed thanks to two rolls. These ones, by rotating at very low distance and exerting a certain pressure, allowed the inclusion of carbon-based composite in the grid. The used steps for slurry laying were the following:

- knead of slurry with hands;
- press on a plastic paper to have a thin layer;
- wet with some droplets of ethanol;
- roll with one large distance between rolls;
- fold up the slurry;
- repeat these two last passages for other 2 times;
- reduce distance between rolls and repeat previous rolling steps;
- reduce for the last time and repeat of rolling steps;
- wet with ethanol;
- cover both sides of the top of a Ti grid with the obtained thin layer of slurry;
- roll at a high distance and repeat previous steps to arrive to the desired thickness;
- remove excess slurry with the help of a cutter;
- leave in oven at 60°C for 24 hours.

On the used machine the initial distance between rolls was "4", while the final one was "2". The instrument to perform rolling was a common pasta machine.

The material deposited on the grid has been weighted and geometrically measured,

in order to have information about area and weight. This allowed normalized calculations of capacitance.

Further trials have been also done by using a steel grid, but with the same procedure. Even a steel foil has been tried to be used in the same manner.

A second slurry, in order to have better results of adhesion on steel and titanium foil has been produced by adopting the following ratio:

- 80% Kuraray active carbons for super-capacitor electrode, model YP-50F;
- 10% TIMICAL SUPER C45 for applications as conductive additive for lithium-ion batteries (carbon black);
- 10% Polyvinylidene (PVDF);
- dimethyl sulfoxide (DMSO).

The final consistence of this new slurry was not a soft and dense one, but a liquid and viscous one. Furthermore, since changing both binder and solvent, even the formation of the slurry was different. For these reasons a completely new technique has been used for the production and incorporation on electrodes.

The steps performed to realize it, were:

- weight 10mg of PVDF;
- add 1mL of DMSO;
- heat at 60°C with stirring for 15 minutes, in order to make the solution more viscous;
- add 80mg of active carbons and 10mg of carbon black;
- heat at 80°C for nearly 24 hours (up to when the slurry started to be more viscous);
- spread the slurry on a metal foil, thanks to a bar with a known high (1.5mm);
- leave the solvent to completely evaporate in vacuum;
- heat at 60°C for 24 hours.

In order to delimit a well defined area on the steel/Ti foils, it was possible to make a little cut with a sharp knife and then remove the excess slurry with few acetone. Particular attention had to be paid in this case, avoiding the damage of the realized electrode.

Finally, even a third slurry has been produced, again with a liquid consistence (like the previously cited one). This last studied components combination was adapted from [77]:

- 0.1mL of ethanol;
- 0.1mL of isopropanol;
- 30 μ L of Nafion[®] solution (5wt.%);
- 5mg of active materials (of which 85% Kuraray active carbons YP-50F and 15% carbon black TIMICAL SUPER C45).

The preparation was really easy, consisting only in the weight of all materials and in the following sonication at 59 kHz for 30 minutes. After that a liquid slurry has been obtained. This has been made drip on the desired support. At the first trial a glassy carbon electrode from MetrOhm has been used, in order to check the goodness of the slurry, successively a larger titanium foil has been used.

The comparison of GC electrode before and after treatment have been shown in figure 6.2, while in figure 6.3 it has been reported the deposition on Ti foil.



Figure 6.2: Glassy carbon electrode before and after the deposition of the slurry 3, obtained when using Nafion[®] resin solution as binder

After all these different preparations on various supports, a further type of electrodes has been developed. This lasts, using the same slurry of the first shown ones, was in the form of small discs, with a diameter of 18mm. This new shape of electrodes could not be used in the same system of the others, needing to be pressed in another type of cell (EL cell, see section 6.4). Results obtained for all those electrodes have been reported in next section.



Figure 6.3: Electrode obtained when using Nafion[®] resin solution as binder, deposited on a titanium foil.

6.2 Results for Glassy Carbon

The measurements performed in this chapter had as general goal the testing of the treated Nafion[®] membrane through supercapacitive electrodes.

In general the aspect of interest was: the functioning or not of the membrane to avoid redox mediator passage and thus also avoiding redox shuttling.

Since all electrodes here presented were based on active carbons, a preliminary test could have been done. In particular, this first trial has been performed with a commercial glassy carbon electrode from MetrOhm.

The measurements performed were of cyclic voltammetry and of charge-hold-discharge. The importance of the first technique lied in finding the correct potential range. The criterion used was of determining the one where the coulombic efficiency was higher than the 98%. The scan rate used for all cyclic voltammetries was 20mV/s.

For the glassy carbon electrode, the range which gave more than 98% of coulombic efficiency was the one $-0.5V \div 0.4V$.

In figure 6.4 it has been presented the cyclic voltammetry obtained in the following system:

- GC as working electrode in chamber (a) of the H cell containing only 0.5M KCl;
- reference and counter electrodes, both in the form of platinum rods, in chamber (b) of the cell, where solution 7 was present (20mM $K_3Fe(CN)_6$ + 0.5M KCl).

In red it has been shown the results for this system case. Then the insertion of some drops of solution 2 (containing 7.5mM $K_3Fe(CN)_6$) in chamber (a) to simulate

leakage of redox mediator has been considered and reported.

As could be seen, the main effect of the presence of $\text{K}_3\text{Fe}(\text{CN})_6$ in the chamber of working electrode, lead to the formation of the redox reversible reaction at around -0.1V and to an increase of the difference in currents before and after the reaction. At a first glance one could thought that this was beneficial for the supercapacitive effect of the electrode, since also the area in the CV increased. However, what increased was only the current, since also the contribution from the reaction of the couple $\text{K}_3\text{Fe}(\text{CN})_6/\text{K}_4\text{Fe}(\text{CN})_6$ was added to the previous behaviour.

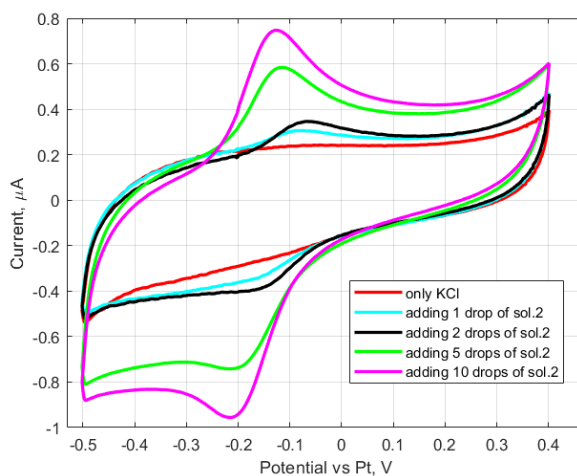


Figure 6.4: Effect of adding redox mediator in the electrolyte when evaluating cyclic voltammetry of the glassy carbon electrode.

In order to better understand the effect of the redox mediator in the system, a new method has been used: the one defined as charge-hold-discharge (CHD). This second method consisted in charging the electrode to the high potential, keeping this for a long time period and then leaving the device to discharge while recording potential variations.

In figure 6.5 it has been shown the comparison between the two cases previously seen in cyclic voltammetry (for cases with redox mediator presence, only the most concentrated one has been represented, being the most significant one).

From the plot it has been easily found the importance of having an ion exchange membrane, in order to keep redox mediator confined. The impact of $\text{K}_3\text{Fe}(\text{CN})_6$ has been, in fact, very dramatic on the device performances.

By considering a discharge time of 1000s, the final potentials were of 97.8% the initial value if the membrane was present, while of 45.3% if some redox mediator drops were added to the solution. This dramatic variation confirmed the need of a

good solution to keep $\text{K}_3\text{Fe}(\text{CN})_6$ away from the electrode.

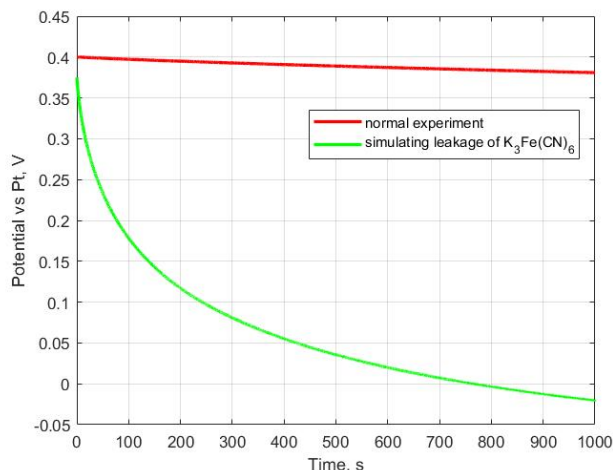


Figure 6.5: Comparison of discharge behaviours for a glassy carbon in normal experiment (when Nafion[®] 117 membrane kept redox mediator away from the GC electrode) or when a leakage is simulated inserting some $\text{K}_3\text{Fe}(\text{CN})_6$ (using 5 drops of solution 2).

6.3 Results for activated carbon electrodes

In the following subsections, the various electrodes produced with active carbon will be discussed, starting by effects found for a glassy carbon.

First of all, however, a presentation of all the produced ones seemed to be necessary. In particular, observations on geometrical or practical problems encountered, with proposed solution will be exploited. After that, the electrodes which showed a good behaviour will be analyzed in more detail, by reporting and commenting results for both CV and CHD.

When explaining results some configurations used will be shown. In particular three situations will be presented: case A, case B and case C. The scheme of the situation has been sketched in figure 6.6.

The chambers of the H cell, as shown in figure, were containing the two solutions called X and Y. Their composition varied according to the experiments and the three most used cases have been classified as:

- **Case A:** Sol. X = 0.5M KCl & Sol. Y = 0.5M KCl;
- **Case B:** Sol. X = 0.5M KCl & Sol. Y = 0.5M KCl + 20mM $\text{K}_3\text{Fe}(\text{CN})_6$;

- **Case C:** Sol. X = 0.5M KCl + 0.5mM $\text{K}_3\text{Fe}(\text{CN})_6$ & Sol. Y = 0.5M KCl + 20mM $\text{K}_3\text{Fe}(\text{CN})_6$.

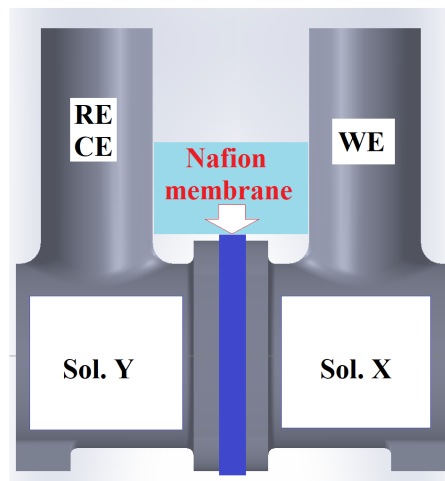


Figure 6.6: Graphical representation of the configurations adopted in the following. RE, CE and WE represented respectively: reference electrode, counter electrode and working electrode. Sol. X and Sol. Y depended instead on the experiment.

6.3.1 Comments on the different configurations

The main difference between the various produced electrodes was the binder employed in the three slurries.

The first electrodes that have been built were those with slurry one, containing PTFE as binder. The first employment for this kind of electrode was that with pressure of the slurry thanks to the pasta machine on a steel grid.

This solution immediately showed its limit: at the first cycle of CV, the steel started to oxidize, releasing thus rust in the solution. Moreover, always due to oxidation of the grid, the resistance increased and the slurry started to detach from the support. Furthermore, the rust in solution could have reacted, altering thus results.

For this reason it has been immediately found that the steel grid was not a viable solution and has not been used in the following.

After this first trial, the same slurry and method have been performed on a titanium grid. This solution avoided the problem of oxidation of the surface of the grid. Cyclic voltammetries have been performed, but giving undesired results. The area of the CV was practically null and a large nearly only resistive behaviour was found. The reason was probably a non-good adhesion of the slurry on the grid.

In order to find if the problem was in the tested electrodes, many proofs with

different ones have been done. The results were always more or less the same. By analyzing physically the electrode, detaching the slurry from the grid with a sharp scalpel, it has been seen that the texture was impressed on the dry slurry surface. According to this it was reasonable to think that the adhesion was good, at least at the moment of electrode fabrication.

Anyway, in agreement with results, it has been supposed that the water pressure may have played the role to detach the active carbons from the grid. This would have been reasonable and would have explained the behaviour of obtained CVs.

The proposed solutions in order to solve this problem were many. The first idea has been to fabricate disc shaped small electrodes, made up of only slurry. After having dried them in oven at 60°C for 24h, they were squeezed on the grid only by pressing them with the help of a PVDF slab. Different geometry of electrodes, varying shape and dimension have been tried. However, after few seconds in water the slurry detached again. Only in one case the slurry remained in condition to work for two cycles, but then it again detached. This result was obviously insufficient.

Since the main problem was the detaching of the slurry, the idea was to keep it confined thanks to the pressure offered by something, even when the electrode was working in water. The first idea was to encapsulate a disc shaped electrode in between of two Ti grids, kept in pressure by Kapton®.

Also this solution didn't work, and so even the use of a paper thin membrane instead of the second Ti grid was not sufficient. The same results were again recorded.

At this point, it appeared obvious that this configuration was not suited to work in a free system, where no pressure to make an electrical contact with the connector was present. Probably grids with different open areas and wire separation, may have produced better results. However, since the limited availability in laboratory, it has been considered this method as not working. For this reason a new list of components has been tried (the one using PVDF as binder).

This new slurry had a liquid composition and it was directly spread on the collector surface. According to this it was no longer possible to use connectors in form of grids, but only of foils.

Two trials were made, by using two different foil materials, a titanium one and a stainless steel one (with a better quality of the one composing the grid). The results for those two devices were the same: a complete detachment of the slurry at the moment of immersion in water. Interestingly, the problem of steel oxidation hasn't been observed with this new configuration, probably according to the higher quality of the material.

After having again discarded the new slurry composition, a last try has been performed by using Nafion® resin solution as binder. The slurry composition has been adapted from [77] and tried at first on a glassy carbon, being provided by the article that attachment in this configuration was good enough for the analysis.

Tries of cyclic voltammetry and CHD have been performed, with quite good results. No detachment was observed and the behaviour of the electrode remained stable with time during different days of measurement.

According to this encouraging result, a try of deposition have been performed on a Ti foil. Results, presented in next subsections, were really good, demonstrating both the need and the ability of the LiCl activated Nafion[®] 117 membrane to keep redox mediator separated.

For sake of completeness and in order to go toward the realization of an integrated HS device, a complete supercapacitor has been performed. The building of this device consisted in the use of disc shaped AC electrodes (made with the first slurry) separated by the activated Nafion[®] 117 membrane, using KCl as electrolyte.

Since the configuration of electrodes tested in the previously built H cell (all except disc shaped ones, which were tried in an EL cell) all showed non negligible resistance, a 90% compensation have been performed. In order to do this, a preliminary electrochemical impedance spectroscopy has been performed to find the resistance value at high frequency, when the imaginary part of impedance was equal to zero. Then, thanks to an option offered by the software Nova, 90% of the recovered value was used in iR compensation.

6.3.2 Deposition on Glassy Carbon

The first working case was the one where the slurry using Nafion[®] resin solution as binder was deposited on the glassy carbon electrode. This configuration has been tried according to previous good results for glassy carbon alone and the suggestion of good attachment from [77].

The cyclic voltammetry has been determined for the same setup used before when studying only the GC electrode. The comparison between the KCl alone case and the one when the IEM membrane was present to avoid redox shuttling, has been shown in figure 6.7.

As could be immediately seen, the electrode seemed to work well. The shape of the cyclic voltammetry resembled the theoretical rectangular shaped one, due to the effect of electrical double layer capacitance. A slight asymmetry has been found, probably imputed to the used system (supercapacitive AC working electrode, while a Pt rod as counter).

The two curves obtained for the two experiments were in high agreement, confirming the possibility to use the studied membrane as separator to keep redox mediator confined. Differences due to different placing of electrodes have been minimized by using the 90% R_u compensation (determining before the uncompensated resistance thanks to EIS).

The capacitance was recovered from the cyclic voltammetry thanks to the equation

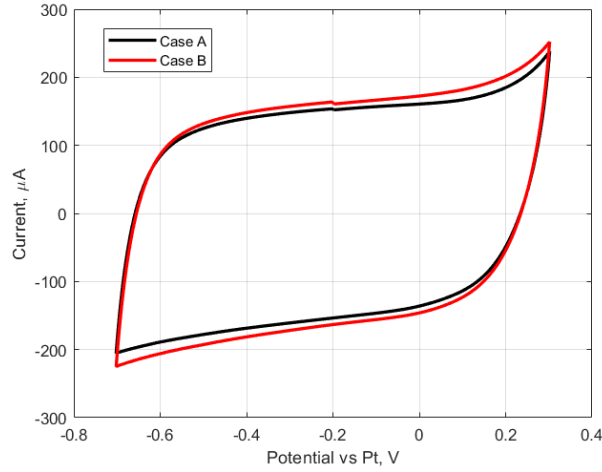


Figure 6.7: Cyclic voltammetry of the treated GC electrode comparing when **case A:** only 0.5M KCl was present and **case B:** redox mediator was kept confined by the treated membrane.

$$C = \frac{1}{2V\nu} \int_{V-}^{V+} i(V)dV \quad (6.1)$$

The found value was of $5.7mF$, which normalized per gram of active material (0.27mg), lead to $21.1F/g$.

The coulombic efficiency was instead of 98.5%.

The system seemed thus to work properly and the analysis could have proceeded with studies of completely laboratory-built electrodes. A proper case has been then found to be necessary when using the charge-hold-discharge evaluation.

This method has been used in order to get information about self-discharge (the real interest in evaluating this system). In fact, the main mechanism of self-discharge when a redox mediator entered in a supercapacitor, was the one of redox shuttling. This last consisted in the discharge of potential at the electrode surface by means of diffusion controlled Faradaic reactions at the interface.

In order to perform correctly the experiment, trials with different holding times have been performed, Results of three cases (1 minute, 10 minutes and 1 hour of holding time) have been plotted in figure 6.8.

The effect was impressing and well represented the possibilities. Using only one minute of holding time it was evident that the self-discharge was very fast. Furthermore, even the iR drop at the first time instant was dramatic. The reasons of this two effects, and in particular of the second one, were due to the charge redistribution effect (see [14] and [13]).

Briefly, the low time allowed to the system in order to balance at the imposed

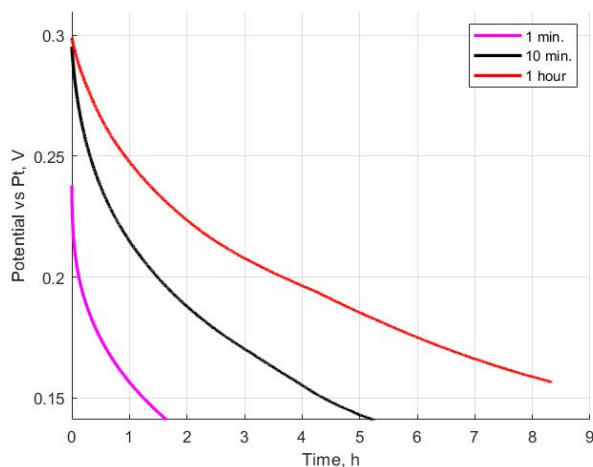


Figure 6.8: Comparison on the effect of different holding time (1 min, 10 min or 1 hour).

potential, was not enough. In this way charges couldn't distribute well in the system. After releasing the charge potential, a rapid falling down has been observed, according to the subsequent rearrangement of charges.

Using 10 minutes improved the quality of the response and one hour has been seen to be even better. According to the availability of time and the quality of results, it has been decided to use 1 hour in following measurements. Probably, results reported in two next subsections could be improved if using higher holding times.

6.3.3 Deposition on Titanium foil

The good results obtained for the treated glassy carbon electrode were encouraging. In order to develop an electrode fully made in laboratory, without depositing slurry on commercial ones, a new one has been realized.

Few drops of the previously produced slurry were deposited on a Ti foil. The technique used consisted in the spread of a drop, wait 10 minutes to let solvent to evaporate and then repeating the process for three other times.

This was the same method used when depositing on glassy carbon. It has also been proofed that the acceleration of times by warming the sample on an heater was not a good idea, since the rapid evaporation of solvents lead to cracks and crumpled structures, with low adhesion to the substrate (as could be seen in figure 6.9).

The amount of material deposited has been weighted and, considering proportions in the solution, it has been found that the deposited carbon quantity was of 1.017mg.



Figure 6.9: Effect of acceleration of dry times using an heater.

The area of deposition has also been determined, but having a not perfectly defined shape, some variations were present. The found value was of 150mm^2 . Anyway, according to the non perfect shape of the deposition, it has been preferred to normalize capacitance value with respect to weight.

The same configuration of previous cases has been used: treated titanium sheet as working electrode and two Pt rods in the opposite chamber of H cell as counter and reference. The membrane placed in between was again a LiCl activated Nafion[®] 117 one, being found in the main part of this work to be a good one for this system. The first experiment has been carried out by filling both chambers of the H cell with a 0.5M KCl solution and then inserting electrodes (Case A). Both cyclic voltammetry and charge-hold-discharge measurements were carried out. After that step, thanks to a pipette, the solution has been removed from the chamber of counter and reference electrode and it has been substituted by solution 7 (20mM $\text{K}_3\text{Fe}(\text{CN})_6$ + 0.5M KCl) (Case B). This step was performed moving the less possible the reference electrode and leaving the working one in its position. In this way, mismatches due to different relative position of electrodes have been minimized (but they weren't completely suppressed).

The last experiment that have been performed was that which simulated a leakage. This test has been done by inserting some redox mediator (adding some drops of solution 2) in the chamber of the working electrode (Case C). Cyclic voltammetry and CHD have been than performed.

The three analyzed cases were those already shown previously in figure 6.6.

In figure 6.10 it has been shown the difference between the CV obtained in the three different cases.

As could be immediately seen, the membrane seemed to work very well, showing results in wide agreement when only KCl was present or when redox mediator was kept confined. Instead, when the leakage occurred, a large variation of results

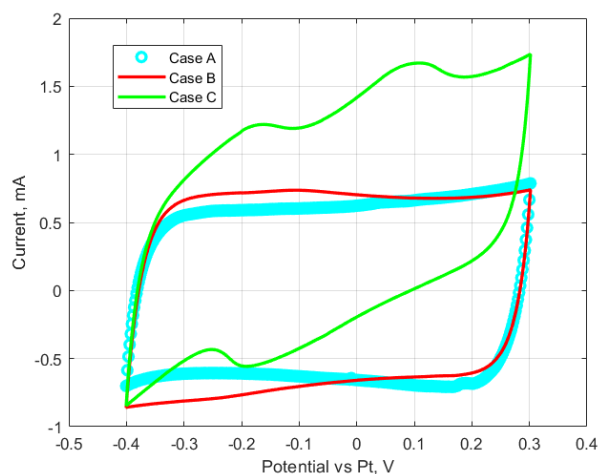


Figure 6.10: Cyclic voltammetry for treated Ti foil. Comparison between: **Case A**, where only KCl was in the cell, **Case B**, where redox mediator was kept confined by the membrane and **Case C**, when simulating a leakage of $\text{K}_3\text{Fe}(\text{CN})_6$.

appeared. The presence of the two nearly symmetrical peaks at around -0.1V has been attributed to the reversible redox reaction. Interestingly, the secondary effect of the reaction was also an increase in current values, as expected. The further proof of the presence of the mediator in case C could be given by comparing with results obtained in the section where glassy carbon was employed instead of titanium.

From the unperturbed case (KCl alone, case A) some important parameters have been obtained, giving the possibility to define it as a supercapacitor. First of all, the potential window was $-0.4\text{V} \div 0.3\text{V}$. Secondary the coulombic efficiency in this range was of 98.1%.

The recovered capacitance was of 29.7mF , which normalized per gram of active material gave 29.2F/g .

The comparison of results for what concerned charge-hold-discharge, instead, have been reported in figure 6.11. From this plot, the impact of some redox mediator traces in the chamber of supercapacitive electrode were very significant.

The importance of doing this kind of measurement arose in order to evaluate self-discharge of the electrode. The other possibility to perform this kind of analysis would have been to kept the potential fixed to the high one (in this case 0.3V) and recording the current required from the system to keep this situation. This method, described by [14], was not used in this work. The method using potential evaluation in open circuit condition has been preferred.

Starting from the figure 6.11, many considerations could be performed. The first

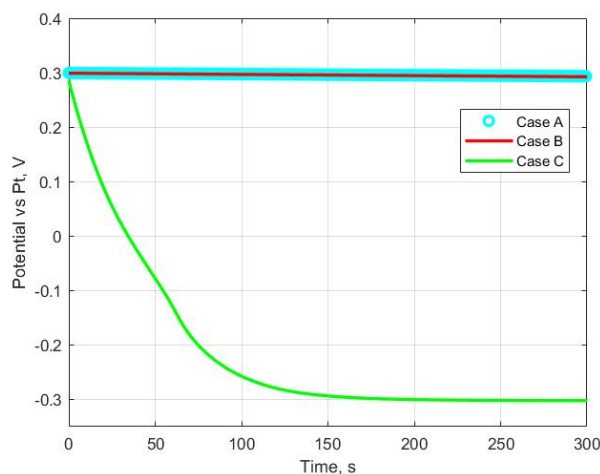


Figure 6.11: Charge-hold-discharge of treated Ti foil. Comparison between: **Case A**, where only KCl was in the cell, **Case B**, where redox mediator was kept confined by the membrane and **Case C**, when simulating a leakage of $\text{K}_3\text{Fe}(\text{CN})_6$.

one, which immediately showed the goodness of this method was for the different time scale of self-discharge. The potential after five minutes for the electrode in bare KCl or when the IEM was present, was higher than 99% of the initial value. When considering the situation with a redox mediator addition, things were dramatically different. After less than three minutes, the value was lower than 15% of the charging potential.

After five minutes, the case C was meaningless, by having a very slow discharge up to the discharged open circuit value. The slowness of this could be attributed to charge redistribution (see figure 6.12).

This very different behaviour implied two things: first of all it has been verified the correct and very good working of the membrane and second it has been demonstrated what was the impact of redox mediator on supercapacitor performances.

The behaviour of self-discharge of the two well behaving systems has been reported in figure 6.12, where the difference for longer times (1 hour) has been shown.

Self-discharge has been generally treated as a black box when evaluating supercapacitors performances. However, many works have been also performed in order to describe the different nature of these processes [14], [13], [78],[79] and [80].

The first check that has been done was devoted to investigate diffusion controlled processes. In particular, they have been evaluated by reporting previous plot vs. the square root of time. If a linear relation was found it would have been probably due to a diffusion controlled Faradaic reaction.

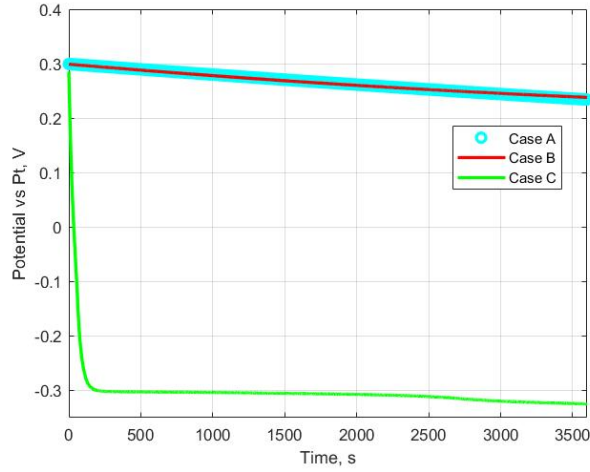


Figure 6.12: Comparison of self-discharge behaviours in CHD between: **Case A**, where only KCl was in the cell, **Case B**, where redox mediator was kept confined by the membrane and **Case C**, when simulating a leakage of $K_3Fe(CN)_6$.

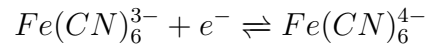
The relation for this kind of process was given by [13]

$$V_t = V_i - \frac{2zFAD^{\frac{1}{2}}\pi^{\frac{1}{2}}c_0}{C}t^{\frac{1}{2}} \quad (6.2)$$

The plot versus square root of time has been reported in figure 6.13. Only the range of interest has been shown.

The two good cases (A and B) showed a nearly constant behaviour, thus they were not dependent on the cited process. The other case (C), instead, showed a linear decrease with square root of time. Therefore it was possible to affirm that the redox shuttling worked thanks to a diffusion controlled Faradaic reaction which made the electrode to discharge.

Obviously the reaction of interest was the one already seen in previous parts of this work:



This has been further proofed, by determining the concentration of redox mediator inserted when simulating a leakage. The found value, obtained by reversing eq. 6.2, lead to a concentration of $K_3Fe(CN)_6$ in the solution of 0.48mM. This value represented a plausible one. Thus, a further proof of the redox shuttling has been provided, confirming also the goodness of the method cited in [13].

In order to determine causes of self-discharge of the two well behaving cases, a new check has been performed. The potential has been plotted on a logarithmic scale

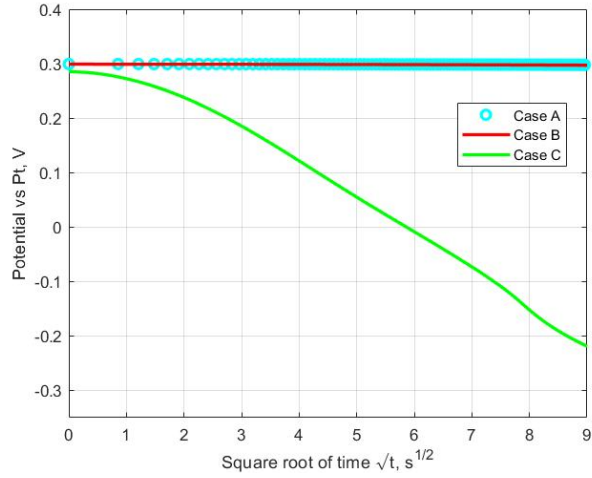


Figure 6.13: Comparison of self-discharge behaviours. Plot of potential vs. square root of time, to highlight the discharge mechanism due to the redox mediator presence.

vs. time (figure 6.14). This has been done according to

$$\ln(V_t) = \ln(V_i) - \frac{t}{RC} \quad (6.3)$$

For the first hour both the behaviours were equal and both followed the expected

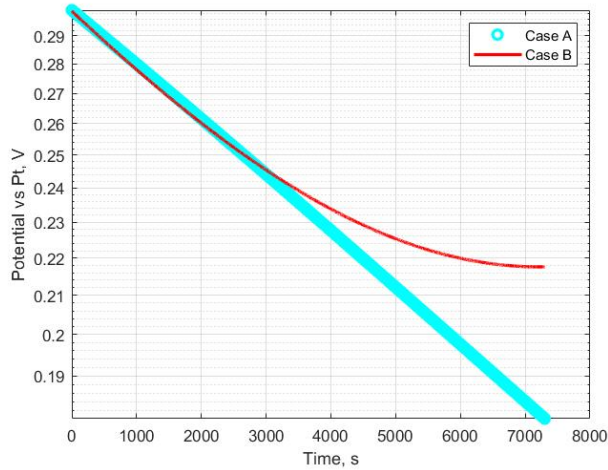


Figure 6.14: Comparison of self-discharge behaviours. Potential has been reported on a logarithmic scale to highlight linear behaviour vs. time for the first hour.

linear trend. This, according to [13], was due to internal ohmic leakages, due

to possible short circuits in the structure of the system and the little passage of current in solution and membrane. After one hour a strange effect appeared: the two curves separated. The fact that the experiment with only KCl behaved worse than the one where the IEM kept redox mediator way was quite counterintuitive. Probably the reason of that came only from the order of the experiments. In fact the measurements with only KCl (case A) have been performed before. Then the electrode remained immersed for a very long time (more than 12 hours) up to when the measurements for the second experiment (case B) have been performed. This could have improved wettability of the electrode and a better charge redistribution. The origin of the plateau of $\ln(V)$ after one hour, in fact was consistent with a charge-redistribution controlled discharge. Further, the different behaviour seemed to be similar to the difference appreciated in the experiment of various holding times for GC (see previous section in figure 6.8). As also confirmed in [14], longer charging times could give large benefits to measurements, according to what has been seen. In order to confirm this, further experiments should be performed using both configurations and leaving them immersed for long and equal times.

6.4 Results for active carbon disc electrodes

The final part of this thesis work used results of previous sections, where the active carbon electrodes were used to represent a supercapacitor.

It has been demonstrated that a supercapacitor could work if a LiCl activated Nafion[®] 117 membrane would be employed to keep confined the redox mediator. Furthermore, it has been verified the ability of active carbon electrodes to work as supercapacitor.

By combining these two results the idea to build a supercapacitor has been born. In particular, it has been wanted to produce a physical device before the end of the project. According to this, a disc shaped flat supercapacitor has been built. The device has been assembled and characterized in an EL cell (fig. 6.15) and the structure was made up of several layers, which could be seen in figure 6.16.

The internal structure of the EL cell has been shown in figure 6.17.

The layers which composed the device were all in the shape of discs with a diameter of 18 mm. In order from the bottom to the top they were: gold collector, AC disc electrode, paper separator, activated Nafion[®] 117 membrane, paper separator, AC disc electrode and gold collector.

The role of collectors was that to provide a good contact between active electrodes and of contacts of the cell. Paper separators, instead, have been found to be useful to avoid the presence of bubbles, which would have compromised the working of the supercapacitor. In fact, since the used IEM tended to wrap when immersed



Figure 6.15: External view of the EL cell containing the studied system.



Figure 6.16: Expanded view of the components of the realized supercapacitor (in order from left to right: gold collector, AC disc electrode, paper separator, activated Nafion[®] 117 membrane, paper separator, AC disc electrode, gold collector).

in water, some voids would have been created between the membrane and the electrodes. This in turn, will have greatly reduced electrical double layer capacitance, reducing device performances. Furthermore, the presence of these separators

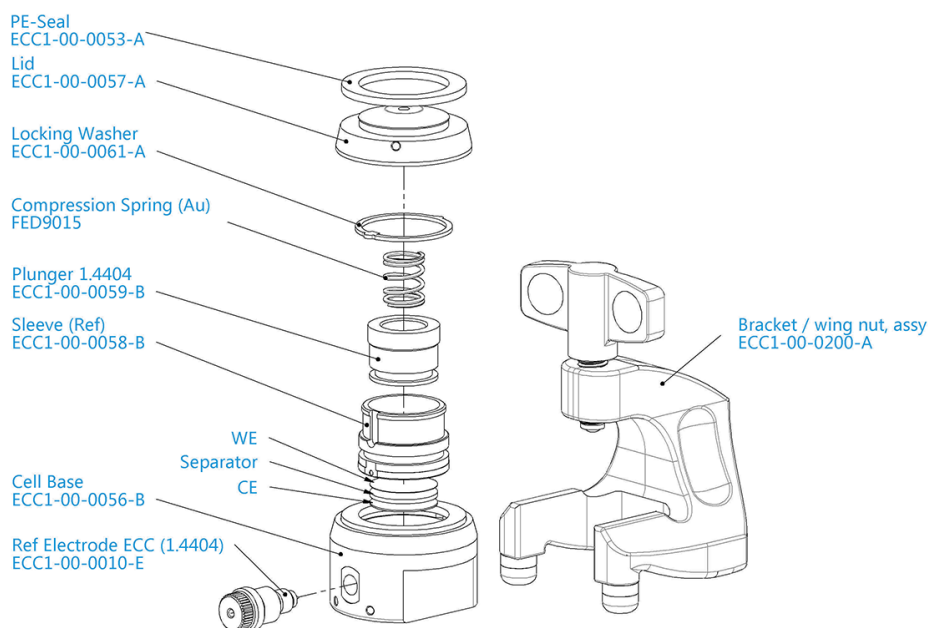


Figure 6.17: Internal structure of the EL cell used for the realization of the supercapacitor, from <https://el-cell.com/>.

increased resistance between the two AC electrodes, reducing thus leakages due to ohmic losses.

The electrodes were prepared with the first slurry, defining their thickness with the help of the pasta machine at the level 2. The resulting thickness after drying for 24 hours at 60°C in oven, was of 1.4mm. The masses of the two used electrodes, were respectively of 35.0mg and 35.5mg.

The electrolyte used for this setup was a solution 0.5M of KCl.

A cyclic voltammetry has been performed in order to evaluate the parameters of the realized supercapacitor. The plot was reported in figure 6.18.

The capacitance of the realized device was calculated and equal to $2.51F$. This value, normalized per mass of electrodes, lead to a capacitance of $37.48F/g$. The operating window was $0V \div 0.8V$, where a coulombic efficiency of 99.1% was recovered. The CV was performed at 20mV/s of scan rate.

Those values seemed to be very good and comparable to examples found in literature (see [24] and [25]).

For sake of completeness also the test of impact of redox mediator (again $K_3Fe(CN)_6$) has been considered. The device has been opened and some droplets of redox

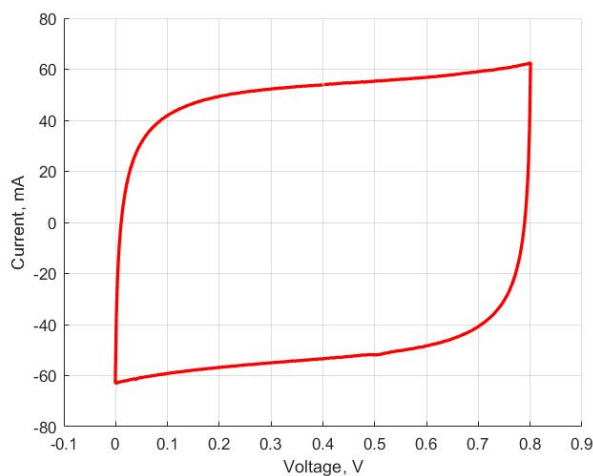


Figure 6.18: Cyclic voltammetry of the realized supercapacitor when 0.5M KCl was used as electrolyte. measurement performed with a scan rate of 20mV/s and a 90% R_u compensation ($R_u = 2\Omega$).

mediator have been inserted, leading to a final concentration of $\text{K}_3\text{Fe}(\text{CN})_6$ of 10mM.

The results of how CV has been deformed have been shown in figure 6.19. The main difference lied in the deformation of the behaviour, making evident the presence of two reversible peaks. Those peaks were quite wide and spread all along the curve, but the potential at which they occurred was still evident (around 0.35V). If this behaviour was compared with the one observed for glassy carbon cases, it should be immediately recovered the presence of mediator, as expected.

The real significant plot was the one of figure 6.20, where a comparison of self-discharge in CHD has been presented.

After less than a hour and a half the device where redox mediator was present, fully discharged. The device containing only the 0.5M KCl electrolyte, instead, at the same instant still kept 70% of initial potential value. After 4 hours, the potential was 0.45V.

It has to be noted that the effect of redox mediator in this device was less dramatic than for the previous cases (see for e.g. the treated Ti foil, where discharge was produced in less than 3 minutes). The reason was that the $\text{K}_3\text{Fe}(\text{CN})_6$ was inserted only on one side of the device. According to this one electrode didn't suffered of redox shuttling and thus performances have been increased.

Obviously this separation could not be guaranteed as for previous cases where the H cell was employed. In fact, in the EL cell, it wasn't possible to seal separate the solutions, even if trying by making a large IEM, which in principle should have

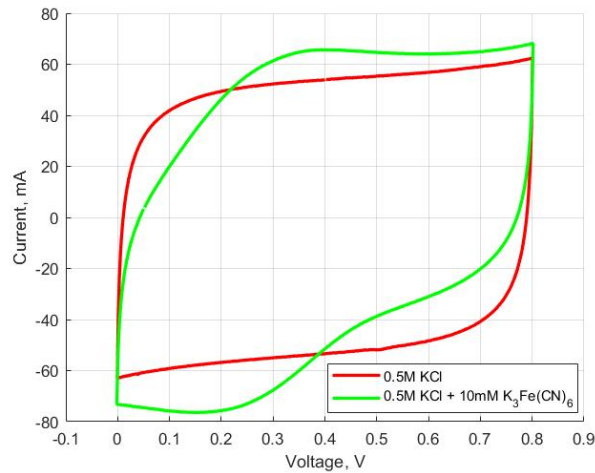


Figure 6.19: Comparison of cyclic voltammetry of the realized supercapacitor when only KCl was present and when K₃Fe(CN)₆ was added.

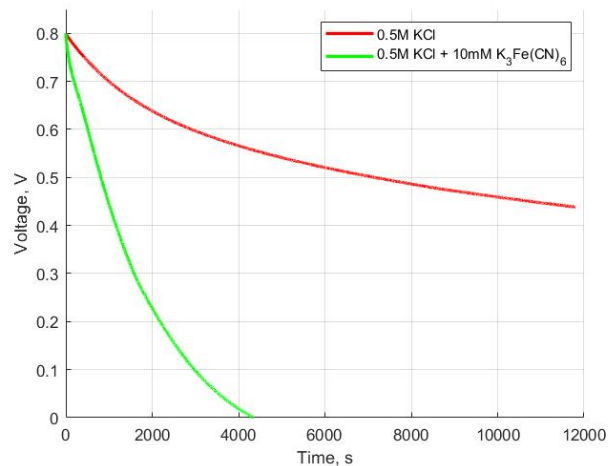


Figure 6.20: Comparison of self-discharge behaviours of the realized supercapacitor when only KCl was present and when K₃Fe(CN)₆ was added.

kept solutions separated. Better geometries of cells should be adopted to study this effect.

Probably, according to the large dimensions of electrodes if compared to those used in previous sections, larger times of charge would have been required to further reduce redistribution of charges. This would have certainly improved the behaviour in self-discharge, increasing retention of potential. However, in order to be consistent with the previous part of this study, one hour of charge has been also

used for this device. Further measurements with longer charging times will thus certainly provide better performances.

According to results, a final HS device were a DSSC should be integrated with a supercapacitor, would require another geometry, even if the elements proposed seemed to be good. In fact, the redox shuttling at one supercapacitor electrode would be a real problem for the working. A new geometry should be proposed, like an opened one, where both electrodes of the supercapacitor should be on the same side of the device. This would allow to kept confined the redox mediator of the DSSC thanks to the studied membrane.

Chapter 7

Conclusions

As widely commented in chapter 2, the energy demand is growing day by day. Furthermore, not only the amount should increase with time, but even the necessity to use renewable sources must be considered. The most important one of them is sun.

It is in fact free, widespread and frequently available. The produced energy can be in form of heat (solar) or electrical (photovoltaic). Many configurations to harvest energy of the sun have been found during the years. One of the most promising technologies is the one of DSSC. These devices are based on the absorption of energy by a dye, which will produce a current, thanks to electrons provided by the electrolyte. In this last element, generally in liquid form, a redox mediator is present, which, thanks to its reactions at the two electrodes, allows for the passage of current, by closing the circuit.

DSSCs are easy to produce, have good indoor efficiencies, quite inexpensive and with a lower environmental impact (with respect to older technologies, like those based on silicon). However, they still present lower efficiency than other solutions, but many studies are producing daily more and more performing devices.

The main limit of using solar energy, anyway, is that it is not always present. In fact, clouds can cover the sun and during night a photovoltaic cell can't work. Thus, a system of storage should be necessary. The first idea which could come in mind consists in the integration of the two parts of harvest and storage of energy. This was the idea at the base of the project, already started, in which the thesis work was inserted, being oriented to the construction of an integrated HS device. According to the previous choice of a DSSC for the production part, a supercapacitor has been chosen to complete the device, providing good characteristics for the storage.

The idea was thus to integrate this two components in order to get a completely working device. However, one big problem immediately appeared to be important. It consisted in the fact that, since the need of the two devices to share the same

electrolyte, the redox mediator used by the DSSC was not compatible with the supercapacitor. In particular, an effect called redox shuttling would have happened, leading to the self-discharge of the storage system.

For this reason, a method to keep the redox mediator confined was necessary. According to many researches found in literature, the decision was to use an ion exchange membrane. Once this was decided, it was necessary to take an important decision: if using or not an aqueous based electrolyte. This, in turn, would have affected also the choice of the membrane.

The initial idea was to use the redox couple I^3^-/I^- in an acetonitrile based electrolyte. However, mainly due to practical limitations like time and material availability, it has been preferred to use the couple $Fe(CN)_6^{3-}/Fe(CN)_6^{4-}$ in water. This simplified manipulations and allowed to work directly in the laboratory room, without the need of an oxygen-free environment.

At this point, once the main choices for the integrated devices were done, the determination of the good behaviour of the membrane was necessary.

The work of this thesis was born in accordance with this need. By briefly resuming the activities, it was found that some important things have been determined to correctly perform the final evaluation.

First of all the choice of microelectrodes allowed to work in the diffusion limited regime when performing cyclic voltammetry. This was very useful, differently from macroelectrode, where the diffusion regime was planar instead that semi-hemispherical. The microelectrodes allowed thus to determine the diffusion coefficient of the studied redox mediator. All methods to clean the surface of these electrodes have been carefully analyzed and tried. In this way a standard and good procedure have been determined to have comparable results in successive experiments.

After having taken a good familiarity with microelectrodes, they have been employed to determine the diffusion coefficient of $K_3Fe(CN)_6$. Three techniques have been analyzed and compared, by studying many effects, the major of which was the effect of supporting electrolyte. After this, with the choice of cyclic voltammetry as the best of the three, a value of diffusion coefficient of $9.13 \cdot 10^{-6} cm^2/s$ has been found.

This parameter was determined since allowed to connect the recorded current to the concentration of mediator in solution. This was fundamental in this work, since the final goal consisted in the evaluation of the ability of the membrane to keep it confined.

After some checks on the membrane main parameters like permselectivity, a final test has been conducted. The membrane was placed in between the two chambers of an H cell. Then the solution containing mediator was placed in one chamber. In the other, where only 0.5M KCl was present, the microelectrode was inserted. Performing cycling voltammetries during a long time (5 days), it has been found

that no traces of $\text{K}_3\text{Fe}(\text{CN})_6$ could be found. This provided that the Nafion[®] 117 membrane used was really good and didn't allow the passage of mediator.

This allowed to think to really use it in the integrated HS device. The work was thus moved to the study of the redox shuttling effect, with again a further proof of the good selectivity of the membrane.

The last chapter was devoted to the realization of supercapacitive electrodes based on active carbons. These could be used in a future supercapacitor included in the integrated device. These electrodes have been studied in the H cell, again using the membrane to keep confined the redox mediator. Results were again really good.

The effect of inserting $\text{K}_3\text{Fe}(\text{CN})_6$ lead to variations in the discharge after 1 hour of more than 90% of the potential of charge. In fact, as experimentally seen, the redox reaction of the mediator made the charge stored on electrodes to completely discharge in few minutes. This was a further proof of the need of the membrane as proposed at the beginning of the work.

The final operation that have been done was to produce a supercapacitor. It was made of two disc shaped carbon based electrodes separated by paper and the studied ion exchange membrane. The electrolyte was 0.5M KCl. Good results have been obtained, indicating that this device could be integrated in future with an aqueous based DSSC.

In conclusion, this work confirmed the possibility to build an integrated HS device made up of a DSSC and a supercapacitor, using the studied membrane to keep $\text{K}_3\text{Fe}(\text{CN})_6$ confined. The choice of electrolyte should fall on an aqueous KCl one, with the redox mediator studied before to regenerate dye for the DSSC. The electrodes of supercapacitor could be made using the slurry cited in chapter 6 and should have an open configuration, with both of them on the same side of the device. The LiCl activated Nafion[®] 117 membrane would be the proper choice to allow this integration.

Bibliography

- [1] *Key World Energy Statistics*. [iea.org](https://www.iea.org/reports/key-world-energy-statistics-2020), 2020. URL: <https://www.iea.org/reports/key-world-energy-statistics-2020>.
- [2] O. Ellabban, H. Abu-Rub, and F. Blaabjerg. «*Renewable energy resources: Current status, future prospects and their enabling technology*». In: *Renewable and Sustainable Energy Reviews* Vol. 29 (2014), pp. 748–764. DOI: 10.1016/j.rser.2014.07.113.
- [3] B. O'Regan and M. Grätzel. «*A low-cost, high-efficiency solar cell based on dye-sensitized colloidal TiO₂ films*». In: *Nature* Vol. 353 (1991), pp. 737–740. DOI: 10.1038/353737a0.
- [4] M. Grätzel. «*Photoelectrochemical cells*». In: *Nature* Vol. 414 (2001), pp. 338–344. DOI: 10.1038/35104607.
- [5] P. Sethupathy, K. Wagner, G. G. Wallace, and D. L. Officer. «*Development of Aqueous Dye Sensitized Solar Cell Electrolytes based on Fe(CN)₆^{4-/3-} and [Co(bpy)₃]^{2+/3+} Redox Couples*». In: *Poster of ARC Centre of Excellence for Electromaterials Science and the Intelligent Polymer Research Institute, University of Wollongong, Australia* (2018), pp. 1–2. URL: <https://www.researchgate.net/publication/326543828>.
- [6] T. Daeneke, Y. Uemura, N. W. Duffy, A. J. Mozer, N. Koumura, U. Bach, and L. Spiccia. «*Aqueous Dye-Sensitized Solar Cell Electrolytes Based on the Ferricyanide–Ferrocyanide Redox Couple*». In: *Advanced Materials* 24 (2012), pp. 1222–1225. DOI: 10.1002/adma.201104837.
- [7] R. Liu, Y. Liu, H. Zou, T. Song, and B. Sun. «*Integrated solar capacitors for energy conversion and storage*». In: *Advanced Energy Materials* Vol. 10 (2017), pp. 1545–1559. DOI: 10.1007/s12274-017-1450-5.
- [8] Z. Fang, X. Hu, and D. Yu. «*Integrated Photo-Responsive Batteries for Solar Energy Harnessing: Recent Advances, Challenges, and Opportunities*». In: *ChemPlusChem* Vol. 85 (2020), pp. 600–612. DOI: 10.1002/cplu.201900608.

- [9] S. Zang and N. Pan. «*Supercapacitors Performance Evaluation*». In: *Advanced Energy Materials* Vol. 5 (2015), pp. 1401401–1401419. DOI: 10.1002/aenm.201401401.
- [10] A. K. Samantara and S. Ratha. *Materials Development for Active/Passive Components of a Supercapacitor*. Springer, Singapore, 2018. Chap. 3, pp. 11–39. DOI: 10.1007/978-981-10-7263-5_3.
- [11] A. Borenstein, O. Hanna, R. Attias, S. Luski, T. Brousee, and D. Aurbach. «*Carbon-based composite materials for supercapacitor electrodes: a review*». In: *Journal of Material Chemistry* Vol. 5 (2017), pp. 12653–12672. DOI: 10.1039/C7TA00863E.
- [12] A. Brandt, S. Pohlmann, A. Varzi, A. Balducci, and S. Passerini. «*Ionic liquids in supercapacitors*». In: *Material Research Society* Vol. 38 (2013), pp. 554–559. DOI: 10.1557/mrs.2013.151.
- [13] J. Black and H. A. Andreas. «*Effects of charge redistribution on self-discharge of electrochemical capacitors*». In: *Electrochimica Acta* Vol. 54 (2009), pp. 3568–3574. DOI: 10.1016/j.electacta.2009.01.019.
- [14] H. A. Andreas. «*Self-Discharge in Electrochemical Capacitors: A Perspective Article*». In: *Journal of the Electrochemical Society* Vol. 162 (2015), pp. A5047–A5053. DOI: 10.1149/2.0081505jes.
- [15] T. Miyasaka and T. N. Murakami. «*The photocapacitor: An efficient self-charging capacitor for direct storage of solar energy*». In: *Applied Physics Letters* Vol. 85 (2004), pp. 3932–3934. DOI: 10.1063/1.1810630.
- [16] A. Scalia, F. Bella, A. Lamberti, S. Bianco, C. Gerbaldi, E. Tresso, and C. F. Pirri. «*A flexible and portable powerpack by solid-state supercapacitor and dye-sensitized solar cell integration*». In: *Journal of Power Sources* Vol. 359 (2017), pp. 311–321. DOI: 10.1016/j.jpowsour.2017.05.072.
- [17] Z. Wang, J. Cheng, H. Huang, and B. Wang. «*Flexible self-powered fiber-shaped photocapacitors with ultralong cyclelife and total energy efficiency of 5.1%*». In: *Energy Storage Materials* Vol. 24 (2020), pp. 255–264. DOI: 10.1016/j.ensm.2019.08.011.
- [18] C. Li, M. M. Islam, J. Moore, J. Sleppy, C. Morrison, K. Konstantinov, S. X. Dou, C. Renduchintala, and J. Thomas. «*Wearable energy-smart ribbons for synchronous energy harvest and storage*». In: *Nature Communications* Vol. 7 (2016), pp. 1–10. DOI: 10.1038/ncomms13319.
- [19] T. Chen, Z. Yang, and H. Peng. «*Integrated Devices to Realize Energy Conversion and Storage Simultaneously*». In: *ChemPhysChem* Vol. 14 (2013), pp. 1777–1782.

- [20] C. T. Chien, P. Hiralal, D. Y. Wang, I. S. Huang, C. C. Chen, C. W. Chen, and G. A. J. Amaratunga. «*Graphene-Based Integrated Photovoltaic Energy Harvesting/Storage Device*». In: *Small journal, material views* Vol. 11 (2015), pp. 2929–2937. DOI: 10.1002/sml1.201403383.
- [21] W. Guo, X. Xue, S. Wang, C. Lin, and Z. L. Wang. «*An Integrated Power Pack of Dye-Sensitized Solar Cell and Li Battery Based on Double-Sided TiO₂ Nanotube Arrays*». In: *Nano Letters* Vol. 12 (2012), pp. 2520–2523. DOI: 10.1021/nl3007159.
- [22] D. Lau, N. Song, C. Hall, Y. Jiang, S. Lim, I. Perez-Wurfl, Z. Ouyang, and A. Lennon. «*Hybrid solar energy harvesting and storage devices: The promises and challenges*». In: *Materials Today Energy* Vol. 13 (2019), pp. 22–44. DOI: 10.1016/j.mtener.2019.04.003.
- [23] T. N. Murakami, N. Kawashima, and T. Miyasaka. «*A high-voltage dye-sensitized photocapacitor of a three-electrode system*». In: *The Royal Society of Chemistry* (2005), pp. 3346–3348. DOI: 10.1039/b503122b.
- [24] V. Vega-Garita, L. Ramirez-Elizondo, N. Narayan, and P. Bauer. «*Integrating a photovoltaic storage system in one device: A critical review*». In: *Progress in Photovoltaics Research and Applications* Vol. 27 (2019), pp. 346–370. DOI: 10.1002/pip.3093.
- [25] S.K. Chirauri, A.K. Dehury, and Y.S. Chaudhary. «*Photosupercapacitors: A perspective of planar and flexible dual functioning devices*». In: *Wires Energy and Environment* Vol. 9 (2020), pp. 1–27. DOI: 10.1002/wene.377.
- [26] A. Scalia. «*New devices for energy harvesting and storage: integrated third generation photovoltaic solar cells and electrochemical double layer capacitors*». In: *Doctoral dissertation, PhD in electrical, electronics and communications engineering* (2019).
- [27] A. Scalia, A. Varzi, A. Lamberti, E. Tresso, S. Jeong, T. Jacobad, and S. Passerini. «*High energy and high voltage integrated photoelectrochemical double layer capacitor*». In: *Sustainable Energy Fuels* Vol. 2 (2018), pp. 968–977. DOI: 10.1039/c8se00003d.
- [28] Z. Yang, L. Li, Y. Luo, R. He, L. Qiu, H. Lina, and H. Peng. «*An integrated device for both photoelectric conversion and energy storage based on free-standing and aligned carbon nanotube film*». In: *Journal of Material Chemistry* Vol. 1 (2013), pp. 954–958. DOI: 10.1039/c2ta00113f.
- [29] A. Scalia, F. Bella, A. Lamberti, C. Gerbaldi, and E. Tresso. «*Innovative multipolymer electrolyte membrane designed by oxygen inhibited UV-crosslinking enables solid-state in plane integration of energy conversion and storage devices*». In: *Energy* Vol. 166 (2019), pp. 789–795. DOI: 10.1016/j.energy.2018.10.162.

- [30] R. G. Compton and C. E. Banks. *Understanding voltammetry*. World Scientific, 2010. Chap. 5, p. 444. DOI: 10.1142/p726.
- [31] K. Aoki. «*Theory of ultramicroelectrodes*». In: *Electroanalysis* Vol. 5 (1993), pp. 627–639. DOI: 10.1002/elan.1140050802.
- [32] C. G. Zosky. *Handbook of Electrochemistry*. Elsevier Science, 2007, p. 934. DOI: 10.1016/B978-0-444-51958-0.X5000-9.
- [33] P. Daubinger, J. Kieninger, T. Unmüßig, and G. A. Urban. «*Electrochemical characteristics of nanostructured platinum electrodes – a cyclic voltammetry study*». In: *Physical Chemistry Chemical Physics* Vol. 16 (2014), pp. 8392–8399. DOI: 10.1039/c4cp00342j.
- [34] D. A. J. Rand and R. Woods. «*A study of the dissolution of platinum, palladium, rhodium and gold electrodes in 1 M sulphuric acid by cyclic voltammetry*». In: *Journal of Electroanalytical Chemistry* Vol. 35 (1972), pp. 209–218. DOI: 10.1016/S0022-0728(71)80089-X.
- [35] L. Jacobse, S. J. Raaijman, and M. T. M. Koper. «*The reactivity of platinum microelectrodes*». In: *Physical Chemistry Chemical Physics* Vol. 18 (2016), pp. 28451–28457. DOI: 10.1039/c6cp05361k.
- [36] T. Biegler, D. A. J. Rand, and R. Woods. «*Limiting oxygen coverage on platinized platinum; Relevance to determination of real platinum area by hydrogen adsorption*». In: *Journal of Electroanalytical Chemistry* Vol. 29 (1971), pp. 269–277. DOI: 10.1016/S0022-0728(71)80089-X.
- [37] D. W. Kumsa, N. Bhadra, E. M. Hudak, S. C. Kelley, D. F. Untereker, and J. T. Mortimer. «*Electron transfer processes occurring on platinum neural stimulating electrodes: a tutorial on the $i(V_e)$ profile*». In: *Journal of Neural Engineering* Vol. 13 (2016), pp. 1–15. DOI: 10.1088/1741-2560/13/5/052001.
- [38] *Differences between digital scans, analog scans and signal integration. AN-EC-007*. MetrOhm, 2019, pp. 1–5. URL: <https://www.metrohm.com/en/applications/AN-EC-007>.
- [39] J. E. Baur and R. M. Wightman. «*Diffusion coefficients determined with microelectrodes*». In: *Journal of Electroanalytical Chemistry and Interfacial Electrochemistry* Vol. 305 (1991), pp. 73–81. DOI: 10.1016/0022-0728(91)85203-2.
- [40] A. J. Bard and L. R. Faulkner. *ELECTROCHEMICAL METHODS. Fundamentals and Applications*. 2nd ed. John Wiley & Sons, Inc., 2001, p. 934. ISBN: 0-471-04372-9.

- [41] P. Wachter, C. Schreiner, M. Zistler, D. Gerhard, P. Wasserscheid, and H. J. Gores. «*A microelectrode study of triiodide diffusion coefficients in mixtures of room temperature ionic liquids, useful for dye-sensitised solar cells*». In: *Microchimica Acta* Vol. 160 (2008), pp. 125–133. DOI: 10.1007/s00604-007-0803-2.
- [42] C. L. Bentley, A. M. Bond, A. F. Hollenkamp, P. J. Mahon, and J. Zhang. «*Voltammetric Determination of the Iodide/Iodine Formal Potential and Triiodide Stability Constant in Conventional and Ionic Liquid Media*». In: *Journal of Physical Chemistry* Vol. 119 (2015), pp. 22392–22403. DOI: 10.1021/acs.jpcc.5b07484.
- [43] F. C. Pereira, L. M. Moretto, M. De Leo, M. V. Boldrin Zanoni, and P. Ugo. «*Gold nanoelectrode ensembles for direct trace electroanalysis of iodide*». In: *Analytical Chimica Acta* Vol. 575 (2006), pp. 16–24. DOI: 10.1016/j.aca.2006.05.056.
- [44] J. Orozco, C. F. Sanchez, and C. J. Jorquera. «*Ultramicroelectrode Array Based Sensors: A Promising Analytical Tool for Environmental Monitoring*». In: *Sensors* Vol. 19 (2017), pp. 475–490. DOI: 10.3390/s100100475.
- [45] N. Frenzel, J. Hartley, and G. Frisch. «*Voltammetric and spectroscopic study of ferrocene and hexacyanoferrate and the suitability of their redox couples as internal standards in ionic liquids*». In: *Physical Chemistry Chemical Physics* Vol. 10 (2010), pp. 28841–28852. DOI: 10.1039/c7cp05483a.
- [46] S. Y. Lee, D. J. Lee, K. H. Yeon, W. G. Kim, M. S. Kang, and J. S. Park. «*A Cyclic Voltammetric Study of Electrodes for Reverse Electrodialysis*». In: *Journal of the Korean Electrochemical Society* Vol. 16 (2013), pp. 145–150. DOI: 10.5229/JKES.2013.16.3.145.
- [47] G. Denuault, M. V. Mirkin, and A. J. Bard. «*Direct determination of diffusion coefficients by chronoamperometry at microdisk electrodes*». In: *Journal of Electroanalytical Chemistry* Vol. 308 (1991), pp. 27–38. DOI: 10.1016/0022-0728(91)85056-U.
- [48] T. R. I. Cataldi, A. Rubino, and R. Ciriello. «*Sensitive quantification of iodide by ion-exchange chromatography with electrochemical detection at a modified platinum electrode*». In: *Analytical and Bioanalytical Chemistry* Vol. 382 (2005), pp. 134–141. DOI: 10.1007/s00216-005-3187-3.
- [49] Y. Wang, E. I. Rogers, and R. G. Compton. «*The measurement of the diffusion coefficients of ferrocene and ferrocenium and their temperature dependence in acetonitrile using double potential step microdisk electrode chronoamperometry*». In: *Journal of Electroanalytical Chemistry* Vol. 648 (2010), pp. 15–19. DOI: 10.1016/j.jelechem.2010.07.006.

- [50] D. Shoup and A. Szabo. «*Chronoamperometric at finite disk electrodes*». In: *Journal of Electroanalytical Chemistry and Interfacial Electrochemistry* Vol. 23 (1982), pp. 237–245. DOI: 10.1016/0022-0728(82)85171-1.
- [51] V.S. Muralidharan. «*Warburg impedance – basics revisited*». In: *Anti-Corrosion Methods and Materials* Vol. 44 (1997), pp. 26–29. DOI: 10.1108/00035599710157387.
- [52] S. R. Taylor and E. Gileadi. «*Physical Interpretation of the Warburg Impedance*». In: *Corrosion Science* Vol. 51 (1995), pp. 664–671. DOI: 10.5006/1.3293628.
- [53] J. Huang. «*Diffusion impedance of electroactive materials, electrolytic solutions and porous electrodes: Warburg impedance and beyond*». In: *Electrochimica Acta* Vol. 281 (2018), pp. 170–188. DOI: 10.1016/j.electacta.2018.05.136.
- [54] Z. A. Rotenberg, A. V. Dribinskii, V. P. Lukovtsev, and N. S. Khozyainova. «*Electrochemical Impedance of Microelectrodes*». In: *Russian Journal of Electrochemistry* Vol. 36 (2000), pp. 879–882. DOI: 10.1007/BF02757062.
- [55] D. Schmidt, M. D. Hager, and U. S. Schubert. «*Photo-Rechargeable Electric Energy Storage Systems*». In: *Advanced Energy Materials* Vol. 6 (2016), pp. 1–11. DOI: 10.1002/aenm.201500369.
- [56] E. Frackowiack, K. Fic, M. Meller, and G. Lota. «*Electrochemistry Serving People and Nature: High-Energy Ecocapacitors based on Redox-Active Electrolytes*». In: *ChemSusChem* (2012), pp. 1–5. DOI: 10.1002/cssc.201200227.
- [57] M. Rahimnejad, G. Bakeri, G. Najafpour, M. Ghasemi, and S. E. Oh. «*A review on the effect of proton exchange membranes in microbial fuel cells*». In: *Biofuel Research Journal* Vol. 1 (2014), pp. 7–15. DOI: 10.18331/BRJ2015.1.1.4.
- [58] A. Zerrouki, M. Kameche, H. Kebaili, I. S. Boukoussa, M. A. Flitti, H. Ilikti, and C. Innocent. «*An investigation on polymer ion exchange membranes used as separators in low-energy microbial fuel cells*». In: *Springer Nature* Vol. 75 (2018), pp. 4947–4965. DOI: 10.1007/s00289-018-2305-2.
- [59] H. Prifti, A. Parasuraman, S. Winardi, T. M. Lim, and M. Skyllas-Kazacos. «*Membranes for Redox Flow Battery Applications*». In: *Membranes* Vol. 75 (2012), pp. 275–306. DOI: 10.3390/membranes2020275.
- [60] D. Chen, M. A. Hickner, E. Agar, and E. C. Kumbar. «*Selective anion exchange membranes for high coulombic efficiency vanadium redox flow batteries*». In: *Electrochemistry Communications* Vol. 26 (2013), pp. 37–40. DOI: 10.1016/j.elecom.2012.10.007.

- [61] C. Jia, F. Pan, Y. G. Zhu, Q. Huang, L. Lu, and Q. Wang. «*High-energy density nonaqueous all redox flow lithium battery enabled with a polymeric membrane*». In: *Science Advances* Vol. 1 (2015), pp. 1–7. DOI: 10.1126/sciadv.1500886.
- [62] S. Kim, J. Yan, B. Schwenzer, J. Zhang, L. Li, J. Liu, Z. G. Yang, and M. A. Hickner. «*Cycling performance and efficiency of sulfonated poly(sulfone) membranes in vanadium redox flow batteries*». In: *Electrochemistry Communications* Vol. 12 (2010), pp. 1650–1653. DOI: 10.1016/j.elecom.2010.09.018.
- [63] J. Sheng, A. Mukhopadhyay, W. Wang, and H. Zhu. «*Recent advances in the selective membrane for aqueous redox flow batteries*». In: *Materials Today Nano* Vol. 7 (2019), pp. 1–9. DOI: 10.1016/j.mtnano.2019.100044.
- [64] J. Lee, P. Srimuk, S. Fleischmann, X. Su, T. A. Hatton, and V. Presser. «*Redox-electrolytes for non-flow electrochemical energy storage: A critical review and best practice*». In: *Progress in Materials Science* Vol. 101 (2019), pp. 46–89. DOI: 10.1016/j.pmatsci.2018.10.005.
- [65] B. Evanko, S. W. Boettcher, S. J. Yoo, and G. D. Stucky. «*Redox-Enhanced Electrochemical Capacitors: Status, Opportunity, and Best Practices for Performance Evaluation*». In: *American Chemical Society* Vol. 2 (2017), pp. 2581–2590. DOI: 10.1021/acseenergylett.7b00828.
- [66] M. Tachibana, T. Ohishi, Y. Tsukada, A. Kitajima, H. Yamagishi, and M. Murakami. «*Supercapacitor using an electrolyte charge storage system*». In: *Electrochemistry* Vol. 79 (2011), pp. 882–886. DOI: 10.5796/electrochemistry.79.882.
- [67] L. Chen, H. Bai, Z. Huang, and L. Li. «*Mechanism investigation and suppression of self-discharge in active electrolyte enhanced supercapacitors*». In: *Energy Environment Science* Vol. 7 (2014), pp. 1750–1759. DOI: 10.1039/C4EE00002A.
- [68] E. A. Sanginov, E. Y. Evshchik, R. R. Kayumov, and Y. A. Dobrovolski. «*Lithium-Ion Conductivity of the Nafion Membrane Swollen in Organic Solvents*». In: *Russian Journal of Electrochemistry* Vol. 51 (2015), pp. 986–990. DOI: 10.1134/S1023193515100122.
- [69] G. Inzelt, A. Lewenstam, and F. Scholz. *Pseudo-reference Electrodes*. Springer, Berlin, Heidelberg, 2013, pp. 331–332. DOI: 10.1007/978-3-642-36188-3_14.
- [70] K. K. Kasem and S. Jones. «*Platinum as a Reference Electrode in Electrochemical Measurements*». In: *Platinum Metals Review* Vol. 52 (2008), pp. 100–106. DOI: 10.1595/147106708X297855.
- [71] IUPAC. *Compendium of chemical terminology*. Vol. 65. 1993, p. 856.

- [72] W. Grot. *Fluorinated Ionomers*. 2nd ed. 2011. Chap. 9, pp. 229–230.
- [73] H. J. Cassady, E. C. Cimino, M. Kumar, and M. A. Hickner. «*Specific ion effects on the permselectivity of sulfonated poly (ether sulfone) cation exchange membranes*». In: *Journal of Membrane Science* Vol. 508 (2016), pp. 146–152. DOI: 10.1016/j.memsci.2016.02.048.
- [74] R. S. Kingsbury, S. Flotron, S. Zhu, D. F. Call, and O. Coronell. «*Junction Potentials Bias Measurements of Ion Exchange Membrane Permselectivity*». In: *Environment Science Technology* Vol. 52 (2018), pp. 4929–4936. DOI: 10.1021/acs.est.7b05317.
- [75] P. Vanýsek. *Ionic conductivity and diffusion at infinite dilution*. 2011, pp. 77–79. URL: https://is.muni.cz/el/sci/podzim2016/C4020/um/pom/Ionic_Conductivity_and_Diffusion_at_Infinite_Dilution.pdf.
- [76] R. S. Kingsbury, S. Flotron, S. Zhu, D. F. Call, and O. Coronell. *Junction Potentials Bias Measurements of Ion Exchange Membrane Permselectivity. SUPPORTING INFORMATION*. 2018, pp. S1–S9. URL: https://pubs.acs.org/doi/suppl/10.1021/acs.est.7b05317/suppl_file/es7b05317_si_001.pdf.
- [77] J. Zeng, C. Francia, C. Gerbaldi, V. Baglio, S. Specchia, A.S. Aricò, and P. Spinelli. «*Hybrid ordered mesoporous carbons doped with tungsten trioxide as supports for Pt electrocatalysts for methanol oxidation reaction*». In: *Electrochimica Acta* Vol. 84 (2013), pp. 80–91. DOI: 10.1016/j.electacta.2013.01.139.
- [78] K. Wang, L. Yao, M. Jahon, J. Liu, M. Gonzalez, P. Liu, V. Leung, X. Zhang, and T. Nga. «*Ion-Exchange Separators Suppressing Self-Discharge in Polymeric Supercapacitors*». In: *American Chemical Society* Vol. 5 (2020), pp. 3276–2384. DOI: 10.1021/acsenerylett.0c01783.
- [79] B. E. Conway, W. G. Pell, and T-C. Liu. «*Diagnostic analyses for mechanisms of self-discharge of electrochemical capacitors and batteries*». In: *Journal of power sources* Vol. 65 (1997), pp. 53–59. DOI: 10.1016/S0378-7753(97)02468-3.
- [80] J. Niu, B. E. Conway, and W. G. Pell. «*Comparative studies of self-discharge by potential decay and float-current measurements at C double-layer capacitor and battery electrodes*». In: *Journal of power sources* Vol. 135 (2004), pp. 332–343. DOI: 10.1016/j.jpowsour.2004.03.068.